



Doctoral Thesis

Design, modeling and optimization of multi-column chromatographic processes

Author(s):

Baur, Daniel

Publication Date:

2017

Permanent Link:

<https://doi.org/10.3929/ethz-a-010881404> →

Rights / License:

[In Copyright - Non-Commercial Use Permitted](#) →

This page was generated automatically upon download from the [ETH Zurich Research Collection](#). For more information please consult the [Terms of use](#).

DISS. ETH NO. 24108

*Design, modeling and optimization
of multi-column chromatographic processes*

A thesis submitted to attain the degree of
DOCTOR OF SCIENCES of ETH ZURICH
(Dr. sc. ETH Zurich)

presented by
Daniel Baur

MSc ETH in Chemical and Bioengineering

born on 04.04.1988
citizen of Zurich, Switzerland

accepted on the recommendation of
Prof. Dr. Massimo Morbidelli, examiner
Prof. Dr. Rudyanto Gunawan, co-examiner

2017

Acknowledgments

Here, at the end of my PhD work, I feel humbled and grateful for the opportunities and support that I was given over the years. This is not just my thesis; too many people have had a part in its creation to mention all of them, but I will certainly try.

First and foremost, my thanks go to Prof. Morbidelli, who has not only given me the opportunity to do my PhD thesis in his wonderful group, but who has accompanied and mentored me since my bachelor studies, keeping always the scientific picture but also my personal progress in mind. I immensely appreciate the opportunity to be a lecturer and teaching assistant for several years. Working with students was certainly the one of most exhilarating parts of being a PhD student. I would also like to express my gratitude to Prof. Gunawan, who has agreed to be the co-examiner for this thesis without hesitation.

It has always been a great pleasure and lots of fun working in Prof. Morbidelli's wonderful research group, and I want to thank each and every member for these joyful and productive years. Special mention goes of course to the chromatography sub-group, including Martin, who supervised my master thesis, Monica, Rushd, David, Fabian, and Nicole, for all the fruitful discussions and fun nights out both in Zurich and abroad. On this list of the “best generation” of master students, I certainly cannot leave out Lucrèce, the great dancer, and Baptiste and Eric, both great musicians and friends.

Being extraordinarily lucky, I was born in Zurich, home of this world-class university, so I never had to miss my friends and family. I cannot thank my family enough for supporting me through all these years of studies, I feel grateful beyond words. Thanks to my dear friends Philippe, James, Döme, Yves, and all the others for always being there for fun and drinks.

Playing the trombone, I had the pleasure of meeting and playing with many a musician over the years, too many to list them all. But a special thank you goes to Kantonsschule Oerlikon and Jugendmusik Zürich 11, where I learned most of my musical skills, as well as the Jazzarmonics Bigband and the 1-2 Bigband, where I still get to play wonderful music every week.

Last but not least I would like to thank my dearest Kirstyn, certainly the most important person I've met through my musical endeavors, for sticking with me through this final phase of my PhD, always caring, and motivating me to keep going.

Contents

	Page
Abstract	I
Kurzfassung	III
Symbols and abbreviations	V
List of figures	IX
List of tables	XII
1 Introduction	1
2 Isolation of α_1-antitrypsin from human blood plasma using multi-column counter-current solvent gradient purification	9
2.1 Introduction	9
2.2 Materials and methods	12
2.2.1 Starting material for α_1 -antitrypsin purification	12
2.2.2 Stationary phases and buffers	12
2.2.3 Analytics	13
2.2.4 Preparative chromatography runs	14
2.2.5 MCSGP process design	15
2.3 Results and discussion	16

2.3.1	Gradient batch operation and MCSGP design	16
2.3.2	Product analysis	18
2.3.3	MCSGP operation and comparison to batch	21
2.4	Concluding remarks	25

3 Optimal model-based design of the twin-column CaptureSMB process improves capacity utilization and productivity in protein A affinity capture 27

3.1	Introduction	27
3.2	Process descriptions	29
3.2.1	Batch chromatography with dual loading flow rate	30
3.2.2	CaptureSMB	32
3.3	Materials and Methods	33
3.3.1	Monoclonal antibody	33
3.3.2	Stationary phase and buffers	33
3.3.3	Preparative chromatography operating conditions	34
3.3.4	Analytics	34
3.4	Process model	35
3.4.1	Model equations with empirical mass transfer model	35
3.4.2	Fixed operating parameters	38
3.4.3	Process constraints for yield, purity and pressure drop	38
3.4.4	Process optimization	39
3.5	Results	42
3.5.1	Model fitting	42
3.5.2	Internal concentration profiles	48
3.5.3	Process optimization	48
3.5.4	Pareto optimal operating points and influence of column length	52
3.5.5	Concluding remarks	55

4	Comparison of batch and continuous multi-column protein A capture processes by optimal design	59
4.1	Introduction	59
4.2	Process descriptions	61
4.2.1	CaptureSMB	63
4.2.2	3-column PCC (3-C PCC)	64
4.2.3	4-column PCC (4-C PCC)	65
4.3	Materials and methods	66
4.3.1	Process model	66
4.3.2	Shrinking core adsorption model	67
4.3.3	Column model	69
4.3.4	Process performance measures and optimization problem . .	70
4.4	Results and discussion	73
4.4.1	Model fitting of batch protein A breakthrough curves	73
4.4.2	Operational parameters considered for optimization	76
4.4.3	Base case optimization results in productivity / capacity utilization trade-off for all processes	78
4.4.4	Influence of CIP time	82
4.4.5	Influence of feed concentration	82
4.4.6	Influence of recovery and regeneration scheduling in the 4-column PCC process	86
4.5	Concluding remarks	90
5	Optimization and comparison of batch and different MCSGP processes for ternary center-cut separations of proteins	93
5.1	Introduction	93
5.2	Process descriptions	96
5.2.1	Gradient batch chromatography	96

5.2.2	The MCSGP process	98
5.3	Materials and methods	102
5.4	Process models	102
5.4.1	Column and adsorption model	102
5.4.2	Process performance	104
5.4.3	Optimization problem	106
5.4.4	Principle component analysis for pareto-curves and stability analysis	106
5.5	Results and discussion	110
5.5.1	Model fitting	110
5.5.2	Purity-yield trade-off	110
5.5.3	Productivity-yield trade-off	112
5.5.4	Influence of operating parameters	116
5.5.5	Buffer consumption	128
5.5.6	Stability analysis	130
5.6	Concluding remarks	131
6	Conclusions and outlook	135
	Bibliography	151
	Curriculum Vitae	152
	List of publications	153
	Conference proceedings	154
	Poster proceedings	155

Abstract

Biopharmaceuticals, and among them, monoclonal antibodies (mAbs), have been the main growth sector in the market for pharmaceuticals in recent years. Chromatography plays a major role in product purification. Currently, most industrial chromatographic processes are run in batch mode. In this work, the application and optimization of multi-column chromatographic processes in the purification of biopharmaceuticals is explored.

First, the multi-column counter-current solvent gradient purification (MCSGP) process is applied for the isolation and purification of a human blood plasma protein. With the example target protein that was chosen, α_1 -antitrypsin (AAT), a purity/yield trade-off could be observed in batch chromatography. To overcome this limitation and reach high purity and high yield at the same time, a 2-column MCSGP process was designed and run into steady state. This proved the feasibility of using MCSGP to isolate and purify blood plasma proteins directly from human blood plasma.

Secondly, the focus was shifted to a recently developed multi-column capture process for monoclonal antibodies, the twin-column CaptureSMB process. In order to investigate how to design and optimize the CaptureSMB process, a model was developed that used batch breakthrough data to accurately predict CaptureSMB performance. Using this model, both the batch and the CaptureSMB processes were thoroughly optimized with regards to two objectives, productivity and capac-

ity utilization. The CaptureSMB process outperformed the batch process in each case and additionally, it was found that even at maximum capacity utilization, the mAb could be retained in only two columns, making a third column in the load train redundant. This notion was further scrutinized by modeling and optimizing several different multi-column processes with different numbers of columns, and comparing them against each other. Each of multi-column processes examined could achieve a capacity utilization close to 100%, dominating the batch process in all cases. The CaptureSMB process was optimal for maximizing the productivity at lower titers, but surprisingly, at high titers, the batch process was optimal for maximizing productivity (but at significant cost in terms of capacity utilization). Finally, the polishing step was more thoroughly examined, by modeling and optimizing a batch process and the 2- and 3-column MCSGP processes. In addition to the purity/yield trade-off, a yield/productivity trade-off arises when the load is increased with constrained purity. The MCSGP processes outperformed the batch process in these objectives, and among the MCSGP processes, the 2-column process performed better in all cases except at the lowest purity. At this purity level, the batch process could achieve the highest productivity among all three processes, albeit a significant loss of yield, and the 3-column process showed a slightly better trade-off.

Overall, it became clear that the optimal number of columns to use depends on the objective and the specifics of the separation problem. In general however, there is a step change in performance between one and two columns, and only marginal improvements when using more than two columns.

Kurzfassung

Biopharmazeutika, und vor allem monoklonale Antikörper (mAbs), waren in den letzten Jahren die grössten Wachstumsträger im Markt für Medikamente. Chromatographie spielt eine entscheidende Rolle in der Aufreinigung der Produkte. Die meisten chromatographischen Prozesse werden heutzutage im Batch-Modus gefahren. Diese Forschungsarbeit befasst sich mit der Anwendung und Optimierung von chromatographischen Mehrsäulenprozessen in der Produktion von Biopharmazeutika.

Zunächst wurde der multi-column counter-current solvent gradient purification (MCSGP) Prozess angewendet, um α_1 -Antitrypsin (AAT) aus menschlichem Blutplasma zu isolieren. Wie erwartet zeigte sich in der Batch-Chromatographie ein Zielkonflikt zwischen Reinheit und Ausbeute. Dieser Zielkonflikt konnte mithilfe des 2-Säulen MCSGP-Prozesses vermieden werden. Dies erlaubte es, hohe Reinheit und hohe Ausbeute gleichzeitig zu erreichen. Es konnte so beispielhaft gezeigt werden, dass der MCSGP-Prozess angewendet werden kann, um Proteine direkt aus menschlichem Blutplasma zu isolieren.

Als zweites rückte ein anderer kürzlich entwickelter Mehrsäulen-Prozess in den Fokus, nämlich der 2-Säulen CaptureSMB-Prozess. Batch-Durchbruchskurven wurden verwendet um ein Modell zu entwickeln, das die Effizienz eines CaptureSMB-Prozesses voraussagen konnte. Dieses wurde verwendet, um Batch und CaptureSMB zu optimieren, und zwar indem Produktivität und Säulenausnutzung ma-

ximiert wurden. Der CaptureSMB-Prozess dominierte den Batch-Prozess in jedem der untersuchten Fälle. Zusätzlich konnte gezeigt werden, dass das Produkt auch bei maximaler Säulenausnutzung in nur zwei Säulen zurückgehalten werden kann, was eine dritte Säule überflüssig macht. Um diese Vermutung weiter zu prüfen wurden mehrere Mehrsäulen-Prozesse, von denen jeder eine andere Anzahl Säulen verwendet, modelliert, optimiert und verglichen. Alle untersuchten Mehrsäulen-Prozesse konnten fast 100% Säulenausnutzung erreichen und damit den Batch-Prozess dominieren. Bei niedrigen Ladekonzentrationen war der CaptureSMB-Prozess optimal zur Maximierung der Produktivität, bei hohen Konzentrationen war aber überraschenderweise der Batch-Prozess optimal für maximale Produktivität, aber nur unter grossen Einbussen in der Säulenausnutzung.

Im letzten Teil wurde der MCSGP-Prozess genauer untersucht, indem Batch und ein 2- und 3-Säulen MCSGP-Prozess modelliert und optimiert wurden. Zusätzlich zum Zielkonflikt zwischen Reinheit und Ausbeute ergibt sich ein Zielkonflikt zwischen Ausbeute und Produktivität wenn die Beladung erhöht wird und die Reinheit einen bestimmten Wert nicht unterschreiten darf. Die MCSGP-Prozesse dominierten den Batch-Prozess, und der 2-Säulen Prozess zeigte die besseren Ergebnisse als der 3-Säulen Prozess, ausser bei niedrigen Reinheitswerten. Der Batch-Prozess konnte bei der niedrigsten untersuchten Reinheitsgrenze die höchste Produktivität erreichen, aber nur unter grossen Einbussen bei der Ausbeute.

Zusammenfassend konnte gezeigt werden, dass die optimale Anzahl Säulen davon abhängt, was optimiert werden soll und was separiert werden muss. Im Allgemeinen wurde aber klar, dass es zwischen Batch- und Zweisäulen-Chromatographie eine sprunghafte Verbesserung der Effizienz gibt, während das Verwenden von mehr als zwei Säulen nur punktuelle Verbesserungen bringt.

Symbols and abbreviations

Symbol	Units	Description
α		Fraction of sites occupied
α_i		Henry prefactor for component i
A		Intercept of the reduced van Deemter equation
A_{Col}	cm^2	Column cross-sectional area
AAT		α_1 -antitrypsin
AT3		Antithrombin-III
β		PLS regression coefficient
β_i		Henry power law exponent for component i
BC	mL mg^{-1}	Buffer consumption
c	mg mL^{-1}	Liquid phase concentration
c_0	mg mL^{-1}	Initial liquid phase concentration
c_{Feed}	mg mL^{-1}	Feed concentration
$c_{\text{Grad,S,E}}$	mg mL^{-1}	Modifier concentration at the gradient start or end
c_{In}	mg mL^{-1}	Concentration at the column inlet
c_{Out}	mg mL^{-1}	Product concentration
c_{P}	mg mL^{-1}	Intra-particle liquid phase concentration
c_{PEW}	mg mL^{-1}	Concentration in product elution window
CIP		Cleaning-in-place
CSMB		CaptureSMB
CU	%	Capacity utilization
CU_{Batch}	%	Capacity utilization of the batch process
CU_{CMSB}	%	Capacity utilization of the CaptureSMB process
CV	mL	Column volume
CV		Charge variant
∂		Partial derivative
ΔP	bar	Pressure drop
D	cm min^{-1}	Pore diffusion fitting parameter
D_0	$\text{cm}^2 \text{min}^{-1}$	Free diffusion coefficient

D_E	$\text{cm}^2 \text{ min}^{-1}$	Effective pore diffusion coefficient
D_L	$\text{cm}^2 \text{ min}^{-1}$	Apparent axial dispersion coefficient
DNA		Deoxyribonucleic acid
d_P	cm	Particle diameter
DR_{PS}		Dilution ratio during product/strong recycle
DR_{WP}		Dilution ratio during weak/product recycle
ϵ		Porosity
ϵ_B		Bed porosity
ϵ_P		Particle porosity
ϕ		Phase ratio
ϕ_P		Particle phase ratio
γ	bar min cm^{-2}	Pressure drop coefficient
GDE3		Generalized differential evolution v3
H		Henry coefficient
H_{Ref}		Henry coefficient at reference conditions
HETP		Height equivalent to a theoretical plate
HPLC		High performance liquid chromatography
HSA		Human serum albumin
IC		Interconnected
IgG		Immunoglobulin G
$k_{A,1,2}$	$\text{mL mg}^{-1} \text{ min}^{-1}$	Adsorption rate constant for site 1 or 2
K_D	mL mg^{-1}	Adsorption equilibrium constant
k_F	cm min^{-1}	Film mass transfer coefficient
k_m	min^{-1}	Mass transfer coefficient
k_m^{max}	min^{-1}	Maximum mass transfer coefficient
k_S	cm min^{-1}	Mass transfer coefficient in the solid phase
k_{tot}	cm min^{-1}	Total mass transfer coefficient
L	cm	Total length
L_{Col}	cm	Column length
LC		Liquid chromatography
mAb		Monoclonal antibody
MCSGP		Multicolumn counter-current solvent gradient purification
mod		Modifier
MS		Mass spectrometry
MW	kDa	Molecular weight
N		Henry coefficient power law exponent
n_{Col}		Number of columns
N_{CV}		Number of charge variants
N_{RR}		Number of columns in recovery and regeneration

P		Product
P_{Batch}	mg mL ⁻¹ h ⁻¹	Productivity of the batch process
P_{CSMB}	mg mL ⁻¹ h ⁻¹	Productivity of the CaptureSMB process
P_{Target}	mg mL ⁻¹ h ⁻¹	Target productivity
PCA		Principle component analysis
PCC		Periodic counter-current chromatography
PEG		Polyethylene glycol
PEW		Product elution window
pH _{Ref}		Reference pH value
PLS		Partial least squares
Pr	mg mL ⁻¹ h ⁻¹	Productivity
Pu	%	Product purity
Pu_{Target}	%	Target purity
q	mg mL ⁻¹	Solid phase concentration
$q_{1,2}$	mg mL ⁻¹	Adsorbed concentration on site 1 or 2
q^*	mg mL ⁻¹	Equilibrium solid phase concentration
q_{Feed}^*	mg mL ⁻¹	Equilibrium concentration at feed liquid concentration
q_0	mg mL ⁻¹	Initial solid phase concentration
q_{sat}	mg mL ⁻¹	Saturation capacity
Q	mL min ⁻¹	Flow rate
$Q_{1,2,3}$	mL min ⁻¹	Pump flow rates in zones 1, 2 and 3
Q_{B}	mL min ⁻¹	Batch loading flow rate
Q_{dil}	mL min ⁻¹	Flow rate of the dilution pump
Q_{Feed}	mL min ⁻¹	Feed flow rate
Q_{Grad}	mL min ⁻¹	Flow rate during gradient
Q_{IC}	mL min ⁻¹	Interconnected loading flow rate
Q_{L}	mL min ⁻¹	Loading flow rate
Q_{max}	mL min ⁻¹	Maximum flow rate
Q_{out}	mL min ⁻¹	Flow rate out of a column
Q_{PEW}	mL min ⁻¹	Flow rate during product elution window
Q_{PL}	mL min ⁻¹	Preload flow rate
$Q_{\text{P/S}}$	mL min ⁻¹	Flow rate during product/strong recycle
Q_{RR}	mL min ⁻¹	Flow rate during recovery and regeneration
$Q_{\text{W/P}}$	mL min ⁻¹	Flow rate during weak/product recycle
R	cm	Radial coordinate
r_{P}	cm	Particle radius
σ	%	PCA variance explained per component
S		Strongly adsorbing impurities
S_1		Maximum hindrance parameter

S_2		Nonlinearity parameter
SDS-PAGE		Sodium dodecyl sulphate polyacrylamide gel electrophoresis
SEC		Size exclusion chromatography
SMB		Simulated moving bed
SMCC		Sequential multi-column chromatography
t	min	Time
t_B	min	Batch time
t_{CIP}	min	Time for cleaning-in-place
t_{Cycle}	min	Cycle time
t_{Elu}	min	Elution time
t_{Equil}	min	Equilibration time
t_{IC}	min	Interconnected time
t_L	min	Loading time
t_{PL}	min	Preloading time
t_{RR}	min	Time for recovery and regeneration
t_{Switch}	min	Switching time
t_W	min	Washing time
TRIS		Tris(hydroxymethyl)aminomethane
u	cm h ⁻¹	Superficial velocity
UV		Ultraviolet
v	cm h ⁻¹	Interstitial velocity
V	mL	Elution volume
V_{Buffer}	mL	Buffer volume used per switch
V_{Col}	mL	Column volume
V_{Feed}	mL	Feed volume
V_{Grad}	mL	Gradient length
V_{PEW}	mL	Duration of the product elution window
$V_{PEW,S,E}$	mL	Start or end position of product elution window
$V_{P/S}$	mL	Duration of product/strong recycle
V_{RR}	mL	Volume used in recovery and regeneration
V_W	mL	Duration of weak elution
$V_{W/P}$	mL	Duration of weak/product recycle
VIP		Variable importance in projection
W		Weakly adsorbing impurities
x	cm	Longitudinal coordinate
x	Various	Process degrees of freedom
Y	%	Yield

List of Figures

2.1	Schematic center-cut separation.	15
2.2	Twin-column MCSGP process schematic.	17
2.3	Design batch with fraction analysis.	18
2.4	LC/MS/MS analysis of MCSGP product and commercial standard.	20
2.5	SDS-PAGE analysis of design batch fractions.	22
2.6	Overlay of the UV-profiles recorded in the MCSGP process.	23
2.7	Change of yield and purity over the course of the MCSGP process.	24
2.8	Pareto-optimal batch pooling strategies and MCSGP operating point.	25
3.1	Process flow charts for batch capture and CaptureSMB.	31
3.2	Breakthrough curves used to fit the power law mass transfer model.	44
3.3	Experimental UV profiles compared to simulation data.	45
3.4	Internal concentration profile of the CaptureSMB process.	50
3.5	Pareto-optimal operating points for the batch process and the Cap- tureSMB process.	54
3.6	Change of operating parameters along the pareto front for the Cap- tureSMB process.	57
4.1	Process flow charts for the multi-column processes.	62
4.2	Shrinking core principle.	67
4.3	Breakthrough curves used to fit the shrinking core model.	75
4.4	Isotherm used in the shrinking core model.	76

4.5	Pareto-fronts for the base case.	80
4.6	Yield loss when increasing productivity.	81
4.7	Influence of CIP time and feed concentration.	83
4.8	Influence of interconnected wash.	86
4.9	Optimal scheduling for the 4-column PCC process.	88
4.10	Base case pareto curves for the 4-C PCC process with optimal scheduling.	89
4.11	High titer pareto curves for the 4-C PCC process with optimal scheduling.	89
5.1	Schematic center-cut batch process with degrees of freedom.	97
5.2	Two column MCSGP process schematic with degrees of freedom.	99
5.3	Three column MCSGP process schematic with degrees of freedom.	101
5.4	Model simulation and experimental UV data for a batch elution.	110
5.5	Purity-yield pareto fronts for the batch and MCSGP processes.	113
5.6	Productivity-yield pareto fronts for the batch and MCSGP pro- cesses, grouped by process.	114
5.7	Productivity-yield pareto fronts for the batch and MCSGP pro- cesses, grouped by purity level.	115
5.8	PCA analysis of the productivity-yield pareto front for the batch process.	118
5.9	PLS regression results for productivity for the batch process.	120
5.10	PCA analysis of the productivity-yield pareto front for the 2-column process.	122
5.11	PLS regression results for productivity for the batch process.	124
5.12	PCA analysis of the productivity-yield pareto front for the 2-column process.	126
5.13	PLS regression results for productivity for the batch process.	127

5.14 Buffer consumption as a function of yield for all processes and all three purity levels.	129
--	-----

List of Tables

3.1	Fitted parameters for the power law mass transfer model.	43
3.2	Operating conditions for the different CaptureSMB runs used to compare the model to the experimental data.	43
3.3	Comparison of model predictions with experimental data for the performance of the CaptureSMB process in different conditions. . .	49
3.4	Summary of optimized operating points (single objective) with op- erating parameters.	53
4.1	Fitted parameters for the shrinking core model.	77
4.2	Operational parameters considered in the optimization.	78
4.3	Optimum process choice depending on feed titer and desired per- formance objective.	87
5.1	Fixed parameters for the charge variant separation.	107
5.2	Fitted parameters for the charge variant separation.	111
5.3	Stability analysis of the batch, 2- and 3-column MCSGP processes.	130

Chapter 1

Introduction

For most of history, all pharmaceutically active substances could either be isolated directly from nature (e.g. herbal extracts), or, in the case of small molecules, chemically synthesized. Over the past decades, biopharmaceuticals have been the fastest growing market in pharmaceuticals overall, however biopharmaceuticals are usually too large and too structurally complex to allow direct chemical synthesis in any cost effective fashion [1–3]. Therefore, the only option to produce biopharmaceuticals is *in vivo*. While some peptides, for example hormones like insulin or human growth hormone [4, 5], are important, recently the main focus of research and development lay on therapeutic proteins [6]. For applications in humans, the proteins are either isolated directly from healthy human biological samples, or produced recombinantly in genetically modified cell lines [7]. The most important source of human therapeutic proteins is human blood plasma, while the most important artificial proteins are monoclonal antibodies (mAbs), Fc fusion proteins and other recombinant proteins. In both cases, similar challenges arise in the isolation and purification of the target protein: The product is embedded in a extremely complex matrix of impurities numbering in the thousands, many of which are very similar to the product [8].

The first large scale isolation of a protein from human blood plasma was implemented in the Cohn process during the second world war, with the goal of isolating the most abundant plasma protein albumin, to be used as substitute for whole plasma transfusions [9]. The Cohn process, just as analogs developed later, such as the Kistler and Nitschmann process [10], is based on successive addition of increasing amounts of ethanol to single donor or pooled human blood plasma at low temperatures, which causes different fractions of proteins to precipitate. Human albumin is at the end of this fractionation cascade and constitutes the main product of the original Cohn process. The remaining supernatant and all of the other fraction however also contain valuable proteins that have potential therapeutic applications, for example in treating genetic disorders, trauma and illness. Two different application modes exist, since the protein can either have a direct therapeutic effect, such as stimulating blood coagulation, or the protein can be used as a replacement in case of deficiencies. When recombinant products are unavailable or cause too strong an immunological reaction, proteins isolated directly from human blood plasma are the only alternative [11,12]. Many different plasma products are available nowadays, such as blood coagulation factors (factors IV, V, VII, VIII, IX) [13–17], proteases and their antagonists (such as thrombin and antithrombin-III, or trypsin and α_1 -antitrypsin) [18, 19], or proteins related to the immune-system (for example immunoglobulins) [20,21]. The Cohn process with its different fraction still remains the backbone of most plasma fractionation plants, but it is of great interest to isolate as many proteins as possible from the side-streams of the Cohn process. Many different techniques have been explored to this end, including cryoprecipitation [11] and PEG-precipitation [22], but chromatography is the most versatile and powerful separation technique to resolve such difficult mixtures [23].

In the isolation and purification of human plasma proteins, both affinity and

non-affinity chromatography play a role, however the application of affinity chromatography is limited to custom-tailored antibodies specific to a target protein immobilized on a solid phase, which is both expensive (due to ligand development costs) and inefficient (due to stability issues and re-usability). The protein heparin is worth mentioning as an exceptional affinity ligand, because it is relatively cheap to produce and can be polymerized for additional ligand stability. Heparin specifically and strongly binds several major human plasma proteins, for example antithrombin-III and factor IX, which are usually extracted from Cohn fraction I, and the von Willebrand factor which can be purified from the cryoprecipitate, which is the fraction of proteins that are insoluble in untreated human plasma at 4°C [24–26]. Non-affinity chromatography is therefore used to purify most human blood plasma proteins, most notably ion-exchange and in some cases size exclusion chromatography. A separation problem involving such a complex mixture as human blood plasma or its fraction will most likely involve a center-cut separation, where some impurities elute before the desired product, while other impurities elute after the product. If the different components are not base-line separated, this leads to a trade-off situation in standard batch chromatography: one can either collect a narrow, highly pure fraction, while discarding overlapping regions and thus compromising yield, or collect more of the product, which means more impurities are pooled with the product and purity is lower. Multi-column chromatography can be used to alleviate this trade-off.

The first multi-column setup to be widely used is the simulated moving bed (SMB) process, which separates two overlapping species with high yield and high purity, while increasing productivity compared to batch [27–30]. While it is possible to use two SMB systems in series to achieve a ternary separation [31,32], as is needed here, sufficient separation can usually only be achieved by gradient chromatography, which is a feature that is not available in SMB systems. In order to achieve

high yield and high purity with gradient chromatography, the multi-column solvent gradient purification (MCSGP) process was developed [33]. Chapter 2 explores the application of MCSGP to plasma fractionation, and gives a first empirical approach on how to design an MCSGP process from a batch separation. As an example target protein, α_1 -antitrypsin (AAT) was chosen, due to its therapeutic applications and due to its relative abundance in human blood plasma. While AAT is industrially purified from Cohn fraction IV precipitate [11], the MCSGP process was applied directly to delipidated, cryopoor plasma, to further prove its capabilities.

With the discovery of how to create and cultivate from a single cell a continuous culture of hybridoma cells, which secrete a specific antibody [34], and major developments in genetic engineering and microbiology, became possible to produce monoclonal antibodies (mAbs) as biopharmaceuticals. The most commonly used therapeutic monoclonal antibodies are of the immunoglobulin gamma (IgG) type, a 144 kDa protein that mediates immune-response, among other functions. A wide range of diseases and conditions can be addressed using mAbs, but the most common targets are autoimmune disorders and cancer cells [35]. Other areas of application include neovascular (eye) disorders, infectious diseases, hemostasis, and transplant/implant rejection [36]. While there are different types of mAbs, namely fully human antibodies, chimeric antibodies, and humanized or recombinant antibodies, we will only focus on the latter in this work. The production process for mAbs is operationally split into two major parts: the upstream part, where the cell line is cultivated and the antibody itself is produced; and the downstream part, where the antibody is isolated from the cells and the other constituents of the cell growth medium, further purified (and in some cases modified), and put into a formulation. In most of the current industry production, these are all batch-wise processes akin to unit operations [37]. In this work, we will focus on improvements

in the downstream part.

The first goal of downstream processing is to isolate the mAb from the cell culture supernatant, which still contains other extracellular proteins, cell debris, growth media components, etc. [8]. The most widely used method to achieve this separation is by protein A affinity chromatography. Protein A is a surface protein found in *staphylococcus aureus* which strongly and specifically binds to the constant region of antibodies especially of the IgG-type [38]. In nature, this is a survival technique because it screens the bacterium from the immune response by binding antibodies in the wrong orientation. In mAb production, protein A immobilized on a chromatographic resin can be used to specifically retain mAbs and capture them from the cell culture supernatant [39]. After several wash steps to remove any weakly bound or unbound components, such as host cell proteins or DNA, a step change in pH is then used to elute the antibody. After the chromatographic column is regenerated, it can be used for another bind and elute cycle [40]. Over time, the chromatographic resin will deteriorate, resulting in lower binding capacity and possible product losses. After a few hundred cycles, the resin must be replaced, which, due to protein A resin being relatively expensive, constitutes the largest cost factor in downstream processing. Typically, protein A columns can only be loaded to around 30 to 50% of their maximum binding capacity, because at higher loads, product would be lost in the breakthrough. This means that much of the resin remains unused, leading to a production cost increase [41,42].

A straight forward solution would be to capture the mAb that is breaking through in a second column. This very simple principle is the basis of a novel multi-column chromatographic capture process, the CaptureSMB or 2-column periodic countercurrent chromatography (2C-PCC) process [43]. Simple, empirical design rules to arrive at a feasible CaptureSMB process from batch breakthrough experiments have been previously developed [43,44]. In chapter 3, we explore the

possibilities and capabilities of the process in more detail, focusing on the trade-off situation between productivity and capacity utilization. Increasing productivity means more product can be processed per unit time on given equipment, therefore saving on process time, while increasing capacity utilization means that more mAb can be produced before the resin must be replaced, therefore reducing resin costs. Optimizing a multi-column process is not a straight forward task, since it reaches a cyclic steady state that cannot be easily predicted due to the internal recycle streams. Therefore, batch capture and the CaptureSMB process were modeled using an empirical mass transfer model, and the resulting model was used in multi-objective constrained optimization, using a modified version of the third iteration of the generalized differential evolution (GDE3) algorithm, to thoroughly and globally optimize both processes *in silico* [45]. This allows a comparison in terms of process performance between batch and two-column capture.

The CaptureSMB process is not the only multi-column process used for the capture of mAbs from cell culture supernatant with protein A affinity chromatography. Several other processes have been proposed and implemented, such as the periodic counter-current chromatography (PCC) process, which uses 3 or 4 columns [46,47], the sequential multi-column chromatography (SMCC) process, which utilizes a variable number of columns [48, 49], or the BioSMB process, which uses up to 12 columns [50]. However, it is not immediately obvious if using more columns yields any benefit. The capital cost obviously increases more or less linearly with the number of columns, since using additional columns incurs the need for additional pumps, valves, detectors, capillaries, etc. The influence on process performance, and therefore running costs, is more difficult to determine on the other hand. Thus, in chapter 4, different multi-column protein A capture processes and batch capture are modeled, optimized using multi-objective constrained optimization, and compared in terms of process performance.

In chapter 2 an empirical approach is described which allows to design an MCSGP process from a batch separation. As with any short-cut method, it is less than likely that this will yield an optimal process, especially if the process contains as many degrees of freedom as the MCSGP process. In the last chapter 5, a lumped kinetic model is used to simulate the separation of mAb charge-variants on an ion-exchange column. Using this model, three processes are optimized: A standard batch separation, and the 2- and 3-column MCSGP processes [51, 52]. Optimization is carried out with respect to purity and yield on the one hand, and with respect to yield and productivity, with constrained purity, on the other hand. The three processes are compared against each other, and principle component analysis (PCA) as well as partial least squares (PLS) regression are then used to identify which process variables are most important to assure optimal and stable operation of each process.

Chapter 2

Isolation of α_1 -antitrypsin from human blood plasma using multi-column counter-current solvent gradient purification

2.1 Introduction

Proteins isolated from human blood plasma have a great many therapeutic applications in treating diseases and conditions caused for example by genetic disorders, trauma or illness. Compared to the alternative of using recombinant proteins, applying human proteins is in most cases more economic and sometimes the only viable alternative, either due to the lack of suitable recombinant products or due to the immunological reactions these products can elicit [11,12].

Ever since its development during the second world war, the Cohn process, and later the alternative Kistler and Nitschmann process, have been the backbone of human blood plasma fractionation [9,10]. While the original Cohn process was

envisioned mainly in order to purify albumin, the most abundant plasma protein, to be used as a more efficient alternative to whole blood or plasma transfusions, a wide range of other products have since been isolated from plasma or side streams of the fractionation cascade. Examples include blood coagulation factors (factors IV, V, VII, VIII, IX) [13–17], proteins related to the immune-system (such as immunoglobulin gamma or immunoglobulin M) [20, 21], or protease inhibitors (e.g. antithrombin III or α_1 -antitrypsin) [18, 19]. New products are being continuously added to this list as new therapeutic uses are identified or as their separation becomes more cost-effective [11].

While the main method of separation in the Cohn process is sequential precipitation induced by adding increasing amounts of ethanol to fresh plasma at low temperatures, other separation techniques have become increasingly important, both for further purifying Cohn-fraction precipitates and as replacement for ethanol-precipitation. Applications include cryoprecipitation [11], PEG-precipitation [22], and, most prominently, chromatography for side-stream purification [23]. Both affinity [26, 53, 54] and non-affinity chromatography [55, 56] play a major role in capturing different proteins from plasma or Cohn-fractionation side streams. In most cases, an efficient affinity ligand like protein A in the case of monoclonal antibodies is not available for plasma proteins, therefore the only option for affinity chromatography is to immobilize custom-made antibodies targeting the desired protein, which is inefficient both economically as well as from a process perspective. A noted exception is the interaction of some proteins with heparin, which can be readily immobilized on chromatographic materials. The major products of heparin affinity chromatography include antithrombin-III, factor IX, and the von Willebrand factor, which are usually purified from Cohn fraction 1 (antithrombin-III and factor IX) and the cryoprecipitate (von Willebrand factor) [24–26].

On the non-affinity side, both ion-exchange chromatography and in some cases size

exclusion chromatography are widely used to achieve the desired purity and recovery. In the case of ion-exchange chromatography, it is preferable to use gradient chromatography improve resolution due to the large number of components (human blood plasma contains several thousand different proteins), and their chemical and biological similarity [57,58].

With such a complex mixture as human blood plasma or fractions thereof, it is expected that a center-cut separation must be performed with impurities eluting both before and after the desired product. Whenever this kind of pooling strategy is required, standard batch chromatography runs into a purity-yield trade-off: either only a very narrow, very pure fraction is collected, resulting in high purity but low yield, or a broader collection window is chosen, resulting in lower purity due to coeluting impurities, but better yield. When manufacturing proteins for therapeutic applications, high purity is a basic requirement, therefore yield is usually compromised, potentially wasting valuable raw material. To break out of such trade-off situations, multi-column counter-current chromatography has been used in many other manufacturing process, starting with the simulated moving bed (SMB) technology for isocratic binary separations of small molecules [27–30]. If a ternary (i.e. center-cut) separation is required, either two SMB processes must be run sequentially [31,32], or a different process must be used. The most important alternative is the multi-column counter-current solvent gradient purification (MCSGP) process, which is based on the principle that overlapping regions of the chromatogram are recycled [33]. Different versions of the MCSGP process exist, using between 2 and 8 columns [51,52,59,60]. In this work, the most recent and arguably simplest variant, the twin column MCSGP process is used to isolate a protein from human blood plasma with both high purity and high yield. As an example target protein, α_1 -antitrypsin (AAT) is chosen, because it has many therapeutic applications, it is relatively abundant in human blood plasma and because

current processes recovering the protein from a Cohn-process side-stream typically have rather poor yield [11]. However, since MCSGP can increase the yield of any center-cut batch separation which achieves the desired purity, any protein for which a batch separation can be designed could potentially be targeted with MCSGP.

2.2 Materials and methods

2.2.1 Starting material for α_1 -antitrypsin purification

The starting material for the purification of α_1 -antitrypsin (AAT) was fresh frozen single donor human blood plasma from whole blood containing citrate phosphate dextrose as anticoagulant, obtained from Interregionale Blutspende SRK AG (Bern, Switzerland). The fresh frozen plasma was thawed at 4 °C, centrifuged for 20 minutes with 3000 x g at 4 °C and decanted to obtain cryosupernatant. In order to remove lipids and lipoproteins, which could damage the chromatographic resins by irreversible adsorption, 80 g L⁻¹ of lipid removal agent (Supelco, Bellefonte, PA, USA) was added to the cryosupernatant. After shaking for 3 hours at 4 °C, the suspension was centrifuged for 20 minutes with 3000 x g at 4 °C, decanted and filtrated with 0.2 μ m cut-off sterile Filtermax vacuum filters (TPP, Trasadingen, Switzerland). One part of the filtrate was diluted with five parts of millipore water to reduce the conductivity to below 3 mS cm⁻¹ and the pH was adjusted to 6.0 to ensure binding in the preparative capture step.

2.2.2 Stationary phases and buffers

For the chromatographic capture step, which was run in bind and elute mode, the fractogel EMD DEAE (M) (Atoll, Weingarten, Germany) resin was used,

prepacked in 5 mm i.d. x 50 mm bed height columns. The binding and equilibration buffer (A) was 40 mM acetate at pH 6.0, the gradient and elution buffer (B) was 40 mM acetate and 400 mM NaCl at pH 6.0. Cleaning-in-place was performed using 0.5 M NaOH with a contact time of 15 minutes. For the design batch, one column was used, while for MCSGP capture, two identical columns were used. Unless otherwise stated, the reagents used for buffer preparation were obtained from Sigma-Aldrich (St. Louis, MO, USA). The pH value of all buffers was adjusted using acetic acid, HCl or NaOH respectively. Prior to use, all buffers were filtered using 0.2 μ m cut-off sterile Filtermax vacuum filters (TPP, Trasadingen, Switzerland).

2.2.3 Analytics

The concentration of AAT was estimated using analytical anion exchange chromatography. The stationary phase was Tosoh TSKgel Q-Stat with an average particle size of 7 μ m, measuring 4.6 mm i.d. x 100 mm bed height (Tosoh, Tokyo, Japan). The buffers used were 25 mM TRIS-HCl at pH 8.5 as equilibration buffer (A) and 25 mM TRIS-HCl with 1 M NaCl at pH 8.5 as gradient and elution buffer (B). The elution was carried out at 1 mL min⁻¹, with a gradient from 0 to 50 % B in 10 minutes. Since human plasma is a very complicated mixture, this analytical procedure only gives a rough estimate of purity and yield, but can be used to compare the batch and MCSGP processes.

Product purity and quality was further evaluated using size exclusion chromatography (SEC) and sodium dodecyl sulphate polyacrylamide gel electrophoresis (SDS-PAGE). SEC chromatography was performed with a TSKgel G3000SWXL column (7.8 mm i.d. x 300 mm length; Tosoh, Tokyo, Japan) and 100 mM Na₂SO₄, 25 mM Na₂HPO₄, 0.5 g L⁻¹ NaN₃, pH 7.0 as mobile phase, at a flow rate of 1 mL min⁻¹ and UV detection at 280nm. All analytical chromatography runs were carried out

on Agilent 1100 HPLC equipment at a temperature of 25 °C and evaluated using the Agilent ChemStation software (Santa Clara, CA, USA).

SDS-PAGE was performed under reduced conditions using NuPAGE® Bis-Tris Pre-Cast gels, Novex® MES SDS running buffer and the XCell SureLock® Mini-Cell from Life Technologies (Carlsbad, CA, USA). Gels were run at a constant voltage of 200 V for 35 min. Staining was performed using the SimplyBlue SafeStain Coomassie Blue staining kit from Life Technologies (Carlsbad, CA, USA). Protein identification was performed using the molecular weight (MW) marker Precision Plus Protein™ from Bio-Rad (Hercules, CA, USA) and an AAT standard solution from Sigma-Aldrich (St. Louis, MO, USA). Furthermore, unknown protein bands appearing in the SDS-PAGE were identified by LC/MS/MS at the Functional Genomics Center Zurich (FGCZ, Zurich, Switzerland).

2.2.4 Preparative chromatography runs

All preparative experiments (both in batch and MCSGP mode) were performed at 25 °C on the Contichrom Lab-10 laboratory scale equipment using the ChromIQ software package (ChromaCon AG, Zurich, Switzerland). The UV absorption at a wavelength of 280 nm was observed at each column outlet, and the pH and conductivity were measured in the product collection outlet.

The appropriate loading, washing, gradient elution and regeneration procedures for the capture step were determined in batch mode. For the design batch, fractions of 1.0 mL volume were collected during the gradient elutions and analyzed as described above. Acceptable separation performance could be achieved with the following conditions: 5 column volumes (CV) equilibration with buffer A, loading of 40 mL delipidized diluted cryosupernatant at pH 6.0 (which results in a loading of about 50 mg AAT per mL resin), gradient elution of 5 –75% B in 30 minutes, 15 minutes CIP with 0.5 M NaOH, 5 CV re-equilibration. All steps were performed

at flow rate of 1.0 mL min^{-1} , resulting in a linear velocity of 300 cm h^{-1} , except the CIP step, where the flow rate was halved. From the resulting design batch, an MCSGP process can be designed.

2.2.5 MCSGP process design

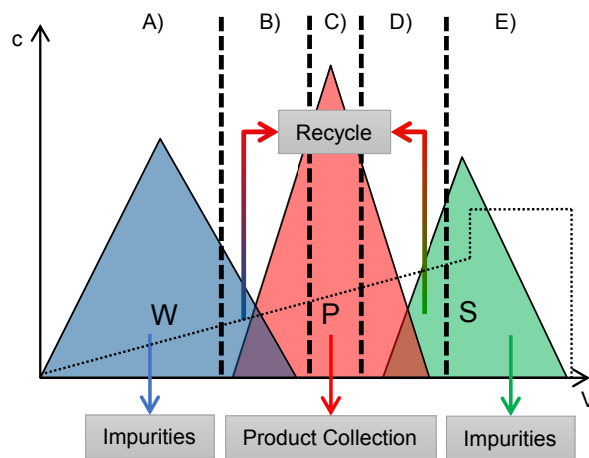


Figure 2.1: Schematic representation of a batch center-cut separation with modifier gradient. In step A), weakly adsorbing impurities (W, blue) elute, then pure product can be collected in step C) (P, red), and last the strongly adsorbing impurities (W, green) elute. After that, the column can be stripped, CIPed and re-equilibrated (step E)). If high yield and high purity are desired, the overlapping regions (B) and D)) must be recycled.

Figure 2.1 shows a schematic center-cut batch separation, with weakly adsorbing impurities (W) eluting before the product (P), and strongly adsorbing impurities (S) eluting after the product. If both high yield and high purity should be achieved, it is easy to see what tasks must be performed in each part of the chromatogram: A) Elute W; B) Recycle the overlapping regions of W and P; C) Elute and collect pure product P; D) Recycle the overlapping regions of P and S; E) Elute S, Strip, CIP and re-equilibrate the column. In the MCSGP process,

these tasks are carried out alternately by two columns, as can be seen in Figure 2.2. The first column follows exactly the steps described before, while the second column takes up the recycle streams and new feed. The design is now straight forward; each change in configuration of columns corresponds to a point in the chromatogram, at a certain elution volume and gradient position. Under the condition that the gradient progress per elution volume is kept the same as in the design batch, the corresponding times, flow rates and gradient concentrations can be calculated. To ensure that the recycled streams adsorb on the second column, an in-line dilution must take place to reduce the ionic strength of the recycled stream. The W/P stream is diluted to reach the same ionic strength as at the beginning of the W/P recycle to ensure W elutes and P adsorbs, and the P/S stream is diluted to reach the same ionic strength as at the beginning of the gradient, to ensure that all P adsorbs. An accelerated startup was performed, where in the first switch, the load volume is equal to the load volume in the design batch. In the subsequent switches, the load volume is reduced to replace the product that is withdrawn from the product stream. This assures that a cyclic steady state is reached as quickly as possible. A more detailed discussion of the design procedures is available in [51, 61, 62], as well as in chapter 5.

2.3 Results and discussion

2.3.1 Gradient batch operation and MCSGP design

Using the elution conditions described above, a design batch chromatogram could be obtained, which is shown in Figure 2.3 along with fraction analysis. As can be seen, most of the main contaminant albumin does not adsorb and is eluted as flow through, along with immunoglobulin G (not shown). From the design batch, using the method described above, an MCSGP process was laid out, separating the

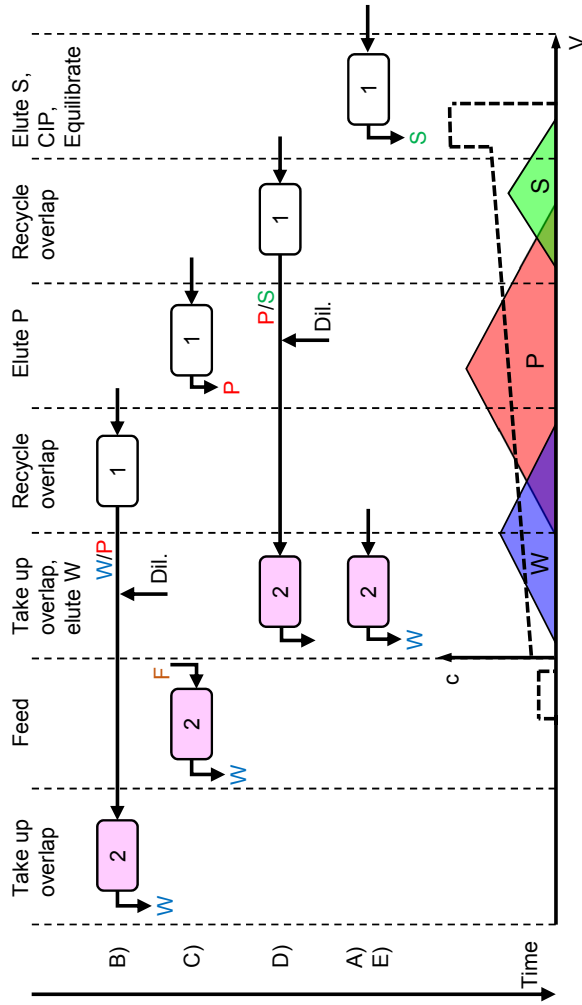


Figure 2.2: Twin-column MCSGP process schematic. In the lower part, a typical center-cut separation task is shown with weakly adsorbing impurities (W) eluting before the product (P) and strongly adsorbing impurities (S) after. The tasks in the chromatogram (elute W, recycle overlap, elute P, recycle overlap, elute S, CIP, equilibrate) can be distributed to the two columns (top part). One switch of the process is shown; after the columns have completed the tasks shown, the two columns swap places and tasks. After another switch, the columns swap back and return to the initial configuration; a whole cycle has passed. Fresh feed (F) is applied to column 2 during product elution in column 1.

region of highest purity at around 12 mL elution volume. An accelerated startup procedure is included in the design, where in the very first switch, the same volume as in the design batch is loaded. After this startup switch, the loading volume is reduced to only load back the product that is withdrawn in the product stream. This allows the process to reach a cyclic steady state much more quickly.

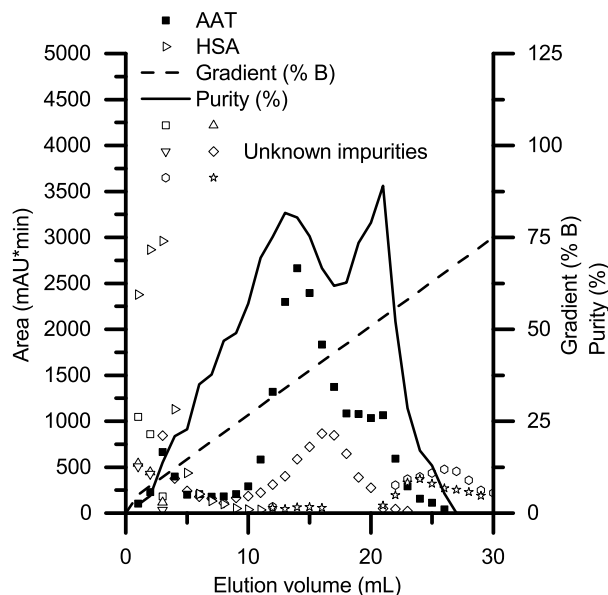


Figure 2.3: Design batch with fraction analysis. The areas reported on the left y axis refer to the integrated peak areas from analytical chromatography. The filled symbols show the AAT content of each fraction, while the empty symbols denote various impurities.

2.3.2 Product analysis

As expected from the fraction analysis of the design batch, there are several components that are co-eluting with AAT. Most of the major impurities have been removed in the MCSGP step, but some very closely related impurities remain. In order to help identify these impurities, SDS-PAGE was performed. The resulting gels are shown in Figure 2.5. The unknown bands in the MCSGP product fraction (lane 17) and the commercial AAT standard (lane 20) were subsequently

identified by LC/MS/MS analysis, see Figure 2.4. From large to small, the bands in the MCSGP product contained: α_2 -macroglobulin (163 kDa) in the first two bands; human albumin (69 kDa) in the third major band; antithromin-III (53 kDa), α_1 -antichymotrypsin (48 kDa), and AAT (47 kDa) in the fourth band; and α_1 -acid glycoprotein (24 kDa), and haptoglobin (45 kDa) and fragments thereof in the remainder of the bands. The bands in the commercial standard contained: human albumin in the first band; antithromin-III, α_1 -antichymotrypsin, and AAT in the second band; and α_1 -acid glycoprotein in the third band. Therefore, apart from α_2 -macroglobulin and haptoglobin, the same impurities were found in the commercially available standard sample as in the MCSGP product. An orthogonal polishing step could be used to remove the remaining impurities and reach the same purity as the commercial standard.

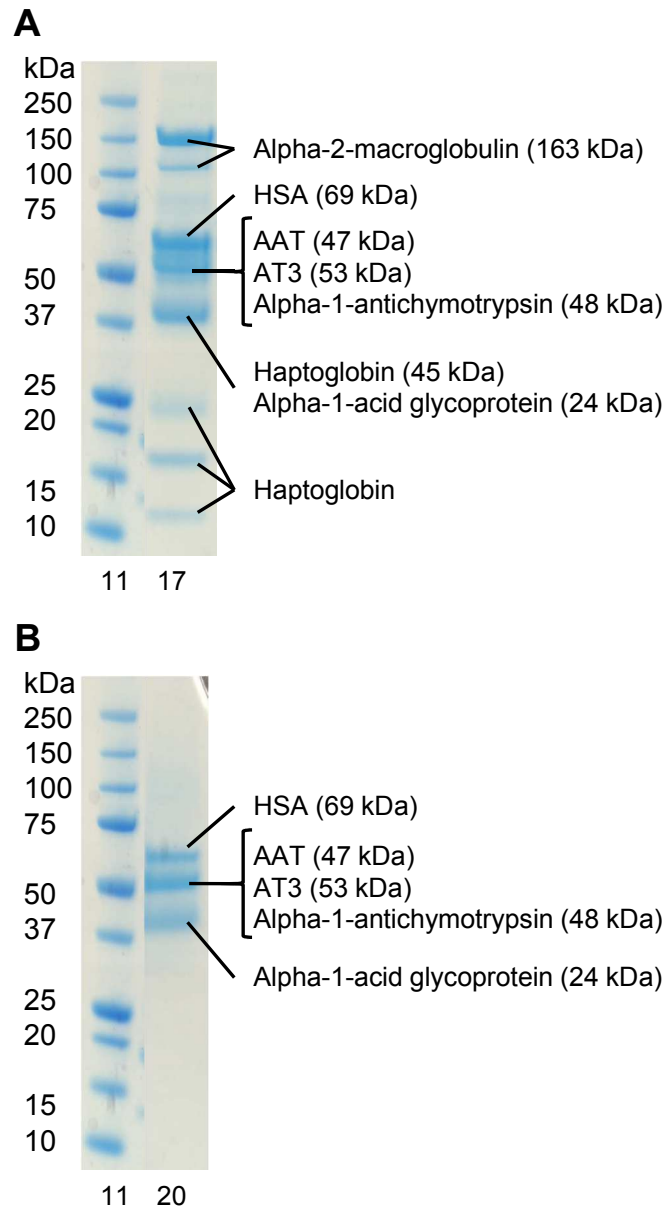


Figure 2.4: LC/MS/MS protein identification of MCSGP product (A) and commercial standard (B), which were in lanes 17 and 20, respectively. Also shown is lane 11 (size standard).

2.3.3 MCSGP operation and comparison to batch

Figure 2.6 shows the UV-profiles from the MCSGP run in an overlay, and shifted to account for the difference of one switch between the two UV detectors. In the first part of the cycle, the gradient elution takes place: first the overlapping region of W/P is eluted and recycled (between 0 and 12 minutes), then the product is eluted and collected (the window marked between 12 and 23 minutes), then product contaminated with strong impurity is eluted and recycled (between 23 and 60 minutes), and finally the columns undergo strip, CIP and equilibration (second window marked between 60 and 73 minutes). In the second part of the cycle, first the W/P recycle is taken up, then fresh feed is loaded which shows in the peak between 85 and 100 minutes, then the P/S overlap is taken up, and lastly the gradient is started. Note that in the very first switch, the UV2 profile is different due to the accelerated startup, where more product is loaded. After this, a cyclic steady state is reached already in the second cycle, when the profiles stay approximately constant. The same effect, reaching a steady state after one cycle, can also be seen in the purity and the transient yield (see Figure 2.7), which do not change much after the third switch. Also note the ramp-up of the yield during the first two switches, which is typical for periodic chromatography processes. The process performance in terms of yield and purity in the batch case of course depends on the pooling strategy. One can either opt to collect a wide window of the chromatogram, resulting in high yield but low purity, or one can collect a narrow window with high purity but lose any product that is not collected this way. This leads to a trade-off situation, where one objective cannot be improved without compromising the other. In the design batch presented here, purities (by HPLC) between 43.8 % and 79.7 % could be achieved, at yields between 84.0 % and 30.5 %, respectively. The MCSGP process on the other hand circumvents this

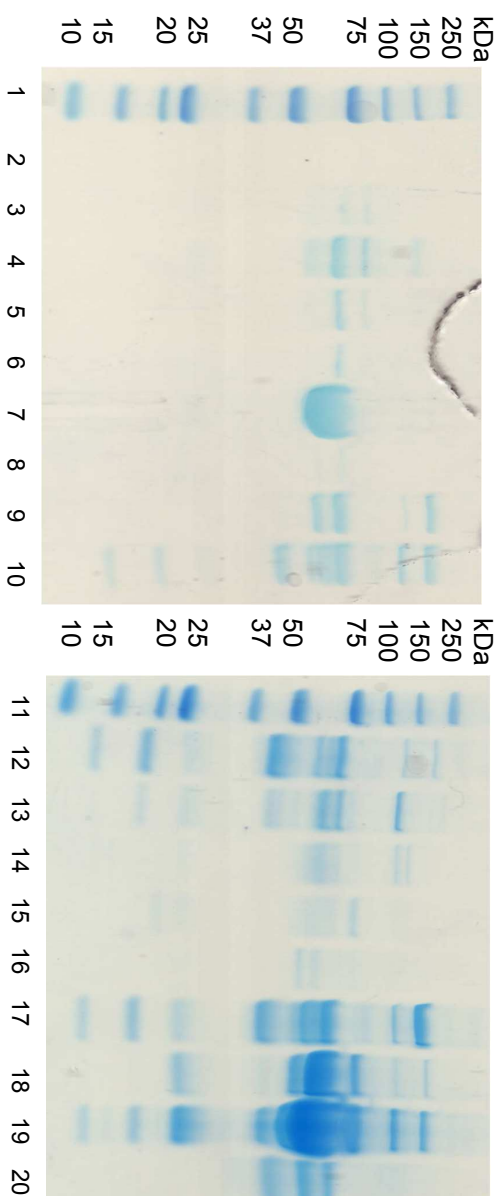


Figure 2.5: SDS-PAGE analysis of design batch fractions. The lanes contained the following samples: 1: Size standard; 2 –10: Batch fractions (1, 4, 7, ..., 25); 12 –16: Batch fractions (28, 31, ..., 40); 17: MCSGP product fraction; 18: MCSGP weak fraction; 19: MCSGP feed; 20: AAT standard (Sigma Aldrich).

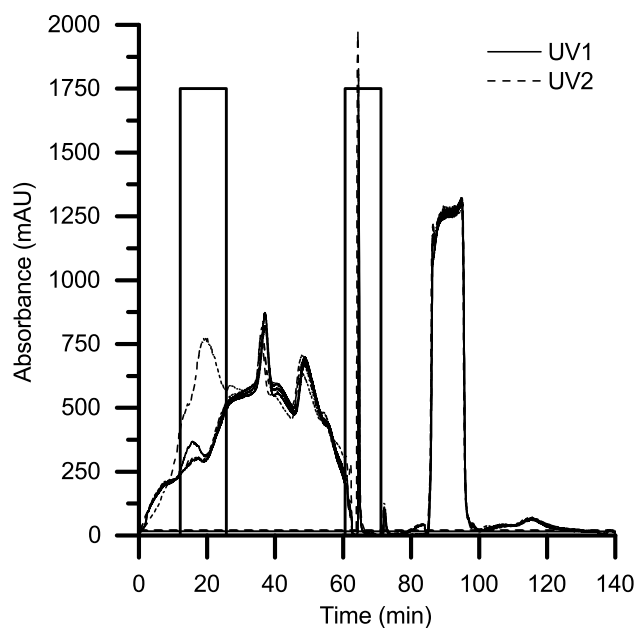


Figure 2.6: Overlay of the UV-profiles recorded in the MCSGP process. The solid line represents the signal recorded by the first UV detector, the dashed line is the signal recorded by the second UV detector. Note that the times of the second UV have been shifted so that both columns start the cycle start at $x = 0$. In addition, two windows are marked: the product elution window between 12 and 23 minutes, and the strip, CIP and equilibration phase between 60 and 73 minutes. Before the first window the W/P recycling takes place, and between the windows, the P/S recycling is carried out.

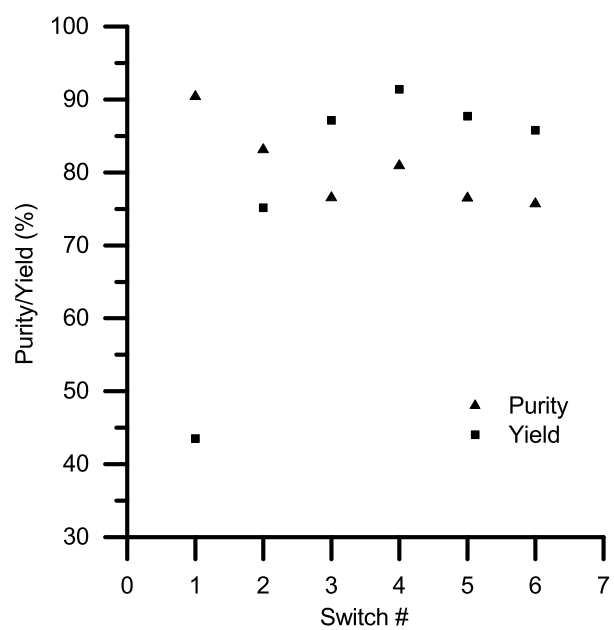


Figure 2.7: Purity and yield values for the MCSGP process in each switch. After the second switch, the process is in cyclic steady state and the values stay approximately constant.

trade-off and achieves both high yield and purity at the same time, in this case a purity of 76.1 % with a yield of 86.7 % in cyclic steady state. The complete batch pareto-curve is shown in Figure 2.8, along with the MCSGP operating point.

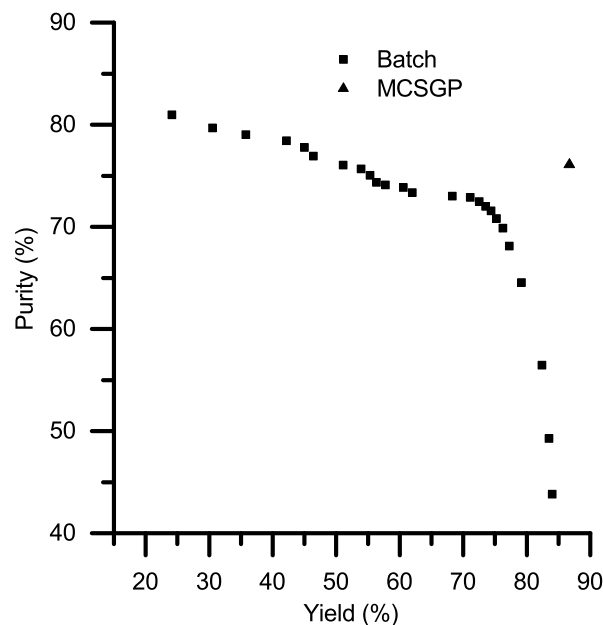


Figure 2.8: Pareto-optimal batch pooling strategies and MCSGP operating point. Note that the MCSGP process can circumvent the intrinsic trade-off present in the batch process.

2.4 Concluding remarks

The feasibility of isolating the protein α_1 -antitrypsin (AAT) directly from delipidated human blood plasma by ion-exchange chromatography has been shown. Since AAT is usually isolated from a side-stream of the Cohn fractionation cascade, which presents a much easier separation problem due to the absence of major contaminants (such as albumin), it is clear that this technology could be applied at any position in the fractionation cascade for human blood plasma. In order to iso-

late AAT, a batch separation process was designed, which suffered from the usual purity/yield trade-off. The batch process could only achieve purities between 43.8 % and 79.7 %, with yield values of between 84.0 % and 30.5 % respectively. Using multicolumn solvent gradient purification (MCSGP) technology, it was possible to run the same separation at high purity (76.1 %) and high yield (86.7 %) simultaneously. A cyclic steady state operation could be reached after just one cycle by using an accelerated startup protocol. While the MCSGP product was of similar quality than a commercial standard, some additional impurities were present. SDS-PAGE and LC/MS/MS were used to identify the impurities. Compared to the commercial standard, which contained the impurities albumin, antithrombin-III, α -1-antichymotrypsin, and α -1-acid glycoprotein, the MCSGP product additionally contained alpha-2-macroglobulin and haptoglobin. These could be removed e.g. by orthogonal chromatography, as is common in state-of-the-art α ₁-antitrypsin production.

Chapter 3

Optimal model-based design of the twin-column CaptureSMB process improves capacity utilization and productivity in protein A affinity capture

3.1 Introduction

In chromatographic purification of biomolecules on a preparative scale, one often deals with very complex mixtures or with solutes that have very similar physical properties. This can lead to cases where baseline separation, and therefore high yield and purity, is very hard to achieve with non-affinity batch chromatography. In the case where no affinity adsorbent is available, continuous countercurrent chromatographic processes, such as SMB or MCSGP and variants thereof have been proposed for binary, ternary and quaternary separations [28,33,59,63–67]. In

cases where an affinity resin material is available, for example in protein A purification of monoclonal antibodies (mAbs), continuous countercurrent chromatography has not been widely used due to the high purities that could be obtained using single-column batch processes available [46,68]. However, protein A affinity resins usually exhibit relatively strong mass transfer limitations, leading to shallow breakthrough curves, and therefore low resin utilization [69,70]. To counteract these limitations, several different continuous multi-column setups have been proposed and implemented, such as periodic counter-current (PCC) [42,71] and sequential multi-column chromatography (SMCC) [48,49] processes, which use sequential loading onto three or more columns to achieve increased performance. Recently, a continuous, two-column capture process has been proposed, which allows for higher productivity and higher capacity utilization than comparable batch processes, while retaining comparable separation performance in terms of yield and purity [43]. Higher productivity means that a larger amount of product can be processed per unit time and unit volume of resin, which reduces the time required to process a given amount of feed stock, while higher capacity utilization means that more product can be processed per unit volume of resin and per cycle, which reduces the number of load, elution and regeneration cycles needed to process a given amount of product. Therefore, capacity utilization means that more product can be produced per unit volume of resin within the life time of the resin. Replacing the resin is a major component of the overall production cost, especially in cases where the resin is expensive [38].

When dealing with a novel process, gaining process understanding is paramount to design an efficient and robust process and to determine the operating regions and optimal process conditions. In order to avoid large time-consuming and resource-consuming experimental campaigns, especially in cases like protein A chromatography for monoclonal antibodies, where both the column material and the feed

are usually very expensive, process modeling and simulation has long since been a vital tool in gaining this understanding [58, 72–74]. Many different models are available to predict the behavior of chromatographic systems under preparative conditions, such as the ideal model [75], Langmuir type models [76, 77], or the steric mass action model [78]. However, these models are generally not very well equipped to predict the behavior of systems with high mass transfer resistances, which are usually observed in protein chromatography. In such scenarios, pore diffusion or general rate models have been applied [27, 73, 79]. In the case of a large protein, such as a mAb, these models can be augmented with features that account for hindrance of mass transfer by proteins blocking pores, which has been shown recently [80, 81]. However, when optimizing a multi-column chromatographic process, these elaborate models tend to be too computationally expensive to complete calculations in a reasonable time frame; therefore a relatively simple model combined with semi-empirical correlations is usually preferable in these cases [82, 83]. In this work, such a model for the twin-column CaptureSMB process is developed, validated experimentally and used to find optimal operating points for the process. The model is held general enough to be easily applied to batch chromatography and other multi-column processes as well.

3.2 Process descriptions

In order to have a fair comparison between the processes, different numbers of resin volumes are used in the CaptureSMB and the batch process. In the batch process, one column is either the same bed height as one column in the CaptureSMB process, or the column in the batch process is twice the bed height of one column in the CaptureSMB process, leading to the same total bed height.

In addition, the purity is assumed to be the same in both processes, and the yield

is kept constant at a high value by enforcing a constraint on the breakthrough (see below). Product quality is assumed to be comparable between the two processes and independent on the operating parameters, which has been proven previously in [43]. Since the recovery and regeneration step can be optimized independently, it is assumed to be fixed and equal in both processes and is not part of the comparison.

3.2.1 Batch chromatography with dual loading flow rate

The affinity batch chromatography process uses a single column, as schematically depicted in Figure 3.1, panel A (top). In the batch process, the column is first equilibrated with a buffer that allows binding of the target compound to the resin material in the column. When the column is equilibrated, the feed solution containing the target compound is loaded onto the column, where the target compound is retained while non-binding impurities are flowing through, ending up in the waste stream (W). One or more washing steps, where the column is flushed with different buffers, can then be applied to clear more impurities. After these washing steps, the target compound is recovered by applying a buffer that allows desorption of the compound from the resin. After the product has been collected (P), the column is cleaned in place (CIP) with a CIP-solution to remove any strongly binding impurities and to sanitize the equipment. When the CIP step is finished, the column is re-equilibrated, preparing the column for the next load-elute cycle.

In the batch process considered, the loading step is further divided into sub-steps. The loading phase encompasses two sub-steps with loading at two different flow rates, Q_{PL} and Q_L for durations t_{PL} and t_L , respectively. The indices PL and L stand for preload and load, respectively.

This dual loading flow rate strategy has been proposed for improvement of batch capture performance [68]. It is used in this work in order to ensure a fair comparison between batch chromatography and CaptureSMB, which also uses a dual

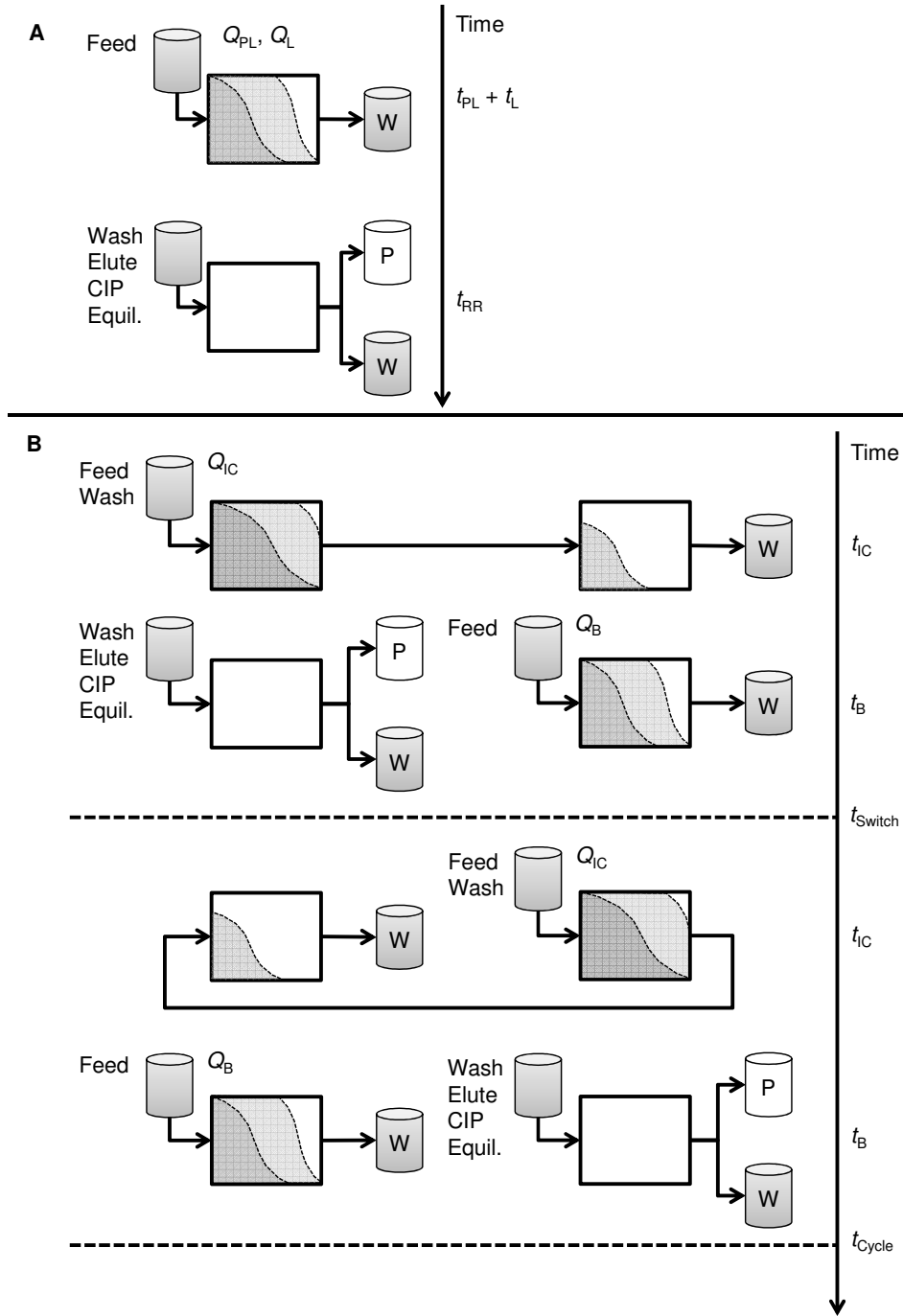


Figure 3.1: Process flow charts for the batch capture process (panel A, top) and the CaptureSMB process (panel B, bottom).

loading flow rate strategy.

The entire elution phase including wash, elute, CIP and re-equilibration has a total duration denoted by t_{RR} . This leads to four design variables that completely describe the process: t_{PL} , t_L , Q_{PL} and Q_L . These are all free variables and there are therefore 4 degrees of freedom for optimization. As mentioned above, the optimization is only applied to the loading step, since optimal procedures for the remaining steps can be determined independently of the loading step.

3.2.2 CaptureSMB

In the CaptureSMB process, two identical columns are used to recover the target compound from the feed mixture. After the columns have been equilibrated, they are interconnected by connecting the outlet of the first column to the inlet of the second column. For a certain time, the feed solution is loaded onto the first column. The fact that there is a second column behind the first one allows for longer feeding compared to the batch case, because the eventual breakthrough is caught by the second column instead of being lost. After this time, the first column enters the recovery and regeneration step, which is equivalent to the batch process described in 3.2.1. During this step, the now disconnected second column is further loaded with feed. As soon as the first column is re-equilibrated and ready to be loaded again, the columns swap roles and continue with the next interconnected step. A process schematic is shown in Figure 3.1, panel B (bottom). In the first part of the switch, the interconnected phase (IC, top), the columns are connected in series and feed is loaded with a flow rate Q_{IC} for a time t_{IC} . At the end of the interconnected phase, the wash step starts for the fully loaded column, while the columns are still interconnected, to catch any product that elutes during this early wash step. Non-adsorbing impurities flow through and go to waste (W). Next, the batch phase (B) follows for a duration t_B , where the fully loaded column is washed

further and more impurities are cleared. After the washing steps, the pure product (P) is eluted and collected. CIP and equilibration steps follow to prepare the column for the next switch. In the meantime, the other column is loaded further with a feed flow rate Q_B . After the first switch, at $t_{\text{Switch}} = t_{\text{IC}} + t_B$, before any product in the second column starts breaking through, the columns switch roles and go through the same procedure again with reversed roles (lower part). After one cycle, at $t_{\text{Cycle}} = 2(t_{\text{IC}} + t_B)$, the columns switch roles again and are back in the initial configuration.

The CaptureSMB process has four design variables that completely describe the process: t_B, t_{IC}, Q_B and Q_{IC} , which are the duration of the batch and interconnected phases, and the loading flow rates during the batch and interconnected phases, respectively. Since one of the columns undergoes recovery and regeneration during the batch phase, this procedure fixes the batch time t_B . This leaves 3 degrees of freedom to optimize the process.

3.3 Materials and Methods

3.3.1 Monoclonal antibody

The cell culture supernatant used in the experimental parts of this study was obtained from JSR (Tokyo, Japan) and contained a monoclonal IgG₁-type antibody in a concentration of $c_{\text{Feed}} = 1.2 \text{ mg mL}^{-1}$. Higher feed concentrations were achieved by spiking the feed with previously captured mAb from the same feed.

3.3.2 Stationary phase and buffers

The protein A stationary phase Amsphere JWT-203 (JSR, Tokyo, Japan) was used for all experiments, in pre-packed columns of dimensions 0.5 x 5 cm (Atoll,

Weingarten, Germany). Two or four such columns were joined in series to form new columns with bed heights of 10 and 20 cm. The buffers were: 20 mM phosphate, 150 mM NaCl, pH 7.5 as equilibration, washing and binding buffer (A); 20 mM phosphate, 1 M NaCl, pH 7.5 as second washing buffer (B); 20 mM citrate pH 3.2 as elution buffer (C); and 0.1 M NaOH as cleaning-in-place (CIP) solution.

3.3.3 Preparative chromatography operating conditions

All preparative batch and CaptureSMB runs were conducted on Contichrom lab-scale equipment (ChromaCon AG, Zurich, Switzerland). The following protocol was used for all elution phases, after a column has been fully loaded:

- Washing: 5 column volumes buffer A, 5 column volumes buffer B, 5 column volumes buffer A
- Elution: 5 column volumes buffer C
- CIP: 15 minutes contact time with the CIP solution
- Equilibration: 5 column volumes buffer A

The very first equilibration step needed before starting the processes is negligible due to the cyclic nature of the processes and the high number of switches to be run. The recovery and regeneration step was carried out at $Q_{RR} = Q_{IC}$.

3.3.4 Analytics

The concentration of mAb in all samples was determined using the method described in [43] using a Poros[®] A-20 analytical protein A chromatography column (2.1 x 30 mm), obtained from Life Technologies (Carlsbad, CA, USA) on an Agilent 1100 series HPLC (Santa Clara, CA, USA). The mobile phases used were 20

mM phosphate, 150 mM NaCl, pH 7.5 (binding and washing buffer), 10 mM HCl, 150 mM NaCl, pH 2.0 (elution buffer) and 20% acetic acid (regeneration solution) and the flow rate was 1.0 mL min⁻¹.

3.4 Process model

3.4.1 Model equations with empirical mass transfer model

The aforementioned chromatographic processes are modeled using a lumped kinetic model [72]:

$$\begin{aligned}\frac{\partial c}{\partial t} &= -v \frac{\partial c}{\partial x} + D_L \frac{\partial^2 c}{\partial x^2} - \phi \frac{\partial q}{\partial t} & t \in [0, t_{\text{Switch}}], x \in [0, L_{\text{Col}}] \\ \frac{\partial q}{\partial t} &= k_m (q^* - q)\end{aligned}\tag{3.1}$$

where c is the liquid phase concentration of the protein, t denotes the time, $v = Q/(A_{\text{Col}}\epsilon)$ is the interstitial velocity, where Q is the volumetric flow rate, A_{Col} is the column cross sectional area and ϵ is the bed porosity, x is the coordinate along the longitudinal axis of the column, L_{Col} is the length of one column, D_L is the apparent axial dispersion coefficient, $\phi = (1 - \epsilon)/\epsilon$ is the phase ratio of the column, q is the solid phase concentration of the protein, k_m is the mass transfer coefficient and q^* is the equilibrium solid phase concentration of the protein.

These partial differential equations are subject to the following boundary and

initial conditions:

$$\begin{aligned}
c(t=0, x) &= c_0(x) \\
q(t=0, x) &= q_0(x) \\
c(t, x=0) &= c_{\text{in}}(t) + \frac{D_L}{v} \frac{\partial c}{\partial x} \Big|_{x=0} \\
\frac{\partial c}{\partial x} \Big|_{x=L_{\text{Col}}} &= 0
\end{aligned} \tag{3.2}$$

Note that the inlet concentration $c_{\text{in}}(t)$ changes with time, because the columns undergo different operations (breakthrough uptake, load, wash, elute, CIP, equilibrate).

The apparent axial dispersion coefficient D_L can be estimated from the reduced van Deemter equation with the correlation [27]:

$$D_L = A \frac{d_P}{2} v \tag{3.3}$$

where A is the intercept of the reduced van Deemter equation and d_P is the average particle diameter.

The bed porosity ϵ can be measured using a pulse injection of a non-adsorbing species.

For the mass transfer coefficient k_m , an empirical correlation is used that approximates the effect of hindered mass transfer due to pore blockage and other effects [83]:

$$k_m = k_m^{\text{max}} \left(S_1 + (1 - S_1) \left(1 - \frac{q}{q_{\text{sat}}} \right)^{S_2} \right) \tag{3.4}$$

where k_m^{max} is the maximum mass transfer coefficient when no protein is adsorbed, S_1 is a coefficient describing the maximum hindrance, for which $0 < S_1 \leq 1$, the coefficient $S_2 > 0$ models the non-linearity of the increase in hindrance and q_{sat} is

the saturation capacity of the resin. The maximum mass transfer coefficient and the parameters of the correlation are fitted from breakthrough curves at different flow rates and concentrations.

The adsorption of the protein is described using a Langmuir isotherm with the pH value as the modifier [33]:

$$\begin{aligned} H &= H_{\text{Ref}} \left(\frac{\text{pH}}{\text{pH}_{\text{Ref}}} \right)^N \\ q^* &= \frac{Hc}{1 + \frac{Hc}{q_{\text{sat}}}} \end{aligned} \tag{3.5}$$

where H is the Henry coefficient (which is proportional to the retention factor $k_{0,f}$), H_{Ref} is the Henry coefficient measured at the reference pH value, pH_{Ref} is the reference pH value and N describes the change of the Henry coefficient with the pH value. H_{Ref} and q_{sat} are fitted from breakthrough curves at different flow rates and concentrations, and N is fitted from elution experiments.

The resulting partial differential equations were discretized along the x coordinate using a first order central finite differences method, and the resulting system of ordinary differential equations was solved in FORTRAN using the solver DLSODES from ODEPACK [84, 85]. The number of grid points was fixed at 100 per column, since a further increase did not show any changes in the solution behavior. The column switching in the CaptureSMB process was conducted numerically by swapping the internal profiles of the columns. This way, the same boundary conditions could be used in every switch. The model is suitable to simulate batch experiments and the CaptureSMB process, but is also kept general enough to be adapted to any multi-column process.

3.4.2 Fixed operating parameters

Some parameters are not part of the optimization, namely the column dimensions and the recovery and regeneration protocol. The following column dimensions were used in the simulations: $A_{\text{Col}} = 0.20 \text{ cm}^2$ and $L_{\text{Col}} = 5$ or 10 cm for a single column in the CaptureSMB case, and $L_{\text{Col}} = 5, 10$ or 20 cm for the column in the batch case.

The elution protocol mentioned above (see 3.3.3) fixes the recovery and regeneration time (which, in the case of CaptureSMB, is equal to the batch loading time) as follows:

$$t_{\text{RR}} = t_{\text{W}} + t_{\text{Elu}} + t_{\text{CIP}} + t_{\text{Equil}} \quad (3.6)$$

where W stands for wash, Elu stands for elution, CIP stands for cleaning in place and Equil stands for re-equilibration.

3.4.3 Process constraints for yield, purity and pressure drop

As mentioned above, the comparison discussed below is performed with constant purity and yield. The impurity clearance is largely dependent on the type of stationary phase and the washing procedure. These are kept identical in the two processes, and it is assumed that the parameters chosen fulfil any purity requirements; therefore the purity is not modelled. On the other hand, yield is a strong function of the operating parameters such as flow rates and durations of the different process steps and it is properly calculated by the model. However, for a high value product such as monoclonal antibodies, a process is not attractive if too much product is lost; yield is therefore treated as a constraint rather than an optimization variable. In the batch process, maximum yield is ensured by loading

only to a volume that corresponds to a certain breakthrough value (e.g. 90% of the volume corresponding to 1% breakthrough [46]). This safety factor of 90% is rather arbitrary; therefore it has not been considered in the optimizations and the constraint is simply that the breakthrough after loading should never exceed 1%. Similarly for the CaptureSMB process, the breakthrough of the second column, which has no column connected to its outlet, must not exceed 1%. With these constraints it is assured that in the comparison discussed below, all process runs lead to equivalent yield values.

In all cases, the pressure drop over the columns must not exceed the maximum allowed pressure drop. The pressure drop is estimated using the following correlation [69]:

$$\Delta P = \gamma u L \quad (3.7)$$

where γ is a coefficient, $u = Q/A_{\text{Col}}$ is the superficial velocity and L is the total bed height, i.e. number of interconnected columns times L_{Col} .

3.4.4 Process optimization

The aim of the process optimization was to maximize the productivity or the capacity utilization. All optimization tasks were done with the built-in genetic algorithm function GA of MATLAB (Mathworks), which implements an evolutionary procedure that drives a randomly distributed initial population of candidate solutions, in this case four sub-populations of 20 members each, towards functional minima. By choosing a relatively large number of individuals, coverage of the solution domain can be improved and the possibility of finding the global optimum is increased.

The productivity represents the amount of antibody which can be produced per unit time and unit resin volume. For the batch process, it can be written as follows

$$P_{\text{Batch}} = Y \cdot \frac{c_{\text{Feed}} (t_{\text{PL}} Q_{\text{PL}} + t_{\text{L}} Q_{\text{L}})}{V_{\text{Col}} (t_{\text{PL}} + t_{\text{L}} + t_{\text{RR}})} \quad (3.8)$$

where Y is the process yield, c_{Feed} is the mAb concentration in the feed and V_{Col} is the volume of one column.

With the constraints discussed above, this leads to the following optimization problem

$$\begin{aligned} & \max_{t_{\text{PL}}, t_{\text{L}}, Q_{\text{PL}}, Q_{\text{L}}} && P_{\text{Batch}}(t_{\text{PL}}, t_{\text{L}}, Q_{\text{PL}}, Q_{\text{L}}) \\ & \text{subject to:} && c(t = t_{\text{PL}} + t_{\text{L}}, z = L_{\text{Col}}) \leq 0.01 c_{\text{Feed}} \\ & && (\gamma u L)_{\text{max}} \leq \Delta P_{\text{max}} \\ & && 0 < t_{\text{PL}}, 0 \leq t_{\text{L}}, 0 < Q_{\text{PL}}, 0 < Q_{\text{L}} \end{aligned} \quad (3.9)$$

Note that the first constraint $c(t = t_{\text{PL}} + t_{\text{L}}, z = L_{\text{Col}}) \leq 0.01 c_{\text{Feed}}$ is equivalent to a yield constraint and assures that the yield is kept high and constant.

A similar expression can be derived for the CaptureSMB process

$$P_{\text{CSMB}} = Y \cdot \frac{c_{\text{Feed}} (t_{\text{IC}} Q_{\text{IC}} + t_{\text{B}} Q_{\text{B}})}{2V_{\text{Col}} (t_{\text{IC}} + t_{\text{B}})} \quad (3.10)$$

Where V_{Col} is the volume of one column in CaptureSMB. The expression (3.10) can be used in (3.9) with analogous constraints and optimization variables.

As mentioned before, with relatively expensive and short-lived resins, maximizing the capacity utilization becomes a very important objective. The capacity utilization is equivalent to the amount of mAb produced per resin volume and cycle normalized with the equilibrium binding capacity at feed concentration. It can be calculated as

$$CU_{\text{Batch}} = Y \cdot \frac{c_{\text{Feed}} (t_{\text{PL}} Q_{\text{PL}} + t_{\text{L}} Q_{\text{L}})}{V_{\text{Col}} (1 - \epsilon) q_{\text{Feed}}^*} \quad (3.11)$$

where CU stands for the capacity utilization and q_{Feed}^* is the equilibrium binding

capacity at feed concentration which can be calculated using equation (3.5). Using the same constraints as in equation (3.9), an analogous optimization problem can be formulated, with CU as the objective to be maximized. Similarly, in CaptureSMB, the capacity utilization is defined as:

$$CU_{\text{CSMB}} = Y \cdot \frac{c_{\text{Feed}} (t_{\text{IC}} Q_{\text{IC}} + t_{\text{B}} Q_{\text{B}})}{V_{\text{Col}} (1 - \epsilon) q_{\text{Feed}}^*} \quad (3.12)$$

Note that the factor 2 in the denominator cancels compared to equation (3.10), since in order to elute both columns, an entire cycle, i.e. two switches, is needed, so equation (3.10) must be multiplied with $2(t_{\text{IC}} + t_{\text{Batch}})$ before normalizing with the equilibrium binding capacity at feed concentration.

The presence of two competing objectives, in this case productivity and capacity utilization, can lead to a trade-off scenario where one of the objectives cannot be improved without having a negative impact on the other. In this case, a set of pareto-optimal operating points can be found, for which no other feasible operating points exist that are better in both objectives at the same time. To find a set of pareto-optimal points, the optimization problem in (3.9), using (3.11) and (3.12) as optimization goal, is modified by adding the constraint:

$$P_{\text{Target}} \leq P \quad (3.13)$$

where P_{Target} , the target productivity, is varied between the optimum values found from the optimization problem (3.9) with productivity as objective, and the productivity value found by optimizing (3.9) for maximum capacity utilization.

3.5 Results

3.5.1 Model fitting

The reduced plate height of pulse injections with a non-adsorbing solute at different flow rates was determined using the method of moments [86]. Linear regression of the data yields the parameter $A = 35.13 \pm 5.451$ which is used in equation 3.3 to calculate the apparent axial dispersion coefficient.

From breakthrough experiments at different flow rates and feed concentrations, the parameters describing the adsorption behavior, k_m^{\max} , S_1 , S_2 , H_{ref} and q_{sat} can be estimated. This is done by minimizing the sum of square errors using a genetic algorithm. In total, 9 breakthrough curves at 5 different flow rates between 0.25 and 3 mL min⁻¹ and 3 different feed concentrations between 1.2 and 4.6 mg mL⁻¹ were used to fit the model parameters. The relatively low value of the maximum mass transfer coefficient $k_m^{\max} = 0.1800 \text{ min}^{-1}$, obtained by fitting, indicates a strongly hindered mass transfer. Furthermore the results indicate that the mass transfer is expected to decrease by almost 38% at saturation, as indicated by the value found for $S_1 = 0.6245 \pm 1.739$ (see equation 3.4) in order to fit the asymmetry and the broadness of the breakthrough curves. A list of all parameters used can be found in Table 3.1.

Examples of the fitted breakthrough curves are shown in Figure 3.2. It is clear that the model can replicate the elution behavior over a wide range of different flow rates and different feed concentrations. An example of simulated and experimental UV signals can be found in Figure 3.3.

A pressure drop coefficient of $\gamma = 0.01020 \pm 5.436 \cdot 10^{-4} \text{ bar min cm}^{-2}$ used in equation 3.7 was determined by linearly fitting the pressure drop values measured at different flow rates.

Table 3.1: Parameters fitted from pulse injections, breakthrough curves at different flow rates and concentrations, and pressure drop measurements at different flow rates, with 95% confidence intervals.

Parameter	Symbol	Units	Estimate
Intercept of van Deemter curve	A	–	35.13 ± 5.451
Bed porosity	ϵ	–	0.368
Maximum mass transfer coefficient	k_m^{\max}	min^{-1}	0.1800 ± 0.5000
Pore blockage coefficient	S_1	–	0.6245 ± 1.739
Pore blockage coefficient	S_2	–	2.071 ± 4.959
Henry coefficient at reference pH	H_{ref}	–	246.8 ± 36.29
Saturation capacity per solid volume	q_{sat}	mg mL^{-1}	94.72 ± 4.282
Pressure drop coefficient	γ	bar min cm^{-2}	$0.01020 \pm 5.436 \cdot 10^{-4}$

Table 3.2: Operating conditions for the different CaptureSMB runs used to compare the model to the experimental data.

Run #	Interconnected time t_{IC} (min)	Interconnected flow rate Q_{IC} (mL min^{-1})	Batch flow rate Q_{B} (mL min^{-1})	R & R flow rate Q_{RR} (mL min^{-1})
1	11.8	2.5	0.67	2.5
2	18.7	2.0	0.63	2.0
3	38.2	1.0	0.50	1.0
4	5.0	2.5	1.1	2.5
5	22.8	1.8	0.5	2.5

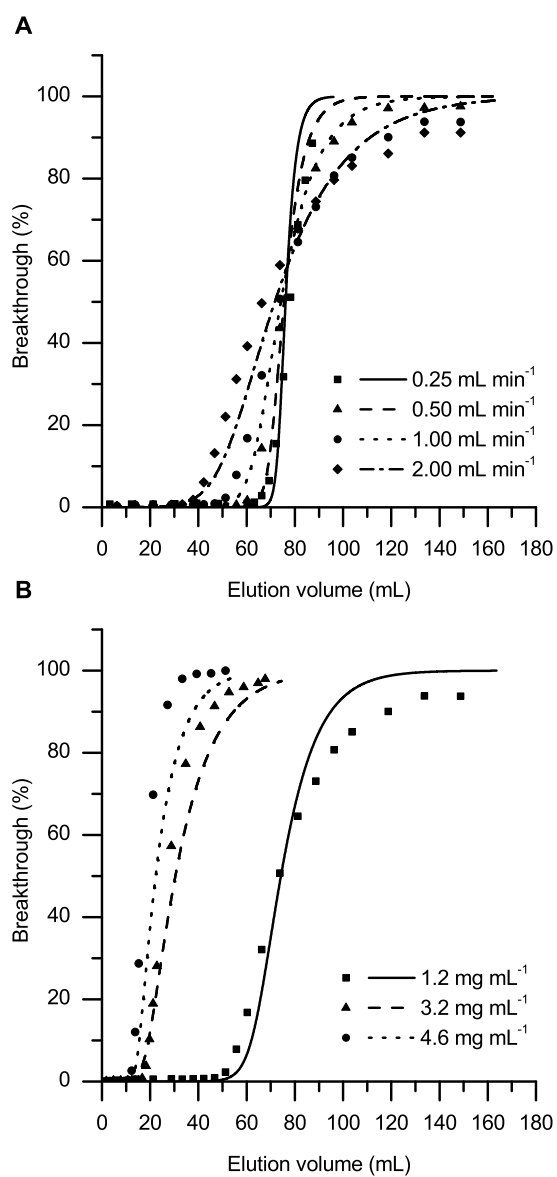


Figure 3.2: Top panel (A): Breakthrough curves at different flow rates (filled symbols) with model data (lines). The feed concentration was 1.2 mg mL^{-1} in these cases. Bottom panel (B): Breakthrough curves at different feed concentrations (filled symbols) with model data (lines). The feed flow rate was 1.0 mL min^{-1} for the experiments with feed concentrations of 1.2 and 4.6 mg mL^{-1} , and 1.5 mL min^{-1} for the run with 3.2 mg mL^{-1} .

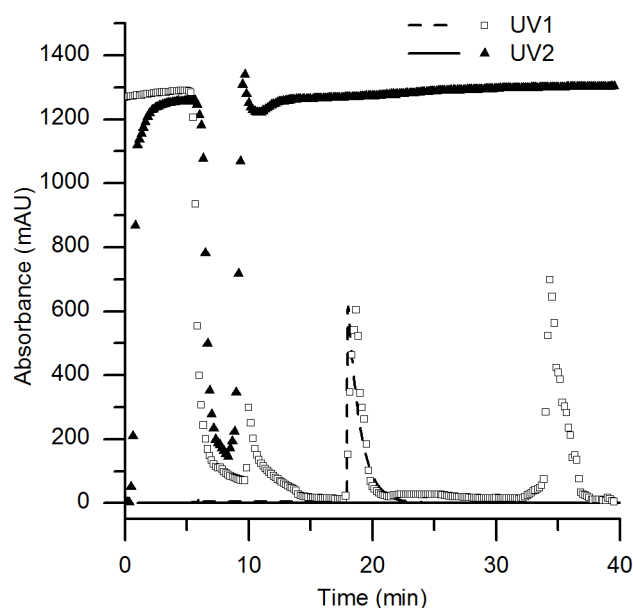


Figure 3.3: Experimental UV profiles (symbols) with model data for the product (lines) for a steady state switch of run 4 (see Table 3.2). Note that the model does not simulate impurities; therefore, the only signal visible in the model data is the product. In the experimental data on the other hand, mostly impurities are visible, except during the elution (UV1 peak at around 20 minutes), and partly during the washing step (UV1 before the elution peak). This can also be seen in the model results, which show a signal increase only during wash and elution. The model predicts a very similar position and shape for the elution peak. At the end of the switch, a slight increase in absorption is visible in the experimental data for UV2, which is due to the displacement of an impurity. This is in good agreement with the model predictions, which show no breakthrough at the outlet of column 2 at the end of the switch.

In order to assess whether the model is able to reasonably reproduce the CaptureSMB process, different operating points were simulated and the output compared to experimental results at these points. The points included a point at high productivity (run 1), a point at high capacity utilization (run 3) and an intermediate point (run 2). Additionally, runs 4 and 5 were used as verification runs, where the operating parameters have been taken from the pareto-optimal set of operating points (see 3.5.4) and then run experimentally. All corresponding operating parameters are reported in Table 3.2. To ensure feasible operation, a safety factor has been added to the operating parameters, i.e. 20% reduced batch loading flow rate. The experiments were run for 3 cycles at each point which was sufficient to reach cyclic steady state.

From the data shown in Table 3.3, it can be seen that the model is able to reproduce the experiments with good accuracy over a wide range of flow rates and loading times. The relative error was smaller than 10% in all performance measures considered, except for the outlet concentration of run 2. Note that all yield losses in both the experiments and the model results are due to losses in the wash, not due to breakthrough. It appears that due to this, increasing the load has a slightly negative impact on yield, but there is no significant correlation. The fact that the capacity utilization seems to be underestimated while the outlet concentration is overestimated might be an indication that the model underestimates the steady state preload, i.e. what fraction of the feed loaded in the interconnected phase breaks through and is loaded onto the second column. If this preload is underestimated, more product ends up in the first column before recovery, leading to a higher concentration, while less product is internally recycled, leading to less product being in the process overall and therefore lower capacity utilization. However, the mass balance not closing in the experiments certainly also plays a role in the inaccuracies in model prediction. As can be seen, run 4, which is optimized

for productivity, offers higher productivity than what was reached in previous experiments that were designed without prior model based optimization. Since run 3 was already very close to the global optimum in terms of capacity utilization, the last point (run 5) was taken from the middle of the pareto curve. Also in this intermittent region, the model is able to replicate the behavior of the system.

3.5.2 Internal concentration profiles

One might expect that using additional columns for sequential could further increase the load and therefore the capacity utilization, but considering the internal concentration profile just before recovery and regeneration that results from solving equations (3.1) and (3.2) at the operating point with maximum capacity utilization (solid line in Figure 3.4), it is obvious that only a very small fraction of the capacity is still available, which is represented as the small grey area in the top right corner of the dashed rectangle, even though the profile is contained in only two columns. Therefore, we can conclude that two interconnected columns are sufficient for an efficient continuous capture process. The internal concentration profile at maximum productivity (dotted line in Figure 3.4) is shown as a reference, which shows a lower capacity utilization, as expected. At the interface of the two columns (vertical dashed line at 10 cm), a discontinuity is visible; This is an effect of the Danckwert's boundary conditions (see equation (3.2)).

3.5.3 Process optimization

A summary of optimum operating points for single objective optimization and their respective values is reported in 3.4 for both processes considered. In this case, the single column length for CaptureSMB was 10 cm, while the batch process was simulated with the same total bed height, resulting in a column length of 20 cm. The feed concentration was 1.2 mg mL^{-1} in all cases.

When maximizing the productivity, the batch process reached a value of $19.7 \text{ mg mL}^{-1} \text{ h}^{-1}$, while the CaptureSMB process reached $27.1 \text{ mg mL}^{-1} \text{ h}^{-1}$. It is clear that the CaptureSMB process shows better performance with respect to productivity, and in addition has a better capacity utilization (79.1% compared to 71.2%) and therefore higher load (35.9 mg mL^{-1} compared to 32.3 mg mL^{-1}) and a higher

Table 3.3: Comparison of model predictions with experimental data for the performance of the CaptureSMB process in different conditions. In parentheses: Relative errors of the simulation output compared to the experimental data.

Run	Yield Y (%)		Mass (%)	balance		Productivity P (mg mL ⁻¹ h ⁻¹)		Capacity utilization CU (%)		Outlet concentration c_{out} (mg mL ⁻¹)	
	Exp.	Sim.		Exp.	Sim.	Exp.	Sim.	Exp.	Sim.	Exp.	Sim.
1	92.9	93.9 (+1.1%)	102.2	100.0	100.0	17.7	18.3 (+3.4%)	67.5	65.3 (-3.3%)	5.48	5.93 (+8.2%)
2	85.3	92.7 (+8.7%)	93.7	100.0	100.0	15.7	17.1 (+8.9%)	82.9	76.2 (-8.1%)	6.06	6.91 (+14%)
3	88.1	88.6 (+0.6%)	97.2	100.0	100.0	10.2	10.4 (+2.0%)	95.5	96.0 (+0.5%)	6.90	7.39 (+7.1%)
4	93.6	94.5 (+1.0%)	101.7	100.0	100.0	19.5	21.0 (+7.7%)	63.8	61.1 (-4.2%)	5.07	5.55 (+9.5%)
5	90.2	94.0 (+4.2%)	99.7	100.0	100.0	16.0	16.9 (+5.6%)	74.8	72.4 (-3.2%)	6.10	6.57 (+7.7%)

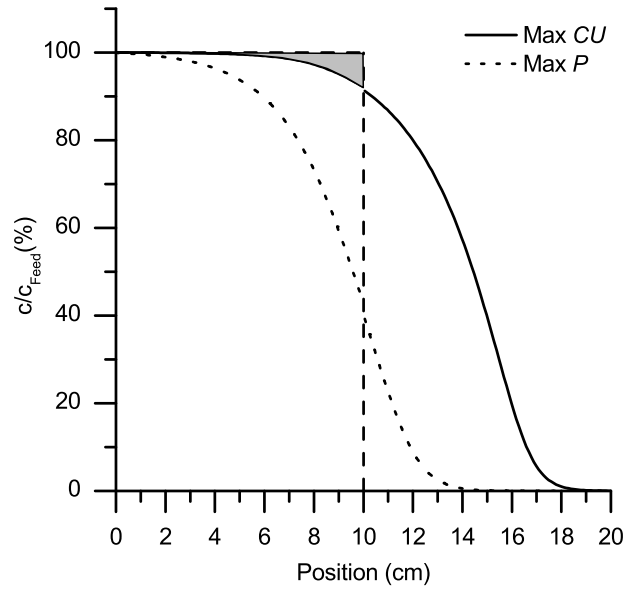


Figure 3.4: Internal concentration profile in the liquid phase of the CaptureSMB process at the end of the interconnected phase, when the first column is fully loaded. The two profiles shown correspond to a process run at maximum capacity utilization (solid line) and an operating point at maximum productivity (dashed line). The gray area represents the resin capacity not utilized at maximum capacity utilization.

outlet concentration (7.18 mg mL^{-1} compared to 6.46 mg mL^{-1}). This also means that fewer cycles are required to process an equal amount of antibody, which leads to slower resin deterioration and therefore lower resin costs.

When maximizing the capacity utilization on the other hand, the batch process shows slightly better values, reaching a capacity utilization of 99.2%, resulting in a load of 45.0 mg mL^{-1} and an outlet concentration of 9.00 mg mL^{-1} , compared to a capacity utilization of 94.8% in the case of CaptureSMB, leading to a load of 43.0 mg mL^{-1} and an outlet concentration of 8.60 mg mL^{-1} . However, in terms of productivity at the operating point with maximum capacity utilization, CaptureSMB shows a vastly superior performance, yielding $16.8 \text{ mg mL}^{-1} \text{ h}^{-1}$ compared to only $1.80 \text{ mg mL}^{-1} \text{ h}^{-1}$ in the batch case.

The difference in capacity utilization is due to the fact that in order to run CaptureSMB, a preload is required that occupies a fraction of the capacity in steady state operation, effectively decreasing the amount of new product that can be loaded per cycle, which is the basis for the calculation of the capacity utilization. In all cases, the specific buffer consumption is comparable between the two processes. At maximum productivity, the CaptureSMB process shows slightly lower buffer consumption than batch (0.766 mL mg^{-1} compared to 0.813 mL mg^{-1}), while at maximum capacity utilization, the CaptureSMB process utilizes slightly more buffer (0.640 mL mg^{-1} compared to 0.584 mL mg^{-1}).

3.5.4 Pareto optimal operating points and influence of column length

It becomes apparent that there is a trade-off between maximizing capacity utilization (i.e. minimizing resin consumption) and maximizing productivity (i.e. speeding up the process). Using the algorithms detailed in 3.5.3, it is possible to generate pareto-curves, on which all points are equally optimal when taking into account both objectives. These curves allow for the complete and exhaustive comparison between the two processes.

A set of pareto-optimal points in the capacity utilization / productivity plane are shown in Figure 3.5. In particular, we consider the batch process with column lengths of 5, 10 and 20 cm and CaptureSMB processes with single column lengths of 5 and 10 cm, at a constant feed concentration of 1.2 mg mL^{-1} . This allows us to estimate the effect of column length on the performance of the processes. In all cases, the pareto curves of different column lengths cross, which means that with short columns, a higher maximum productivity can be achieved, while with long columns it is easier to achieve higher capacity utilization. It is simple to show mathematically that the gradient of the objectives is non-zero in the domain of the operating parameters, therefore at each optimal point, at least one constraint must be active. In all points along the pareto curve, the active constraint was the breakthrough constraint (see equation 3.9). In addition, at the high-productivity end of the pareto curves, the pressure drop constraint became active.

It is clear that, except at very low productivity, CaptureSMB always dominates batch processes with the same or higher column lengths and is therefore an improvement in terms of both capacity utilization and productivity. Additionally, CaptureSMB enables operating points with productivity values far above the maximum possible productivity in batch mode, while simultaneously maintaining high

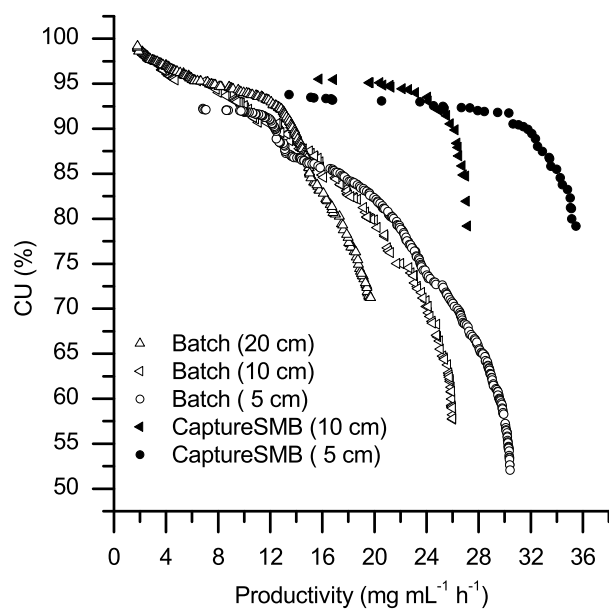


Figure 3.5: Pareto-optimal operating points for the batch process (open symbols) and the CaptureSMB process (full symbols) with different column lengths. In the CaptureSMB case, the column length refers to the length of a single column.

capacity utilization and therefore increasing the load and the outlet concentration. It can be seen that in the batch case, it is always possible to run the process at such low flow rates that the capacity utilization tends to 100%, regardless of column length, but this leads to very low productivity values. In the CaptureSMB process, a preload is needed; therefore there is a difference in maximum capacity utilization between the different column lengths, albeit very small. So in cases where very low productivity, i.e. almost 10 times lower than the maximum achievable productivity, is acceptable, and very high capacity utilization, i.e. close to 100%, is needed, the batch process is preferred over the CaptureSMB process.

When examining the change of the operating parameters t_{IC} , Q_{IC} , and Q_B along the pareto front of the CaptureSMB process, one finds that with increasing productivity, the interconnected loading flow rate Q_{IC} is increasing, while the interconnected time is decreasing. Since there is a trade-off between the objectives, increasing the capacity utilization leads to the inverse behavior, namely longer loading times but smaller loading flow rates. The batch loading flow rate Q_B increases only very slightly with productivity (and hence decreases with increased capacity utilization) over the pareto front. Figure 3.6 displays a graph visualizing these behaviors.

3.5.5 Concluding remarks

In this work we compared batch and CaptureSMB for a mAb capture using a protein A resin in terms of capacity utilization, that is how much product can be processed per resin volume and load/elute cycle, and productivity, that is how much product can be processed per resin volume and per time, at constant yield and purity. A dual loading flow rate strategy was used in both processes. A model for the description of both batch breakthrough experiments and continuous capture processes for protein A chromatography has been developed and verified. In order to fit the model, only a small number breakthrough experiments at different

flow rates (and different concentrations, if desirable) in batch mode are needed, requiring only a small amount of feed. The resulting model has been validated for the CaptureSMB process and is a useful tool in predicting the performance in different operating points and optimizing the processes.

Using the model, a batch capture process and the twin-column CaptureSMB process have been optimized with respect to two different objectives, capacity utilization and productivity, with constant yield and purity. Due to the trade-off between the two objectives, pareto-fronts have been identified for both processes. Judging from these fronts, the CaptureSMB process shows an increase in productivity of around 40% at a given capacity utilization and an increase in capacity utilization of around 25% at a given productivity, compared to a batch process with the same total resin volume. In general, the CaptureSMB process shows better performance than the batch process, except if a very low productivity value (less than 10% of the maximum possible value) is admissible; in these cases the batch process shows slightly higher maximum capacity utilization than the CaptureSMB process.

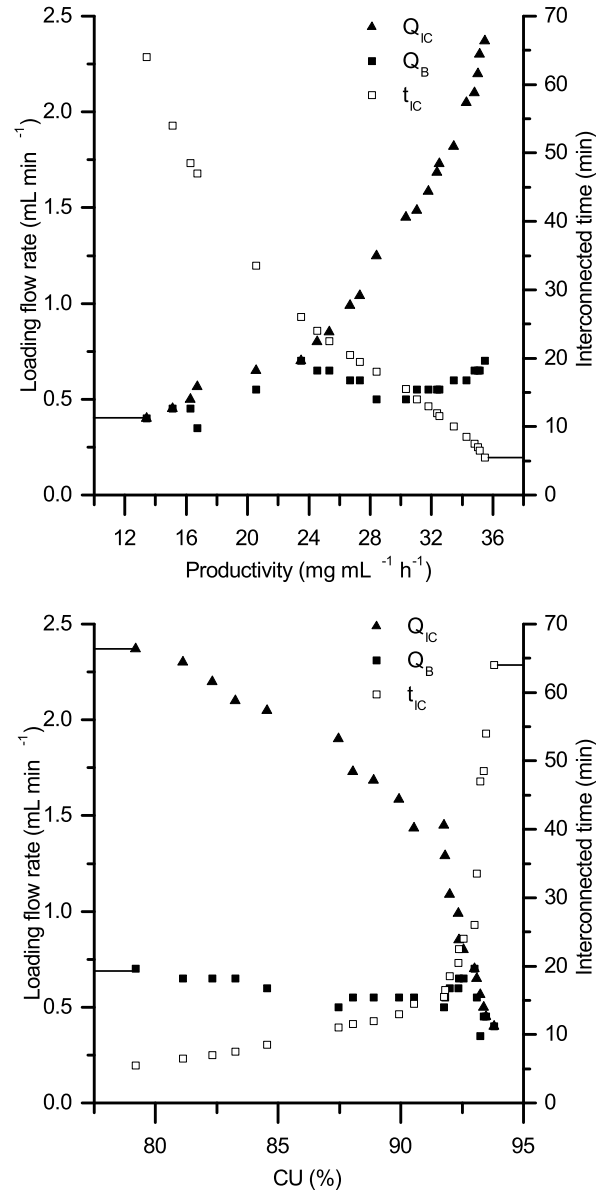


Figure 3.6: Change of operating parameters along the pareto front for the 5 cm CaptureSMB case. Dependence on productivity is shown in the top panel, dependence on capacity utilization in the bottom panel. The loading flow rates (Q_{IC} and Q_B) are plotted as full symbols on the left axes, the interconnected loading time (t_{IC}) is shown on the left axis as empty symbols.

Chapter 4

Comparison of batch and continuous multi-column protein A capture processes by optimal design

4.1 Introduction

Due to their fast growing market share and high value, monoclonal antibodies (mAbs) are one of the most important classes of biopharmaceuticals today [36]. Rapid progress in cell line development, resulting in greatly increased fermentation productivity and titers [2,87] has increased the output of existing bioreactors and prompted the use of smaller fermenters and flexible manufacturing for new products. These developments require high-productivity, flexible downstream processes. Continuous upstream has become an attractive option in many cases, triggering the use of continuous downstream processes. In order to fulfill these requirements, novel downstream processes have been developed in the recent years,

specifically in the field of chromatography, which is still the main process step in downstream purification [86, 88]. While the use of SMB technology has a long history in downstream processing [28, 89, 90], its operating principles (binary separation, many columns) make it generally a sub-optimal choice for affinity capture or polishing steps, where usually a ternary separation must be carried out. The new continuous chromatographic processes operate with two or more identical columns, enabling also counter-current principles. For polishing steps, multi-column counter-current solvent gradient purification (MCSGP) [52, 59, 60, 65], has been successfully used and displayed superior performance compared to batch chromatography. It has been shown that for protein A capture of mAbs, it can be advantageous to use multi-column setups, rather than batch chromatography, such as the twin-column CaptureSMB process (which is semi-continuous when an interconnected wash is applied) [43] or continuous processes with more columns, such as sequential multi-column chromatography (SMCC) processes [48, 49], or periodic counter-current (PCC) processes with interconnected wash, which are typically run with 3 or 4 columns [46, 47], or the BioSMB process, which uses up to 12 columns [50]. In general, counter-current chromatography offers several advantages, mainly increased productivity, better resin utilization and smaller specific buffer consumption, but these come at the price of higher hardware complexity and increased investment cost [91].

Common among these multi-column setups is that the product breakthrough of one column is directed into another column to adsorb, allowing the use of higher loading flow rates and loading times without compromising yield by product breakthrough. This leads to higher productivity and higher loadings of the resin. Resin capacity utilization is proportional to product pool concentration and inversely proportional to buffer consumption and resin costs [43].

For many years, modeling has been a valuable tool for understanding and optimiz-

ing these multi-column processes, precisely because of the high investment costs and typically the high value of the products involved [72, 74]. A novel modeling approach for the diffusive behavior of the monoclonal antibodies inside the affinity resin particles, based on a shrinking core model, is applied here. It has been shown above that fitting batch breakthrough experiments is sufficient for predicting the performance of the CaptureSMB process (see section 3.5.1, page 42). With the column model available, the capture process can be laid out in order to maximize two objectives: Productivity, that is mAb produced per column volume and time, and capacity utilization, that is how much mAb is loaded onto the columns compared to the maximum theoretically possible amount. It is possible to identify operating points biased towards one or the other objective, depending on manufacturing needs or cost targets. In this work we show that the trade-off is present for all investigated processes with 1-4 columns. Comparing the processes under these important aspects might shed some light on their advantages, disadvantages and usefulness for capture applications.

4.2 Process descriptions

As an example capture problem in this work, the purification of an IgG₁ monoclonal antibody (mAb) from clarified cell culture harvest is considered. The processes examined here are: single-column batch capture, twin-column CaptureSMB [43], and periodic counter-current (PCC) processes with interconnected wash step with three (3-C PCC) and four (4-C PCC) columns [46, 71] (Figure 4.1). Note that the recovery and regeneration phase can be optimized separately and is independent of the process type. The total column volumes of buffers used in the different steps of the recovery and regeneration phase are assumed to be the same in all processes. Moreover it was assumed that the same recovery and regenera-

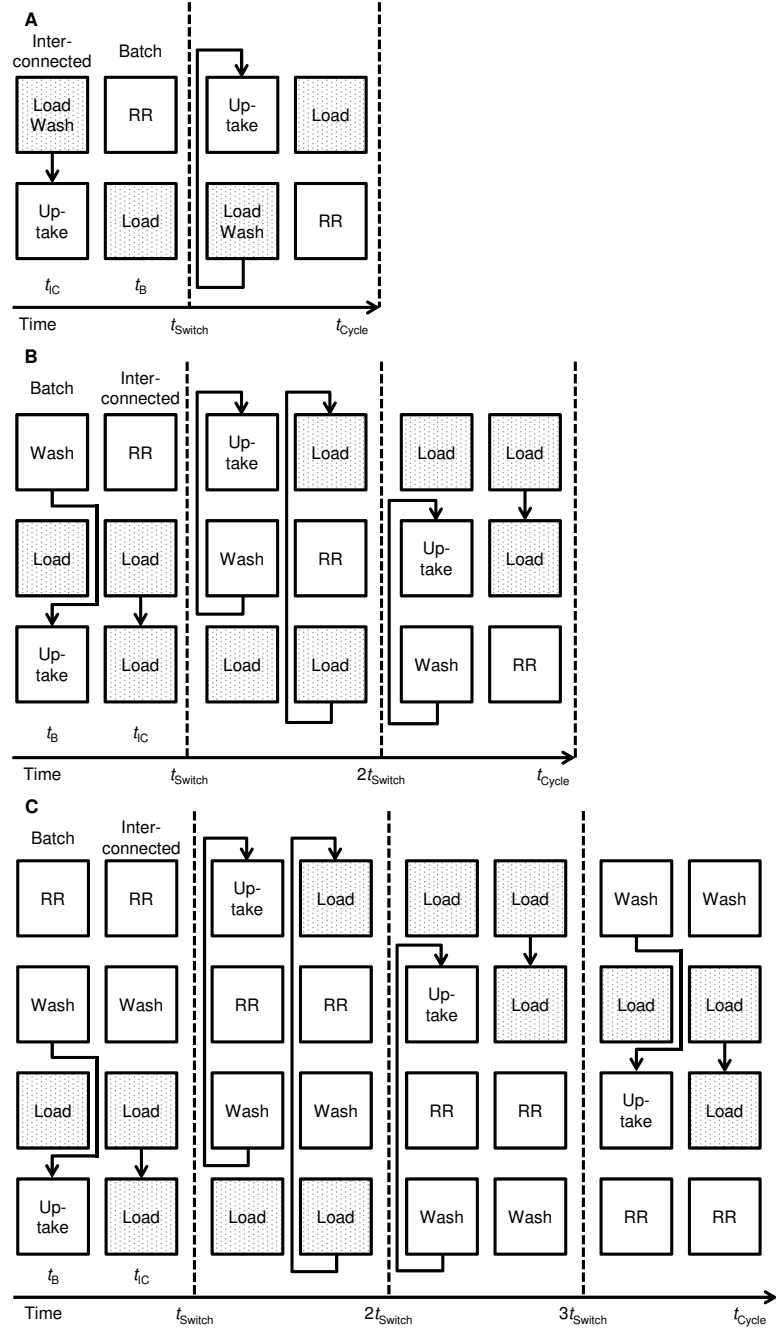


Figure 4.1: Flow chart of the multi-column processes. Panel A (top): CaptureSMB; Panel B (middle): 3-column PCC; Panel C (bottom): 4-column PCC. For each process, an entire cycle is shown.

tion protocol was used in every cycle. Therefore, it is not part of the optimization considered in this work. All flow rates of the recovery and regeneration phase that are not associated with loading, namely interconnected wash, wash, elution and equilibration, are assumed to be run at a constant flow rate Q_{RR} of 1.5 mL min^{-1} (corresponding to a linear velocity of 450 cm h^{-1}). The cleaning in place (CIP) step uses a constant contact time, i.e. its duration is independent on column size. The described processes have in common that steps with sequential loading of two columns and steps with single column loading alternate, each pair of these steps is referred to as “switch” in the following. However, in 3C- and 4C-PCC processes, the interconnected loading step and the recovery and regeneration procedure run simultaneously while in CaptureSMB they run sequentially.

4.2.1 CaptureSMB

The CaptureSMB process uses two columns, as shown in the process schematic in Figure 4.1 (panel A, top). A detailed description is available in [43]. During the interconnected phase, which has the duration t_{IC} , the columns are loaded in series, with the flow rate Q_{IC} . After the load, a first interconnected wash step is performed to flush any protein still present in the liquid phase into the second column. After this wash step, the first column is fully loaded and the columns are disconnected. While the first column enters the recovery and regeneration procedure the second column continues to be loaded. This step is denoted as the “batch” phase, with a duration of t_B , and a loading flow rate of Q_B for the second column. Three variables are used to design the process (t_{IC} , Q_{IC} and Q_B), with the constraint that no breakthrough should occur, ensuring high yield in all operating points. Since the first column undergoes recovery and regeneration during the batch phase, the duration of this step, t_B , is fixed by the recovery and regeneration protocol, which ensures constant purity and product quality.

4.2.2 3-column PCC (3-C PCC)

The 3-column PCC process uses three identical columns. A process schematic, adapted from [42], can be found in Figure 4.1 (middle panel B). A different 3-C PCC process has been published by the same group in [71], however in this work we refer to the newer process. The first part of a switch consists of an interconnected wash step where the first, fully loaded column is washed and the wash is recycled into the third column, while the second column is loaded in a disconnected mode. Since the feed is applied to a disconnected column, this phase is denoted as the batch phase, with the duration t_B and the feed flow rate Q_B . When the interconnected wash step is finished, the first and the third column are disconnected and the first column continues in the recovery and regeneration procedure, with further wash steps, the elution, the CIP and the equilibration step. In the meantime, the two other columns are loaded in an interconnected manner using a flow rate Q_{IC} ; therefore this part of the switch is called the interconnected phase, which lasts for the time t_{IC} . After the interconnected phase is complete, all columns are moved one position upstream relative to the liquid phase flow, which denotes the beginning of a new switch. When three switches have passed and the columns are back in the initial configuration, one cycle has passed.

The duration of the interconnected wash dictates the duration of the batch step. The duration of the recovery and regeneration procedure, which happens during the interconnected phase, puts a lower bound on the duration of this step, since it is permitted to load for a longer time than it takes to wash, elute, clean and equilibrate one column. It is therefore permitted that the first column is inactive for certain periods of time following recovery and regeneration. The 3-column PCC process has three degrees of freedom, namely the two loading flow rates Q_B and Q_{IC} and the interconnected loading time t_{IC} .

4.2.3 4-column PCC (4-C PCC)

The 4-column PCC process uses four identical columns that are loaded and eluted sequentially [46]. A process schematic can be found in Figure 4.1 (bottom panel C). In the setup investigated in this work, there are two different steps, during which different columns are interconnected. In the first part of the switch, the column in the first position, which has been washed in the previous switch, is eluted. Meanwhile, the second column undergoes the first part of the wash step, during which product from the liquid phase of the first column is directed to the cleaned and regenerated column in the last position. During this time, the column in the third position is disconnected and loaded with feed with a flow rate of Q_B . Since the loading happens in a single column batch manner in this part of the switch, it is denoted as the batch phase, which has the duration t_B . When the interconnected part of the wash step is completed, the second column is disconnected and the recovery and regeneration continues. Product elution from the first column finishes during this phase, and CIP and regeneration follow. Meanwhile, the other two columns are interconnected and feed is applied to the third column, with a different flow rate Q_{IC} . After this, one switch has passed and the columns are moved one position upstream. Because the feed is applied to two interconnected columns in this part of the switch, it is denoted as the interconnected phase with a duration of t_{IC} . Since the interconnected wash step is fixed, the duration of the batch step, t_B , is fixed. However, it is again permitted to load for a longer time than it takes to clean and equilibrate a column and the first column is permitted to be inactive after regeneration, so there is a only lower bound on the interconnected time t_{IC} . Therefore, the 4-column PCC process has three degrees of freedom, namely the two loading flow rates Q_B and Q_{IC} and the interconnected time t_{IC} .

4.3 Materials and methods

The cell culture supernatant used in the experimental parts of this study was produced at ETH Zurich by continuous fermentation and contained a monoclonal IgG₁-type antibody in concentrations between 0.20 and 0.75 mg mL⁻¹. For the breakthrough experiments at higher concentrations, clarified cell culture supernatant with a concentration of 0.3 mg mL⁻¹ was spiked with elution product of previous capture runs to obtain feed concentrations of 1.5 mg mL⁻¹ and 2.5 mg mL⁻¹. As stationary phase, MabSelect SuRe (GE Healthcare Life Sciences), in pre-packed columns of dimensions 0.5 x 5 cm (Atoll, Weingarten, Germany) was used for all experiments. Two such columns were joined in series to form columns with bed heights of 10 cm. The preparative conditions and analytical method (analytical protein A chromatography) were the same as reported in sections 3.3.3 (page 34) and 3.3.4, (page 34) with two differences in the preparative part: The duration of the CIP step was varied as a process variable, and recovery and regeneration was always performed at maximum flow rate, therefore $Q_{RR} = Q_{max}$.

4.3.1 Process model

Since adsorption of mAbs on protein A ligands is very fast compared to diffusion through the resin particles, the radial profile of adsorbed protein in the particles shows a very steep front, as has been shown in theory and also experimentally by confocal x-ray spectroscopy [92–96]. This property is used as a basis for a model that avoids completely the radial discretization of the resin particles. Shrinking core models have been proposed previously for catalyzed chemical reactions in porous particles [97], and the analogy between a fast chemical reaction and an adsorption process justifies its use in chromatography. Therefore, the same approach is used to describe the moving front of adsorbed protein.

4.3.2 Shrinking core adsorption model

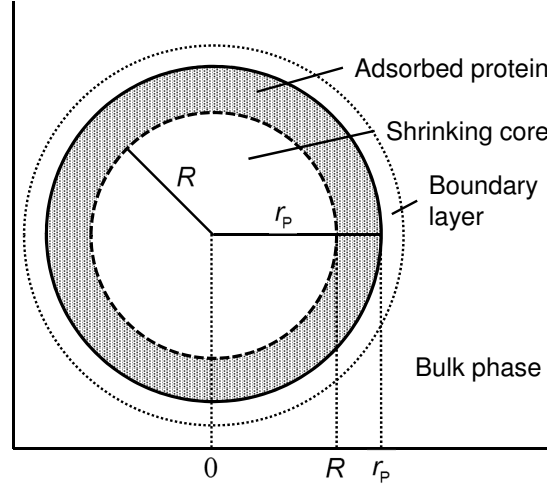


Figure 4.2: Visualization of the moving front inside a resin particle according to the shrinking core model.

According to the shrinking core model, the protein has to diffuse through a stagnant film between the bulk phase and the solid phase particle, and a layer of antibody-saturated protein A sites of thickness $r_p - R$, where r_p is the resin particle radius and R is the radial position of the antibody front progressing through the particle, before adsorbing on a free protein A adsorption site. This process is visualized in Figure 4.2. The total mass transfer coefficient is therefore given as a combination of these two contributions:

$$k_{\text{tot}} = \left(\frac{1}{k_F} + \frac{1}{k_S} \right)^{-1} \quad (4.1)$$

where k_F is the film mass transfer coefficient and k_S is the pore mass transfer coefficient. By combining the fact that the molar flow rate of the protein through the saturated layer is constant, and by using a linear driving force assumption, the following expression can be used to calculate the pore mass transfer coefficient (*more*

details in *F. Steinebach et al., in review*) [97]:

$$k_S = D \frac{(1 - \alpha)^{1/3}}{1 - (1 - \alpha)^{1/3}} \quad (4.2)$$

where $D = \epsilon_P D_E / r_P$ is a fitting parameter that is related to the pore diffusion coefficient for diffusion through saturated pores D_E and α is the fraction of total adsorption sites occupied, i.e.

$$\alpha = \frac{q_1}{q_{\text{Feed}}^*} = \frac{q_1}{q_{\text{sat}}} \frac{1/K_D + c_{\text{Feed}}}{c_{\text{Feed}}} \quad (4.3)$$

where q_1 is the solid phase concentration on the first adsorption site (see equation (4.6)), q_{Feed}^* is the equilibrium solid phase concentration of protein at feed concentration, q_{sat} is the saturation capacity of the resin, c_{Feed} is the protein concentration in the feed and K_D is the equilibrium constant of the adsorption process.

The film mass transfer coefficient k_F on the other hand can be estimated from a classical semi-empirical correlation [86]:

$$k_F = \frac{D_0}{2r_P} \cdot \frac{1.09}{\epsilon_B} \left(\frac{2r_P u}{D_0} \right)^{1/3} \quad (4.4)$$

where D_0 is the protein diffusivity in free solution, ϵ_B is the porosity of the packed bed and $u = Q/A_{\text{Col}}$ is the superficial velocity, where Q is the volumetric flow rate, and A_{Col} is the column cross sectional area.

The intra-particle liquid phase is therefore described by the equilibrium with the bulk liquid phase and the adsorption terms:

$$\frac{\partial c_P}{\partial t} = \frac{3k_{\text{tot}}}{r_P} (c - c_P) - \phi_P \cdot \left(\frac{\partial q_1}{\partial t} + \frac{\partial q_2}{\partial t} \right) \quad (4.5)$$

where c_P is the intra-particle liquid phase concentration, c is the bulk liquid phase

concentration, $\phi_P = (1 - \epsilon_P) / \epsilon_P$ is the particle phase ratio, where ϵ_P is the particle porosity, and q_i are the adsorbed phase concentrations for each adsorption site. The particle porosity, and therefore the intra-particle liquid phase volume, is assumed to be independent of adsorption and therefore constant.

For immobilized recombinant protein A ligands two to three adsorption sites are actually available per ligand [86], and since the adsorption rate constant decreases with increasing number of mAbs bound to a ligand due to steric hindrance, only the first two adsorption possibilities are taken into account here. This leads to the following expressions for the change in adsorbed phase concentrations [44]:

$$\begin{aligned}\frac{\partial q_1}{\partial t} &= k_{A,1} \left[c_P (q_{\text{sat}} - q_1) - \frac{q_1}{K_D} \right] \\ \frac{\partial q_2}{\partial t} &= k_{A,2} \left[c_P (q_1 - q_2) - \frac{q_2}{K_D} \right]\end{aligned}\tag{4.6}$$

where $k_{A,i}$ are the adsorption rate constants for two sites. Note that in the formula for the second adsorption site, the current concentration of the first site appears in place of the saturation capacity. This reflects the fact that the second site is a hindered site, which can only be occupied when a mAb is already adsorbed on the first site.

4.3.3 Column model

As in the standard lumped kinetic model, the equations above describing the adsorption process are combined with the transport equations for the liquid phase [72]:

$$\frac{\partial c}{\partial t} = -v \frac{\partial c}{\partial x} + D_L \frac{\partial^2 c}{\partial x^2} - \frac{3k_{\text{tot}}}{r_P} (c - c_P) \quad t \in [0, t_{\text{Switch}}], x \in [0, L_{\text{Col}}] \tag{4.7}$$

where t denotes the time, $v = u/\epsilon_B$ is the interstitial velocity, x is the coordinate along the longitudinal axis of the column, D_L is the apparent axial dispersion coefficient, and L_{Col} is the bed height of one column.

These partial differential equations are subject to the following boundary conditions and initial conditions:

$$\begin{aligned}
c(t=0, x) &= c_0(x) \\
c_P(t=0, x) &= c_{P,0}(x) \\
q_i(t=0, x) &= q_{i,0}(x) \\
c(t, x=0) &= c_{in}(t) + \frac{D_L}{v} \frac{\partial c}{\partial x} \Big|_{x=0} \\
\frac{\partial c}{\partial x} \Big|_{x=L_{Col}} &= 0
\end{aligned} \tag{4.8}$$

The apparent axial dispersion coefficient was estimated as described in section 3.4.1 (page 35), and the same solution procedure was used to solve the system of partial differential equations.

4.3.4 Process performance measures and optimization problem

Apart from impurity clearance, the three most important performance measures in preparative affinity chromatography are yield, productivity and capacity utilization. Since the main factors influencing product purity are the type of stationary phase and the recovery and regeneration protocol, it is not modeled and considered constant and in specification for all investigated processes. Yield and productivity by contrast are strongly influenced by the operating parameters, namely the flow rates and durations of the different process steps, and they are properly calculated in the model. In capture processes, columns are typically not fully loaded

since this would compromise yield. In batch capture of monoclonal antibodies for example, 90% of the volume corresponding to 1% breakthrough [46] is loaded to ensure maximum and constant yield. Since this does not directly translate to multi-column processes and different implementations of a safety factor will make a fair comparison difficult, the constraint applied for all processes in this work is that the breakthrough value of a disconnected column must not exceed 1%. This assures a high yield value for all processes considered.

Flow rate constraints were implemented based on product information provided by the manufacturer. For MabSelect SuRe a maximum linear velocity of 500 cm h⁻¹ is reported, resulting in a maximum flow rate of $Q_{\max} = 1.67 \text{ mL min}^{-1}$ (GE Healthcare, Data file 11-0011-65 AC, retrieved online 07/2014).

It is important to highlight that the processes described were not optimized under a feed continuity constraint as described in [42] for full integration with continuous upstream manufacturing without an intermediate balancing container. Instead, a setup as described in [71] was assumed, with a balancing container (“surge bag”) at the interface of upstream and downstream processing. This setup requires only the average inflow and outflow of the container to be equal, allowing flexible feed flow rates on the side of the downstream capture, i.e. different feed flow rates in the interconnected and batch phases of multicolumn capture, allowing better process performance. Moreover this setup appears advantageous from a risk perspective. It also covers the state-of-the-art mAb fed-batch fermentation, where the entire harvest becomes available at a certain point in time. Due to the risk of product degradation, this scenario requires the harvest to be processed within a certain time period, typically around 24 hours, however this capture mode does not require the feed flow rate to be constant. The first optimization target is productivity, which is defined as the amount of product produced per resin volume

and unit time, can be written as follows for all processes:

$$P = Y \cdot \frac{c_{\text{Feed}} (t_{\text{IC}} Q_{\text{IC}} + t_{\text{B}} Q_{\text{B}})}{n_{\text{Col}} V_{\text{Col}} (t_{\text{IC}} + t_{\text{B}})} \quad (4.9)$$

where Y is the process yield, c_{Feed} is the mAb concentration in the feed, n_{Col} is the number of columns the process uses, and V_{Col} is the volume of one column. Note that for batch chromatography, there is no interconnected phase, and the recovery and regeneration time has to be added to the switch time in the denominator.

The second optimization target is the capacity utilization CU , which is defined as the actual load per cycle divided by the maximum possible load. Therefore, the higher the capacity utilization, the more antibody can be produced per volume of resin before the resin needs to be replaced, since fewer load and elute cycles are needed to process a given amount of antibody. Thus, higher capacity utilization leads to lower resin costs. The capacity utilization can be calculated as follows:

$$CU = Y \cdot \frac{c_{\text{Feed}} (t_{\text{IC}} Q_{\text{IC}} + t_{\text{B}} Q_{\text{B}})}{(1 - \epsilon_{\text{B}}) V_{\text{Col}} q_{\text{max}}} \quad (4.10)$$

where q_{max} is the maximum possible amount that could theoretically be loaded per column volume at a given feed concentration, which can be calculated as follows:

$$q_{\text{max}} = \frac{c_{\text{Feed}}}{(1/K_{\text{D}} + c_{\text{Feed}})} q_{\text{sat}} \quad (4.11)$$

Summarizing the constraints and objectives discussed above, the following optimization problem can be formulated:

$$\begin{aligned}
& \max_x && P(x), CU(x) \\
& \text{subject to:} && c(x = L_{\text{Col}}) \leq 0.01c_{\text{Feed}} \\
& && Q \leq Q_{\text{max}} \\
& && 0 < x \\
& && t_{\text{RR}} \leq t_{\text{IC}}
\end{aligned} \tag{4.12}$$

where x are the degrees of freedom of the capture process with $x = [t_{\text{B}}, Q_{\text{B}}]$ as the degrees of freedom for batch single column chromatography and $x = [Q_{\text{B}}, t_{\text{IC}}, Q_{\text{IC}}]$ as degrees of freedom for the multicolumn processes. Note that the first constraint $c(x = L_{\text{Col}}) \leq 0.01c_{\text{Feed}}$ is, as mentioned above, effectively a yield constraint that applies only for columns that are being loaded and have no column connected to their outlet. This effectively assures that the first column in the loading zone is loaded to a very high breakthrough value (typically above 60%) as well. The last constraint $t_{\text{RR}} \leq t_{\text{IC}}$ only applies to the 3- and 4-column PCC processes. For numerical optimization, a multi-objective genetic algorithm, i.e. a modified version of the third iteration of the generalized differential evolution algorithm (GDE3) was used [45].

4.4 Results and discussion

4.4.1 Model fitting of batch protein A breakthrough curves

From the breakthrough experiments described in the materials and methods section. the parameters D , $k_{\text{A},1,2}$, K_{D} , and q_{sat} , used in equations (4.2), (4.3) and (4.6) can be estimated. This is done by minimizing the sum of square errors using

the GDE3 algorithm. 13 breakthrough curves at 3 different linear velocities between 150 and 450 cm h⁻¹ (resulting in flow rates between 0.5 and 1.5 mL min⁻¹), and 5 different feed concentrations between 0.2 and 2.5 mg mL⁻¹ were used to fit the model parameters. The data set includes columns of bed heights of 5 and 10 cm. A full list of all the parameters and their value is reported in Table 4.1. The intra-particle diffusion coefficient k_S and the film mass transfer coefficient k_F obviously depend on the solid phase and feed concentrations, and the current flow rate, respectively. The values of the intra-particle diffusion coefficient k_S were typically in the range of 0.001 cm min⁻¹, while the film mass transfer coefficient k_F was typically in the range of 10 cm min⁻¹. Therefore, as expected in protein chromatography, intra-particle diffusion was the rate limiting step. Several breakthrough curves with fitted model results are displayed in Figure 4.3. Clearly the model is applicable for simulating breakthrough curves at different flow rates and different feed compositions, and can accurately account for different column lengths. The root mean square error in each experiment was in the range of 1.20 to 3.98 percentage points, averaging at 2.49 percentage points. As expected in protein A chromatography, the isotherm resulting from the fitted parameters is nearly rectangular. The isotherm is shown in Figure 4.4.

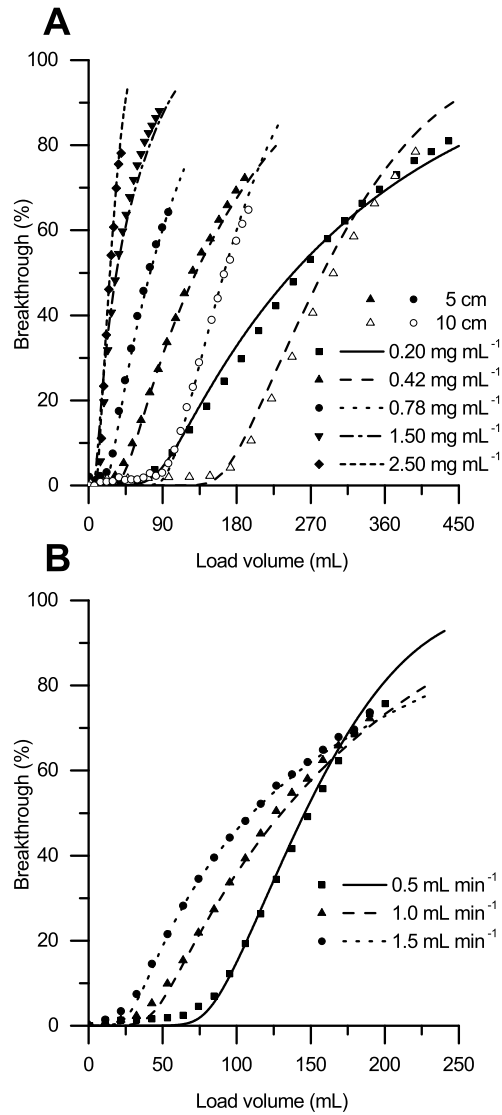


Figure 4.3: Top panel (A): Experimental breakthrough curves at different feed concentrations (symbols) compared with simulation data (lines). The feed flow rate was 1.0 mL min^{-1} (300 cm h^{-1}) for feed concentration below 1.0 mg mL^{-1} , 1.5 mL min^{-1} for the curve at 1.5 mg mL^{-1} and 0.75 mL min^{-1} (225 cm h^{-1}) for the curve at 2.5 mg mL^{-1} . Bottom panel (B): Experimental breakthrough curves at different feed flow rates (symbols) compared with simulation data (lines). The feed concentration was 0.42 mg mL^{-1} , the bed height was 5 cm and the column diameter was 0.5 cm in all cases.

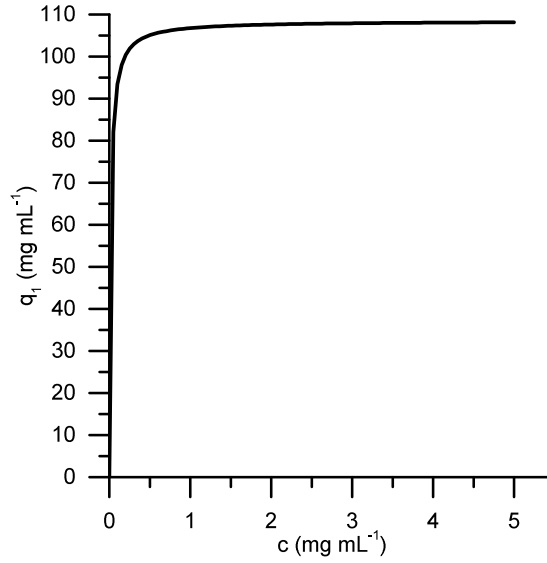


Figure 4.4: Isotherm for the first adsorption site computed from the parameters given in Table 4.1. As expected for protein A chromatography, the isotherm is nearly rectangular.

4.4.2 Operational parameters considered for optimization

Along with the optimization, the influence of four different operational parameters on the optimal operating points of the capture processes was examined: The cleaning-in-place contact time, the number of column volumes used in the interconnected wash step, the bed height of a single column and the feed concentration. An overview of the cases examined is reported in Table 4.2. In a first scenario, the processes were optimized for cleaning (CIP) durations of 15, 30 and 60 min. In a second scenario the optimization was done for washing in series (interconnected) for 0, 3 and 6 CV, respectively. In a third scenario, the optimization was done for feed concentrations of 0.5, 1.5, 2.5, and 5.0 mg mL⁻¹. In the base case, for which a CIP time of 30 minutes, 3 column volumes interconnected wash and a feed concentration of 1.5 mg mL⁻¹ was used, bed heights of 5 and 10 cm were considered, which results in loading zone bed heights of 5, 10 or 20 cm. Since

Table 4.1: Parameters fitted from pulse injections, breakthrough curves at different flow rates and concentrations, with 95% confidence intervals.

Parameter	Symbol	Units	Estimate
Intercept of van Deemter curve	A	–	0.3535 ± 28.1
Bed porosity	ϵ_B	–	0.36
Particle porosity	ϵ_P	–	0.52
Intra-particle mass transfer coefficient	$D = D_E/R$	cm min^{-1}	$2.227 \cdot 10^{-3} \pm 5.54 \cdot 10^{-4}$
Adsorption rate constant	$k_{A,1}$	$\text{mL mg}^{-1} \text{ min}^{-1}$	$6.771 \cdot 10^4 \pm 0.969 \cdot 10^4$
Adsorption rate constant	$k_{A,2}$	$\text{mL mg}^{-1} \text{ min}^{-1}$	$3.179 \cdot 10^4 \pm 0.771 \cdot 10^4$
Adsorption equilibrium constant	K_D	mL mg^{-1}	61.47 ± 1.73
Saturation capacity per column volume	q_{sat}	mg mL^{-1}	69.44 ± 0.542

columns with bed heights of less than 10 cm are generally not considered to be reproducibly packable at large scale, and minimal single column bed height appears to be optimal because this shortens the recovery and regeneration procedure, the investigation of the effect of changing the operational parameters was limited to 10 cm columns. Any scaling up can then be done by increasing the column diameter, which is not expected to have any impact on process performance unless radial flow distribution becomes an issue [86].

Table 4.2: Operational parameters considered in the optimization.

	t_{CIP} [min]	IC Wash [CV]	c_{Load} [mg mL ⁻¹]
Low value	15	0	0.5
Base case	30	3	1.5
High value	60	6	2.5
Extrapolation	30	3	5.0

4.4.3 Base case optimization results in productivity / capacity utilization trade-off for all processes

Figure 4.5 shows pareto-optimal operating points in the capacity utilization (CU) versus productivity plane for the base case, at fixed purity and yield values. The data confirms the expected trade-off of operating with high productivity but low capacity utilization or at high capacity utilization but low productivity. In terms of column bed heights, it is evident that with 5 cm bed height columns, a higher maximum productivity per column volume can be achieved than with 10 cm bed height columns for all processes. When comparing the different processes, the batch process is clearly inferior to the multi-column processes in terms of capacity utilization, but can achieve a similar maximum productivity value, although at the expense of a strong decrease in capacity utilization. Among the multi-column processes, the 4-column PCC process shows the worst performance, because more

capacity utilization is lost when increasing the productivity. The CaptureSMB and 3-column PCC processes can achieve a similar maximum productivity, which is the highest maximum productivity for both bed heights. The multi-column processes all show a similar maximum capacity utilization close to 100%, independent of bed height. These operating points at high capacity utilization of course exhibit a corresponding decrease in productivity. In all cases considered, the pareto-fronts show the same behavior in terms of process constraints: Each and every pareto-optimal point has exactly 1% breakthrough (see equation (4.12)), which is obvious because as long as the breakthrough constraint is not active, one can simply load faster (increasing productivity) or more (increasing capacity utilization). The end points of the pareto-curves are marked by any other constraint becoming active: At maximum capacity utilization (and minimum productivity), the loading flow rates reach the lower bounds (set at 0.01 mL min^{-1} to avoid points where nothing is loaded at all), or the capacity utilization approaches 100%, where no further benefit can be gained by reducing the productivity. On the other hand, at maximum productivity (and minimum capacity utilization), either the maximum loading flow rate is reached, or, in the case of the multi-column processes, the minimum loading time due to the additional constraint that the regeneration of one column must be finished when a switch ends. Note that this minimum time is higher in the 3-column PCC process than in the 4-column PCC process, because the recovery and regeneration step is spread out over fewer columns, leading in some cases to abrupt stops in the pareto-curves. In the case of CaptureSMB, the fixed loading time in the batch phase is generally less of a concern because its impact can be diminished by reducing the batch loading flow rate. In any case, if the minimum loading time is reached before the maximum loading flow rate is reached, any attempts to increase the productivity by increasing the loading flow rate or the loading time will simply result in yield loss, because the breakthrough

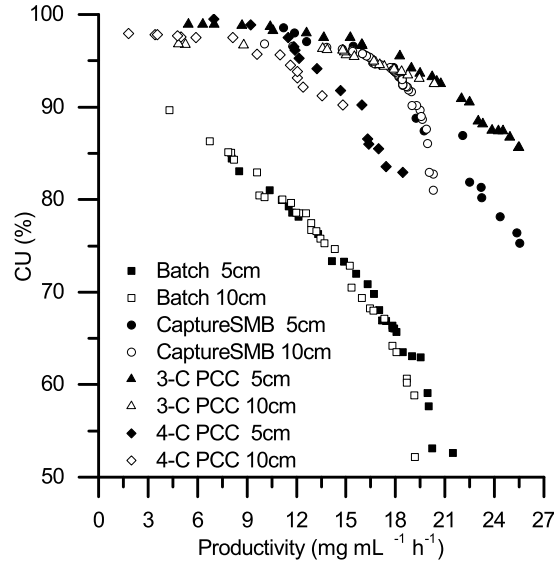


Figure 4.5: Pareto-optimal operating points (at fixed yield and purity) for the base case ($t_{CIP} = 30$ min, $Wash_{IC} = 3$ CV, $c_{Feed} = 1.5$ mg mL⁻¹). Filled symbols show results for 5 cm single column bed height, empty symbols show the results for 10 cm single column bed height.

constraint is already active, therefore negating any possible gains in productivity. This behavior is illustrated in Figure 4.6. Different operating conditions may change the exact position of the steep drop relative to the optimum, but in no case is this kind of yield loss avoidable. The model predicts an average increase in productivity of 39% when going from batch to CaptureSMB, which is in good agreement with the values reported in [43], where an average increase of 37.5% was found, albeit for a different IgG₁-type antibody. At high loading flow rates, which corresponds to operating points with high productivity, an average increase in capacity utilization of around 46% is predicted by the model, which corresponds well to the value of 42% that has been reported in [43].

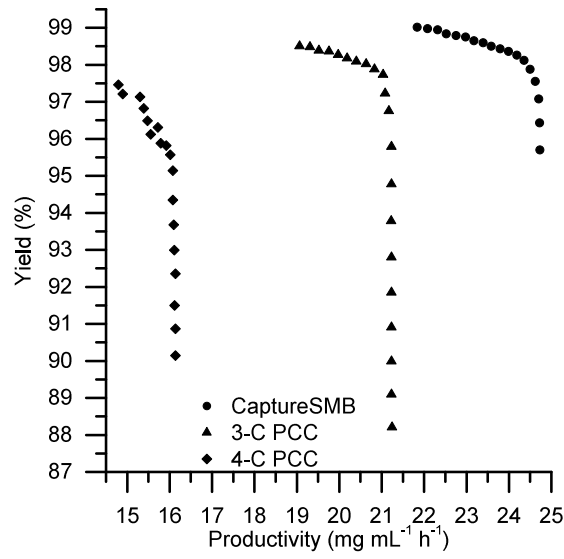


Figure 4.6: Yield loss caused by attempting to increase the productivity beyond the maximum found in the pareto-optimization for $t_{CIP} = 30$ min, $Wash_{IC} = 3$ CV, $c_{Feed} = 2.5$ mg mL⁻¹ and 10 cm single column bed height. It is obvious that increasing the productivity beyond a certain value is impossible for each process because the yield decreases proportionally, effectively nullifying all possible gains.

4.4.4 Influence of CIP time

In the subsequent optimizations starting from the base case, the CIP time was varied. As can be seen in Figure 4.7 (top, panel A), an increased CIP contact time leads to decreased maximum productivity in all processes. This is expected, as cleaning is “not productive” in the sense that no product is loaded or eluted during cleaning. It must be noted that the maximum capacity utilization is basically independent of CIP contact time. This is obvious in the case of batch chromatography, as the CIP step has no impact on the loading of the column. On the other hand, in the CaptureSMB process, a longer CIP time leads to a longer fixed loading time by increasing t_B , but this can be compensated by changing the batch loading flow rate and the interconnected time. In the PCC processes, a longer CIP time simply raises the lower bound on the interconnected loading time, so as long as this constraint is not active (which is the case at high capacity utilization, where the flow rates are low and the loading times are high), the CIP time has no impact on the loading. When comparing the different processes, the same trends as in the base case can be observed: the batch process is inferior in terms of capacity utilization, but can reach similar values of maximum productivity. Among the multi-column processes, again all processes can reach very high capacity utilization, and the CaptureSMB process can achieve slightly higher productivity than the 3-column PCC process, but at a larger cost in terms of capacity utilization. The 4-column PCC process again shows the worst performance among the multi-column processes.

4.4.5 Influence of feed concentration

Changing the feed concentration changes the behavior of the processes most significantly as can be seen in Figure 4.7 (bottom, panel B). As expected, the maximum productivity increases with increased feed concentration for all processes. This

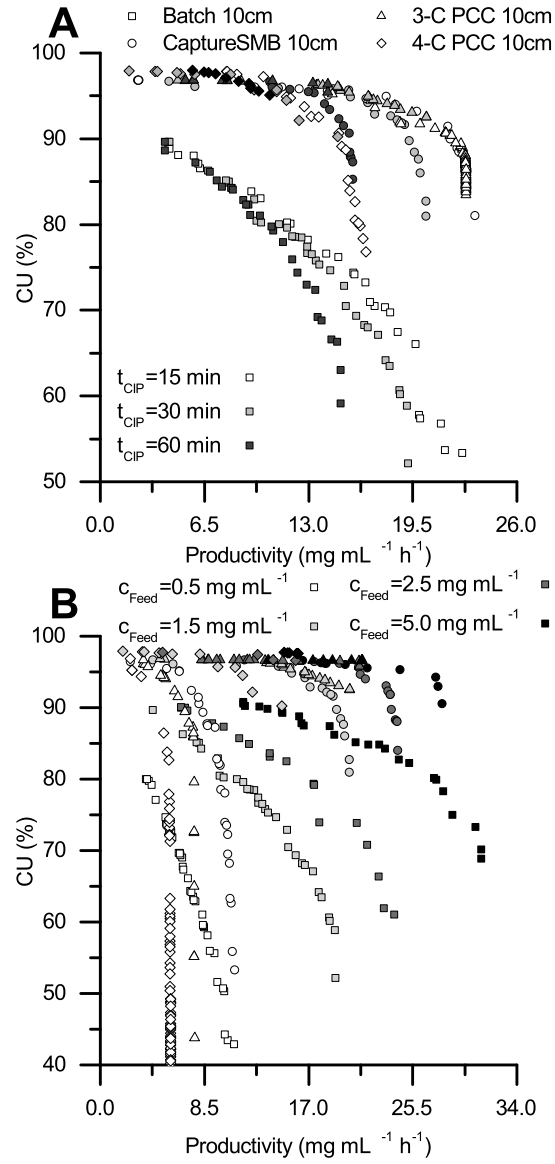


Figure 4.7: Top panel (A): Influence of changing t_{CIP} from 15 to 30 to 60 minutes. The other parameters correspond to the base case, i.e. 3 column volumes interconnected wash and 1.5 mg mL⁻¹ feed concentration. Bottom panel (B): Effect of changing c_{Feed} between 0.5 and 5.0 mg mL⁻¹. The other parameters correspond to the base case.

improvement is mainly due to a decrease of the loading time, which decreases with increasing titer. With decreasing loading time, the time required for recovery and regeneration becomes dominant and the improvement in productivity levels off with increasing titer. On the other hand, the maximum achievable capacity utilization stays approximately constant. At lower feed concentrations, again batch is inferior to the multi-column processes in terms of capacity utilization. But in this region, the CaptureSMB process dominates the other processes. This is due to the fact that the maximum loading flow rate can be used without breakthrough being an issue, which causes the pareto-fronts to become vertical. In this case, additional columns convey no benefit. At higher feed concentrations, two changes can be observed: Firstly, the 3-column PCC process reaches its maximum productivity value before the CaptureSMB process exhibits any significant drop in capacity utilization, giving the CaptureSMB process a much better trade-off, in addition to its higher maximum productivity value. This is caused by the additional constraint on the loading time for the PCC processes ($t_{IC} \leq t_{RR}$) becoming active. Secondly, the batch process becomes more competitive in terms of maximum productivity, eventually outperforming all multi-column processes at 5.0 mg mL^{-1} . This can be explained by the fact that loading times become very short in this region, and the complete decoupling of loading and elution gives batch an advantage in this case. As in the other cases however, the batch process has a worse trade-off than the multi-column processes. It should be noted that the results for 5.0 mg mL^{-1} feed concentration are extrapolated data, as there were no experiments performed at this concentration. The main uncertainty introduced by this extrapolation concerns the assumption of a sharp shrinking core front inside the particles. This assumption becomes weaker because the mass transfer, which is proportional to the concentration gradient inside the particle, becomes faster. This should mainly impact the shape, but not the position of the breakthrough curves, which is only

important to determine how much is recycled, but should have little impact on the process performances.

In conclusion, the optimal process choice depends on the feed titer and the desired objective (maximum productivity, maximum capacity utilization or best possible trade-off between the objectives). The best choice for each combination based on the optimization results is reported in Table 4.3. Of the processes examined, CaptureSMB offers the best trade-off, i.e. how much capacity utilization is lost when increasing the productivity, at low ($< 1.5 \text{ mg mL}^{-1}$) and high titers ($> 2.5 \text{ mg mL}^{-1}$). In the intermediate range, the 3-column PCC process exhibits the best trade-off. In terms of maximizing capacity utilization, it is clear that any of the multi-column processes is suitable for all feed titers, outperforming batch in every case. For achieving maximum productivity, CaptureSMB is optimal at low and medium titers ($< 2.5 \text{ mg mL}^{-1}$), while batch becomes optimal at high feed titers. The 2-4 column capture processes each contain an interconnected wash step that follows the sequential loading. The wash step is required to wash unbound material from the liquid volume of the first column into the second column for adsorption [46]. Moreover, due to change of the equilibrium conditions when flushing with wash buffer, product may desorb from the first column and needs to be captured in the second column requiring washing volumes of more than one column volume. The model predicts negligible impact on capacity utilization and productivity when changing the interconnected wash step for all multi-column processes. These results are shown graphically in Figure 4.8.

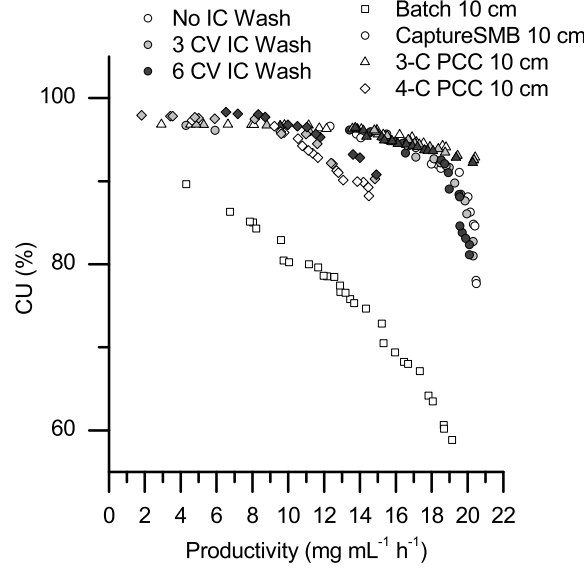


Figure 4.8: Influence of changing the interconnected wash from 0 to 3 and to 6 column volumes. The other parameters correspond to the base case, i.e. 30 minutes of CIP contact time and 1.5 mg mL⁻¹ feed concentration.

4.4.6 Influence of recovery and regeneration scheduling in the 4-column PCC process

The 4-column PCC process differs fundamentally from the other processes in that there is more than one column in the recovery and regeneration phase at any one time. If there is no constraint that the switching times in all positions must be the same, the recovery and regeneration can be scheduled more efficiently in the 4-column PCC process, as shown in Figure 4.9. Instead of having only one column undergo regeneration per t_{RR} , two columns can be scheduled in a way that makes two fresh column available every t_{RR} . For example, after the first switching time at t_{Switch} , column 1 has just finished recovery and regeneration and is moved to the end of the loading train. Column 3 is fully loaded and begins recovery and regeneration. Column 4 moves up to the start of the loading train to be fully loaded. Meanwhile, column 2 is in the middle of recovery and regeneration, and

Table 4.3: Optimum process choice depending on feed titer and desired performance objective.

Feed titer	Objective	Productivity	Capacity utilization	Trade-off
Low ($\sim 0.5 \text{ mg mL}^{-1}$)		CaptureSMB	CaptureSMB / 3- / 4-C PCC	CaptureSMB
Medium ($\sim 1.5 - 2.5 \text{ mg mL}^{-1}$)		CaptureSMB	CaptureSMB / 3- / 4-C PCC	3-column PCC
High ($\sim 5.0 \text{ mg mL}^{-1}$)		Batch	CaptureSMB / 3- / 4-C PCC	CaptureSMB

simply continues. As with the non-optimal scheduling above, after 4 switches, at t_{Cycle} , the initial configuration is reached again. This relaxes the last constraint in equation (4.12) from $t_{\text{RR}} \leq t_{\text{IC}}$ to $t_{\text{RR}}/N_{\text{RR}} \leq t_{\text{IC}}$, where N_{RR} is the number of columns in the recovery and regeneration phase at the same time, in this case $N_{\text{RR}} = 2$. In the non-optimized scheduling, the lower bound on the loading time

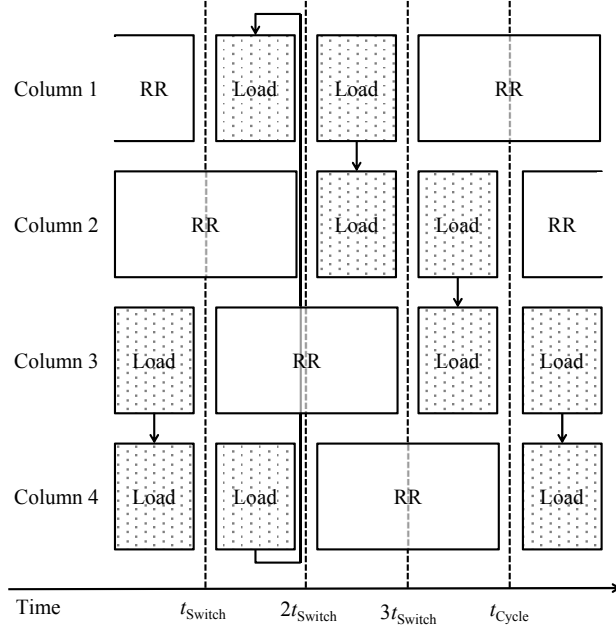


Figure 4.9: *Optimal scheduling for the 4-column PCC process. At each switching time, three of the four columns change their tasks, while the fourth column stays in recovery and regeneration (RR). Note that the inter-connected wash is not shown for brevity.*

was the limiting factor on productivity in the 4-C PCC process. Therefore, with optimum scheduling, the 4-C PCC process behaves differently than before. Figures 4.10 and 4.11 show the pareto curves for the base case and a high concentration case (at a feed titer of 5.0 mg mL^{-1}). Due to the more efficient recovery and regeneration, the optimized scheduling improves the process performance in both cases, as expected. In high titer scenarios however, the constraints imposed by the recovery and regeneration phase become ever more dominant, and since this is the

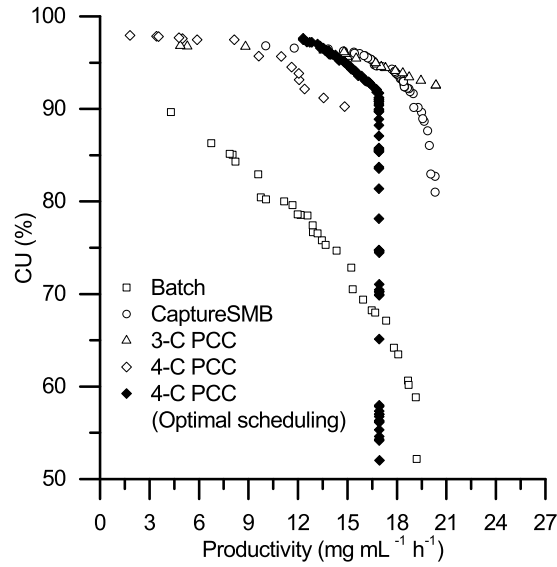


Figure 4.10: Base case pareto curves for the 4-C PCC process with optimal scheduling for 10 cm single column bed height.

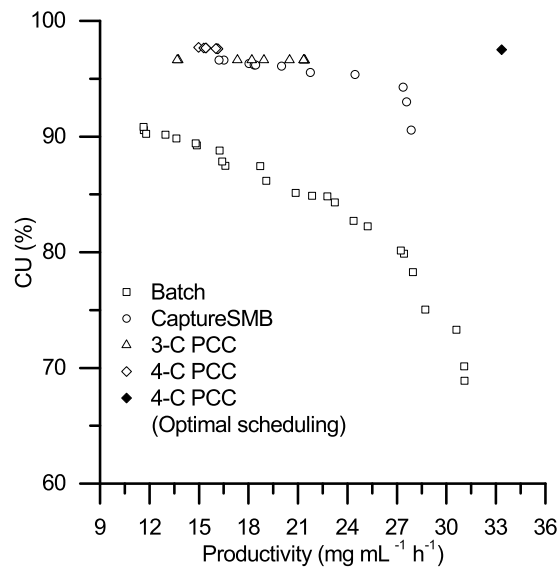


Figure 4.11: High titer pareto curves for the 4-C PCC process with optimal scheduling. The feed titer is 5.0 mg mL^{-1} , while all other parameters correspond to the base case, i.e. 10 cm single column bed height, 30 minute CIP time and 3 column volumes interconnected wash.

main factor constraining productivity in all processes, the 4-C PCC with optimal scheduling process now clearly dominates all processes at higher feed titers. Note that there is no trade-off in this case; There is a single global optimum. This is due to the fact that the loading time is minimal, which prevents a higher loading flow rate and thus a higher productivity, and the capacity utilization is already at the theoretical maximum (100% minus losses in the wash). In this case, further improvements in productivity would only be possible by further increasing the number of columns in the recovery and regeneration train, leading to a BioSMB-like process. This gain in performance comes at a great cost however; Since the columns undergo different steps of the recovery and regeneration protocol simultaneously, one can expect an increase in hardware complexity cumulative with the increase that having four (or more) columns already conveys.

4.5 Concluding remarks

Batch capture and three different continuous multi-column protein A mAb capture processes (2-column CaptureSMB and 3- and 4-column PCC) were numerically optimized and compared in different operating regimes with respect to capacity utilization and productivity, at constant yield and purity. The model used for this task was tuned on ad-hoc batch breakthrough experiments. This resulted in sets of pareto-optimal operating points, showing a trade-off between capacity utilization and productivity.

In the base case examined (3 CVs interconnected wash, 30 min CIP time, 1.5 mg mL⁻¹ feed titer), the multi-column processes show a productivity increase from 5 to 19 mg mL⁻¹ h⁻¹ for the CaptureSMB, an increase from 5 to 20 mg mL⁻¹ h⁻¹ for the 3-C PCC, and an increase from 5 to 15 mg mL⁻¹ h⁻¹ for the 4-C PCC compared to the batch process at a fixed capacity utilization of 90%. On the other

hand, at a fixed productivity of $14 \text{ mg mL}^{-1} \text{ h}^{-1}$, an increase from 75% to 97% in capacity utilization is obtained for a fixed productivity when using CaptureSMB or 3-C PCC, and an increase from 75% to 90% is reached in the 4-column PCC process compared to batch capture. In the special case where one allows for different switching times for each column, the recovery and regeneration in the 4-C PCC process can be scheduled more efficiently, which improves the process performance significantly. The optimally scheduled 4-column process reaches a productivity of $16 \text{ mg mL}^{-1} \text{ h}^{-1}$ at 90% capacity utilization, a capacity utilization of 95% at a fixed productivity of $14 \text{ mg mL}^{-1} \text{ h}^{-1}$, and a much better trade-off overall.

The standard multi-column processes with fixed switching times completely dominated the batch process in all cases (except when maximizing productivity at high titers), with the CaptureSMB showing best performance in terms of productivity and all three multi-column processes showing optimal and comparable performance in terms of capacity utilization. At both low and high feed concentrations, CaptureSMB showed the best trade-off situation, while the 3-column PCC process has the best trade-off in an intermediate region. When increasing the feed concentration to 5.0 mg mL^{-1} , an interesting change can be observed: In this case, the CaptureSMB process still has the best trade-off between capacity utilization and productivity, but the performance of the multi-column processes in terms of productivity drops off below the values achievable in the batch process, albeit at a considerable decrease in capacity utilization. This is due to the fact that there are additional constraints on the loading time in the multi-column processes, because sequential loading and recovery and regeneration are performed in parallel, which does not allow for fast enough loading to achieve higher productivity values. If non-equal switching times are allowed, the picture changes drastically: The optimally scheduled 4-C PCC process clearly dominates all processes in both objectives. In fact, it exhibits a single global optimum, suggesting that adding even more columns

in the recovery and regeneration train to further relax the constraints would lead to a further improvement. In all cases however, the improved capacity utilization provided by the multi-column processes translates into a proportional decrease in resin costs and buffer consumption, while product concentration increases proportionally.

Finally, it should be pointed out that the increased performance of the multicolumn processes comes at the cost of higher investments and more complex hardware. The hardware demand (pumps, valves, detectors, and piping) generally increases linearly with the number of columns. However, given that a step change in performance takes place when moving from a batch process to a two column process the increase in hardware investment can be justified since significant savings in operating expenditures and increased speed of processing is achieved. In conclusion, among the multicolumn processes for mAb capture the two column process is preferable as it combines minimum hardware investment and risk with maximum process performance and flexibility.

Chapter 5

Optimization and comparison of batch and different MCSGP processes for ternary center-cut separations of proteins

5.1 Introduction

Biopharmaceuticals, such as recombinant monoclonal antibodies, are exhibiting some of the largest growth in the market for new medication [2, 6]. Since these molecules are typically too large and too complex to be manufactured by traditional chemical methods, they are produced using genetically engineered cell lines. Therefore, the products have to be captured from a complex mixture, containing impurities such as growth medium components, host cell proteins, DNA fragments and protein aggregates [8]. As for any medication, the purity requirements on the final products are very strict, which necessitates several polishing steps after the initial capture from the cell culture supernatant. The most widely used technique

to tackle these very difficult separation problems is chromatography [98]. In the case of monoclonal antibodies specifically, protein A affinity chromatography is used to first remove the product from the cell culture supernatant, then several ion exchange steps, usually run with a solvent or modifier gradient, follow as polishing steps [99, 100]. Since chromatography is a relatively expensive unit operation, many process related improvements have been developed over the recent years. Arguably the most significant improvement is the implementation of continuous, counter-current principles to improve process performance in both economical and ecological objectives [28, 42, 43, 101].

The currently most widely used continuous, counter-current chromatographic process is the simulated moving bed (SMB) process [28, 102]. The standard SMB process is run isocratically and separates two fractions, therefore it can only handle binary separation problems, for example chiral separations [29, 91, 103], or cases where two groups of related components are separated, as for example in sugar processing [104–106]. SMB is mainly used for the separation of small molecules, where its main advantage compared to a standard batch separation is that the SMB process can achieve high purity and yield simultaneously, and reach higher productivity [28]. The separation problems encountered in the purification of biomolecules mostly require a center-cut separation, that is a ternary separation, where some impurities elute before the product, and some impurities elute after the product. In principle, this can be achieved by SMB either by using two SMB in series, each performing one binary separation [31], or by using a different, more complex SMB setup [107, 108]. However, these solutions are expensive to implement, and in addition, to achieve adequate separation often the use of a solvent or modifier gradient is required, which cannot be easily done in an SMB system. To overcome these limitations, the multicolumn counter-current solvent gradient purification (MCSGP) process was developed, which performs center-cut separa-

tions with a solvent or modifier gradient [59]. The basic principle of the process is to internally recycle overlapping regions of the chromatogram, while collecting a pure center-cut fraction. Initially, the MCSGP process was fully continuous (steady input and output streams), using five [33] or six columns [59]. Subsequently, the process has been simplified to save capital cost for valves, pumps and resin material, employing three columns that alternate between different sets of tasks, making the process semi-continuous [52]. The three-column concept has since been expanded to include a fourth column, which provides either continuous loading or multiple different kinds of cleaning-in-place (CIP) steps [109]. Most recently, a twin-column setup has been developed, where only two columns are required to achieve both high purity and high yield in a center-cut separation problem that requires a solvent or modifier gradient [51]. In a further development, it has been shown that multiple product fractions can be collected in a single run, which was previously impossible [64].

When considering the investment costs, it is quite clear that using fewer columns results in lower costs, since each additional column not only requires resin material, but also pumps, valves and detectors. The main factor determining the running costs on the other hand is process performance, expressed through productivity, buffer consumption and yield [110]. It is not immediately obvious how changing the number of columns will change the performance, if each process is thoroughly optimized. In the protein A capture step for example, it has been shown that it might be optimal to use batch, a two-column, a three-column or an even more complex process, depending on the requirements on process performance (see chapter 4).

In this work, the separation of charge variants of a monoclonal antibody on an ion exchange resin is modeled, and this model is used to assess and compare the performance of batch purification and different MCSGP processes. In order to en-

sure a fair comparison, all processes are optimized separately using multi-objective constrained optimization. Furthermore, the resulting optimal operating points are used to gather insights for process design by identifying the most important operating parameters using multivariate analysis.

5.2 Process descriptions

Three different processes which are able to perform center-cut gradient driven separations were considered: Batch chromatography, and MCSGP with different numbers of columns, namely the 2-, and the 3-column MCSGP processes. It is important to note that the 6-column process is the same as running two 3-column processes with the same switching times in parallel, therefore removing a degree of freedom. This means that the 6-column process can never outperform the 3-column process, and could therefore be omitted from the comparison. Furthermore, the 4- and 5-column processes mentioned above implement specialized, different process schemes compared to the other processes and could therefore not be directly compared to the other processes.

5.2.1 Gradient batch chromatography

The first process considered for the comparison was state-of-the-art gradient batch chromatography. To achieve separation, a mixture of components is loaded onto a column, and usually some wash steps are performed to wash out non-adsorbing or weakly adsorbing impurities. After that, a modifier gradient is applied to elute the components one by one, and more or less pure fractions can be collected at the outlet of the column. When all target components have been collected, strip, cleaning-in-place and equilibration steps are applied, after which the column is ready for another separation. In the majority of complex separation tasks, a

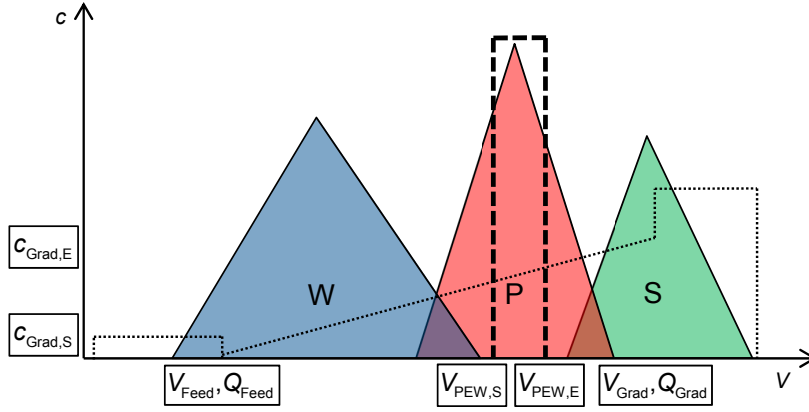


Figure 5.1: Schematic representation of a center-cut batch gradient separation. The process degrees of freedom are highlighted, namely: The loading volume V_{Feed} , the loading flow rate Q_{Feed} , the total gradient volume V_{Grad} , the flow rate during the gradient elution Q_{Grad} , the modifier concentrations at the start and the end of the gradient, $c_{\text{Grad},S}$ and $c_{\text{Grad},E}$, and the position of the product elution window $V_{\text{PEW},S}$ and $V_{\text{PEW},E}$.

center-cut separation must be performed to purify a target component, since some impurities will adsorb more strongly than the product, and therefore elute later, while the other impurities will adsorb more weakly than the product, which causes them to elute earlier. If the impurities and the product are very similar, no baseline separation can be achieved. Such a case is depicted in Figure 5.1. Depending on the pooling policy, one can either achieve high purity by only collecting a narrow fraction of the product, which compromises the yield because much of the product is discarded, or high yield by collecting more of the product, which compromises purity because impurities are collected together with the product.

In total, the batch process has 8 degrees of freedom: The loading volume V_{Feed} and flow rate Q_{Feed} , the duration of the gradient V_{Grad} and the flow rate during the gradient Q_{Grad} , the start and end points of the gradient ($c_{\text{Grad},S}$ and $c_{\text{Grad},E}$), and the pooling policy (start position of the product elution window $V_{\text{PEW},S}$ and its end point $V_{\text{PEW},E}$).

5.2.2 The MCSGP process

In order to counteract the intrinsic purity/yield trade-off observed in batch chromatography, the MCSGP process has been developed. It can be run with different numbers of columns, but the operating principle is the same for all processes: A narrow, highly pure fraction of product is collected, while the overlapping regions of the chromatogram (containing impurities) are recycled into additional columns. In addition, separation is enhanced by the use of counter-current principles.

Twin-column MCSGP

The most recently developed, and arguably simplest, MCSGP process is the twin-column MCSGP process. It distributes the subtasks of the separation over two columns (see Figure 5.2): the first column performs the gradient elution, eluting first the overlapping region of weak and product, then pure product (which is collected), then the second overlapping region of product and strong. After the elution, the column undergoes strip, CIP and equilibration, as in the batch process. Meanwhile, the second column first takes up the recycle stream containing weak and product, then receives fresh feed (including any wash steps if needed). Then, after taking up the second recycle stream (which contains product and strong), this column can already start the gradient elution while the first column undergoes regeneration. After all these steps, the columns swap positions and tasks; and after two such switches, the columns are back in the initial configuration, which denotes the end of a cycle. An MCSGP process can be laid out completely from a design batch chromatogram, by translating the elution volumes and gradient positions that correspond to the tasks mentioned. However, this design procedure was only used as a way to find feasible starting points for the subsequent optimizations, which were independent of any design rules. Note that the recycle streams must

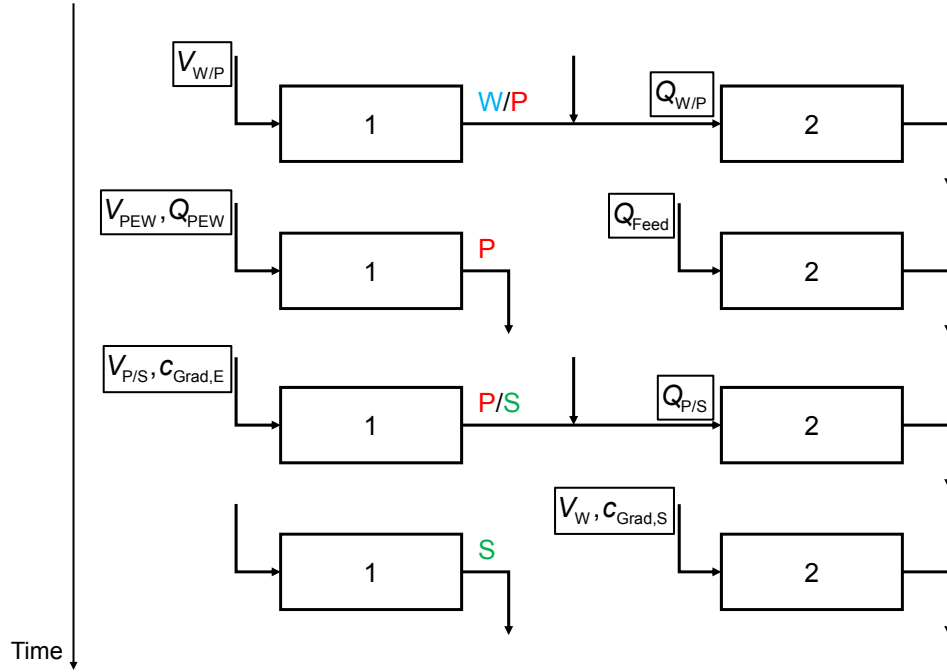


Figure 5.2: Two column MCSGP process schematic with the degrees of freedom highlighted. The degrees of freedom are: The buffer volumes eluted in the different parts of the gradient V_W , V_{WP} , V_{PEW} and V_{PS} , the total interconnected flow rates Q_{WP} and Q_{PS} , the flow rate during the product elution window Q_{PEW} , the dilution ratios for the recycling streams DR_{WP} and DR_{PS} , the feed flow rate Q_{Feed} , and the gradient defined by $c_{Grad,S}$ and $c_{Grad,E}$.

be diluted to a suitable level of conductivity, otherwise their contents are not adsorbed on the second column. Usually, the first recycle stream is diluted to reach the conductivity level at the start of the first recycle window, which allows the product to adsorb but continues to elute the weak impurities, while the second recycle stream is diluted the conductivity level at the start of the gradient, which allows all product to adsorb. However, since these are only rules of thumb and the flow rates were expected to have a large impact on the performance, the dilution ratios were left as a degree of freedom instead.

Under the constraint that the gradient is linear over the elution volume, the twin-column MCSGP process has 12 degrees of freedom: The elution volumes in the different parts of the gradient V_W , V_{WP} , V_{PEW} and V_{PS} , the total flow rates in the interconnected phases and the flow rate in the product elution window (Q_{WP} , Q_{PEW} and Q_{PS}), the dilution ratios in the interconnected phases $DR_{WP} = Q_1/Q_{WP}$ and $DR_{PS} = Q_1/Q_{PS}$ (where Q_1 is the flow rate for the first column during these phases), the feed flow rate Q_{Feed} , and the gradient start and end points ($c_{Grad,S}$ and $c_{Grad,E}$). Note that the duration of the last sub-step t_4 is fixed by the duration of the strip, CIP and regeneration protocol, which together with V_W also defines the flow rate in second column during that phase.

3-column MCSGP

As can be seen in Figure 5.3, in the 3-column MCSGP process, the three columns are alternately interconnected or disconnected (batch phase). While the twin-column case can by its nature not distinguish counter-current from co-current movement, we have a true counter-current movement in this case, i.e. with every switch, the columns move against the liquid flow direction, akin to an SMB system. In the interconnected phase, the overlapping regions of the chromatogram are recycled; the stream containing product and strong goes from the first column to

the second column, while the stream containing weak and product is going from the second column to the third column. Between the columns, inline dilution is applied to ensure that a) the strongly adsorbing impurities cannot elute from the second column and b) the product is adsorbed on the third column. In the batch step, where the columns are disconnected, each performs a different task: the first column undergoes strip, CIP and equilibration, the second column elutes pure product, and the third column elutes weakly and non-adsorbing impurities, while taking up new feed. The counter-current principles can be seen at work here; if the modifier concentrations in each of the positions is kept at just the correct value, then the weakly adsorbing impurities will move with the liquid flow to the right, eluting from the third column, the product will stay in the center, eluting from the second column, and the strongly adsorbing impurities move with the (simulated) solid flow to the left, eluting from the first column in the strip or CIP phase.

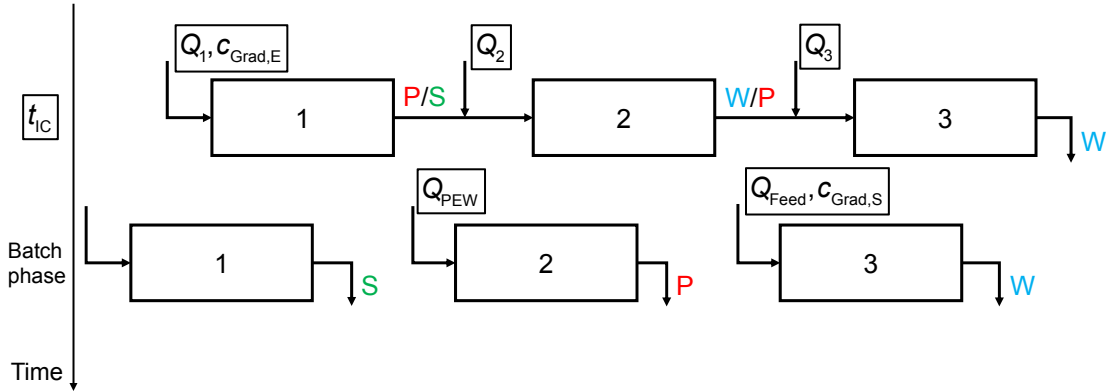


Figure 5.3: *Three column MCSGP process schematic with the degrees of freedom highlighted. One switch is depicted, which is further partitioned in to two phases, the interconnected phase (IC) and the batch phase. After the switch, the columns move one position against the direction of the liquid flow, i.e. column 3 goes to position 2, 2 goes to 1 and 1 goes to 3. The degrees of freedom are: The duration of the interconnected phase t_{IC} , the flow rates during the interconnected phase $Q_{1,2,3}$, the flow rate in the product elution window Q_{PEW} the feed flow rate Q_{Feed} , and the gradient, as defined by $c_{Grad,S}$ and $c_{Grad,E}$.*

Enforcing again the constraint that the gradient be linear over the elution

volume, the 3-column MCSGP process has 8 degrees of freedom: The duration of the interconnected phase t_{IC} , the flow rates in the interconnected phase $Q_{1,2,3}$, the flow rate during the product elution window Q_{PEW} , the feed flow rate Q_{Feed} and the start and end points of the gradient ($c_{Grad,start}$ and $c_{Grad,end}$). Note that the time of the batch phase t_B , when the columns are disconnected, is fixed by the duration of the strip, CIP and regeneration protocol.

5.3 Materials and methods

Separating charge variants of a monoclonal antibody on a fractogel DEAE S column using gradient ion-exchange chromatography was used as a model separation task.

5.4 Process models

5.4.1 Column and adsorption model

The processes were modeled with a lumped kinetic model, applied to each charge variant:

$$\begin{aligned}\frac{\partial c_i}{\partial t} &= -v_i \frac{\partial c_i}{\partial x} + D_{L,i} \frac{\partial^2 c_i}{\partial x^2} - \phi_i \frac{\partial q_i}{\partial t} \\ \frac{\partial q_i}{\partial t} &= k_{m,i} (q_i^* - q_i)\end{aligned}\tag{5.1}$$

$$t \in [0, t_{Switch}], x \in [0, L_{Col}], i \in [1, N_{CV}]$$

where c_i is the liquid phase concentration of charge variant i , t is the time, v_i is the interstitial velocity of charge variant i , x is the longitudinal coordinate along the column, L_{Col} is the column length, $D_{L,i}$ is the apparent axial dispersion coefficient of charge variant i , $\phi_i = (1 - \epsilon_i) / \epsilon_i$ is the phase ratio of the column as seen by charge variant i , N_{CV} is the number of charge variants, q_i is the solid

phase concentration of charge variant i , $k_{m,i}$ is the lumped mass transfer coefficient for charge variant i , and q_i^* is the equilibrium solid phase concentration of charge variant i .

It was assumed that the modifier is inert with respect to the solid phase and does not adsorb. Its behavior was therefore modeled with a simple PDE:

$$\frac{\partial c_{\text{mod}}}{\partial t} = -v_{\text{mod}} \frac{\partial c_{\text{mod}}}{\partial x} + D_{L,\text{mod}} \frac{\partial^2 c_{\text{mod}}}{\partial x^2} \quad t \in [0, t_{\text{Switch}}], x \in [0, L_{\text{Col}}] \quad (5.2)$$

The initial and boundary conditions were applied to each charge variant and the modifier:

$$\begin{aligned} c_i(t=0, x) &= c_{i,0}(x) \\ q_i(t=0, x) &= q_{i,0}(x) \\ c_i(t, x=0) &= c_{\text{in},i}(t) + \frac{D_{L,i}}{v_i} \left. \frac{\partial c_i}{\partial x} \right|_{x=0} \\ \left. \frac{\partial c_i}{\partial x} \right|_{x=L_{\text{Col}}} &= 0 \\ i &\in [1, N_{\text{CV}}] \text{ or mod} \end{aligned} \quad (5.3)$$

The mixing nodes in the multicolumn processes were modeled as perfect and instantaneous mixers for all components. Therefore, the following inlet concentrations c_{in} were applied to columns after a mixing node:

$$\begin{aligned} c_{\text{in},i} &= \frac{Q_{\text{out}} c_{\text{out},i}}{Q_{\text{out}} + Q_{\text{dil}}} \\ c_{\text{in},\text{mod}} &= \frac{Q_{\text{out}} c_{\text{out},\text{mod}} + Q_{\text{dil}} c_{\text{dil},\text{mod}}}{Q_{\text{out}} + Q_{\text{dil}}} \end{aligned} \quad (5.4)$$

where Q_{out} is the flow rate exiting the column that is before the mixing node, c_{out} is the concentration of the charge variant or modifier eluting from the column before the mixing node, Q_{dil} is the flow rate of the pump connected to the mixing

node, and $c_{\text{dil,mod}}$ is the concentration of the modifier in the stream coming from the pump connected to the mixing node.

The apparent axial dispersion coefficients $D_{L,i}$ were estimated using the HETP values calculated from the peak widths of isocratic elution experiments. The bed porosities ϵ_i were estimated from pulse injections with non-adsorbing species. The lumped mass transfer coefficients $k_{m,i}$ were calculated from empirical correlations. For the equilibrium solid phase concentrations of the charge variants, a multi-component Langmuir isotherm with a power law for the modifier dependence was used:

$$H_i = \alpha_i c_{\text{mod}}^\beta$$

$$q_i^* = \frac{H_i c_i}{1 + \sum_{k=1}^{N_{\text{CV}}} \frac{H_k c_k}{q_{\text{sat},i}}} \quad (5.5)$$

The partial differential equations were solved as described in section 3.4 (page 35), including the counter-current switching of the internal profiles in the multi-column processes.

5.4.2 Process performance

The most important performance objective in a polishing step are product purity (product quality), yield (recovery), productivity (amount of product purified per resin volume and time), and buffer consumption (amount of buffer used per amount of product purified). Note that among these, product purity is different because it is usually a process constraint that has to be fulfilled, while the other variables can be subject to optimization. The performance objectives were calculated for

each process as follows:

$$\begin{aligned}
Pu &= \frac{c_{\text{PEW},P}}{\sum_{i=1}^{N_{\text{CV}}} c_{\text{PEW},i}} \\
Y &= \frac{\int_{V_{\text{PEW},S}}^{V_{\text{PEW},E}} c_P dV}{V_{\text{Feed}} c_{P,\text{Feed}}} \\
Pr &= \frac{Y \cdot V_{\text{Feed}} c_{P,\text{Feed}}}{N_{\text{Col}} V_{\text{Col}} t_{\text{Switch}}} \\
BC &= \frac{V_{\text{Buffer}}}{Y \cdot V_{\text{Feed}} c_{P,\text{Feed}}}
\end{aligned} \tag{5.6}$$

where Pu is the purity, $c_{\text{PEW},i}$ is the concentration of charge variant i in the product elution window, Y is the yield, $V_{\text{PEW},S,E}$ is the elution volume where the product elution window starts or ends, c_P is the concentration of the product at the column outlet, V_{Feed} is the amount fed (per switch in the MCSGP processes), $c_{P,\text{Feed}}$ is the concentration of the product in the feed, Pr is the productivity, N_{Col} is the number of columns involved in the process, V_{Col} is the resin volume in a single column, t_{Switch} is the time needed for a switch (or the total time from start of the loading to the end of the CIP and regeneration procedure in the batch case), BC is the buffer consumption, and V_{Buffer} is the volume of buffer used during a switch (or bind and elute step in the batch process). In particular:

$$\text{Batch: } V_{\text{Buffer}} = V_{\text{Grad}} + V_{\text{RR}}$$

$$2 \text{ column MCSGP: } V_{\text{Buffer}} = V_{\text{W}} + V_{\text{WP}}/DR_{\text{WP}} + V_{\text{PEW}} + V_{\text{PS}}/DR_{\text{PS}} + V_{\text{RR}}$$

$$3 \text{ column MCSGP: } V_{\text{Buffer}} = (Q_1 + Q_2 + Q_3) \cdot t_{\text{IC}} + Q_{\text{PEW}} \cdot t_{\text{B}} + V_{\text{RR}}$$

where V_{RR} is the buffer volume required for strip, CIP and equilibration.

5.4.3 Optimization problem

Using the performance variables discussed above, an optimization problem was formulated for each of the processes:

$$\begin{aligned} \max_x \quad & Y(x), Pr(x), -BC(x) \\ \text{subject to: } & Pu_{\text{Target}} \leq Pu(x) \\ & Q \leq Q_{\max} \\ & 0 \leq x \end{aligned} \tag{5.7}$$

where x are the process degrees of freedom (as discussed above), Pu_{Target} is the desired minimum purity, and Q_{\max} is the maximum allowed flow rate due to pressure drop. Note the minus sign in front of the buffer consumption, which should obviously be minimized instead of maximized. Also note that the performance variables change during the transient startup of the multi-column processes, but eventually reach steady state values. These steady state values were used in the optimization. As example purity requirements, 80%, 90% and 95% were chosen. Table 5.1 contains a list of all fixed operating parameters that were not fitted or changed during the optimization.

5.4.4 Principle component analysis for pareto-curves and stability analysis

Along the pareto-curves, the operating parameters are expected to be highly correlated, for example a feeding flow rate might decrease while the corresponding feeding time increases. Therefore, in order to visualize the impact of the different operating parameters on the productivity/yield pareto-curves, principle component analysis (PCA) was performed [111]. In PCA, the coordinate system in

Table 5.1: Fixed parameters for the charge variant separation.

Parameter	Symbol	Units	Value
Single column bed height	L_{Col}	cm	5
Modifier concentration at 0% B	c_{mod}	mg mL ⁻¹	0.55
Modifier concentration at 100% B	c_{mod}	mg mL ⁻¹	18.35
Maximum flow rate	Q_{max}	mL min ⁻¹	1.0
Buffer use for CIP and equilibration	V_{RR}	mL	10
Total feed concentration	c_{Feed}	mg mL ⁻¹	1.77 (mod); 8.0 (mAb total)
Feed composition	$c_{i,\text{Feed}}$	%	11 (W1); 33 (W2); 32 (P); 15 (S1); 9 (S2)

which the data set resides is rotated and stretched in a way so that the first coordinate axis corresponds to the direction of the largest variance in the data set as a linear combination of the original variables. The second axis (or principle component) is again the direction of largest variance orthogonal to the first new axis. Each further principle component is orthogonal to all previously found components and describes the direction of largest variance remaining. When only the first two principle components are plotted, most of the information from the data set, in this case the pareto-optimization, can be captured. This provides a simple visualization of the relationship of the different operating parameters and target variables. The built-in PCA function of MATLAB was used, which implements singular value decomposition to find the principle components.

In addition, partial least squares regression (PLS) was performed to quantify the relative impact that each of the operating parameters has on the process performance in terms of purity and productivity [112]. In PLS regression, similar to PCA, an orthogonal decomposition of the predictor variables is performed, but each subsequent component found explains as much as possible of the covariance between the predictor variables and the target variable. Each variable contributes more or less to the transformed coordinate space, which gives a measure for its importance in the projection (variable importance in projection, VIP). Along with the normalized regression coefficient for each variable, these two measures allow to find the important predictor variables that determine the behavior of the target variable. Note that due to the trade-off, any impact on productivity corresponds to an inverse impact on the yield. PLS regression and subsequent analysis is performed using MATLAB with the toolbox `lib_pls` (www.libpls.net, retrieved July 2015).

Process stability is a very important factor in quantifying process performance, since small disturbances in the pump flow rates and buffer preparations cannot

be avoided. In order to examine process stability, 10 points, spaced evenly along each pareto-curve, were selected, and at each point all of the operating parameters were varied by a random amount. Flow rates were changed in a range of $\pm 0.5\%$ (along with the corresponding pumped volumes), and buffer concentrations were varied in a range of $\pm 1\%$, which are both normally achievable in practice. At each of the 10 points, 500 runs with different random changes were performed, with each of the 500 points taken from a normal random distribution with mean 0 and standard deviation $0.5/3\%$ or $1/3\%$, which means that around 99.7% of the points were expected to lie within the ranges specified. The fraction of failed runs, defined as runs that did not reach steady state or did not achieve the required purity, and the maximum deviation in purity provided a measure of the process stability in each point.

5.5 Results and discussion

5.5.1 Model fitting

Figure 5.4 shows the model prediction and the experimental UV data of an elution. In Table 5.2, and overview of the fitted parameters can be found. These values were used to simulate the batch polishing as well as the MCSGP processes, since it has previously been shown that the performance of MCSGP processes can be accurately predicted using batch fitting data [82].

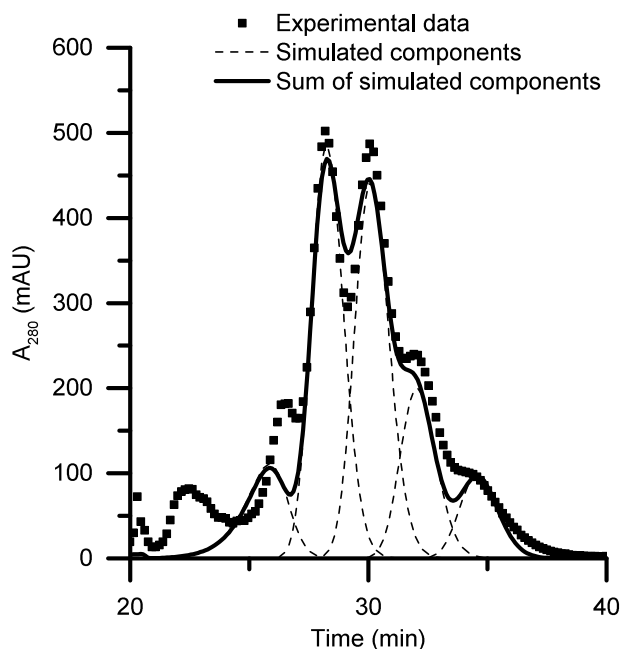


Figure 5.4: Model simulation and experimental UV data for a batch elution.

5.5.2 Purity-yield trade-off

Figure 5.5 shows purity-yield pareto curves for all three processes when purity and yield are used as the only objectives for optimization. In the batch process, it

Table 5.2: Fitted parameters for the charge variant separation.

Parameter	Symbol	Units	Value
Henry coefficient constants	$\log_{10}(\alpha_i)$		2.40 (W1); 3.19 (W2); 4.01 (P); 5.21 (S1); 6.45 (S2)
Henry coefficient exponents	β_i		-3.16 (W1); -3.68 (W2); -4.34 (P); -5.42 (S1); -6.26 (S2)
Axial dispersion coefficient (all CVs)	$D_{L,i}$	cm	0.0855 (all CVs), 0.046 (mod)
Mass transfer coefficient	$k_{m,i}$	min ⁻¹	8.69 (W1); 7.84 (W2); 6.76 (P); 5.63 (S1); 4.98 (S2)
Saturation capacity (all CVs)	q_{sat}	mg mL ⁻¹	65
Porosity (all CVs)	ϵ_i		0.48 (all CVs), 0.70 (mod)

was quite expected that there would be a trade-off between purity and yield, as discussed above. However, the MCSGP processes also showed a trade-off between purity and yield, albeit greatly alleviated. Among the MCSGP processes, the two-column process showed a slightly better trade-off still. If 80% purity was required, the batch process could reach 88% yield, the two-column process could reach 99% yield and the three-column process could reach 96% yield. At 90% purity, yield was strongly compromised in the batch process, at a value of 68%. The two-column process could still reach 99%, while the three-column process reached 93%. If the purity specification was very strict at 95%, the batch process could only reach a yield value of 40%, while the MCSGP processes were still at acceptable levels (97% for the two-column and 86% for the three-column process, respectively). The two-column process was clearly dominating in the purity-yield objectives; even at 100% purity, yield values of over 90% could still be achieved. The difference between the two MCSGP process could be explained by the fact that in the three-column process, the two recycling windows are not independent of each other, because these elutions happen at the same time and in series as part of the same liquid stream. Especially at high purity requirements, this interdependence seemed to compromise the maximum achievable yield value.

5.5.3 Productivity-yield trade-off

Since the purity is usually a constraint rather than an optimization variable, the more important trade-off for process performance is between productivity (amount produced per time and column volume) and yield (amount produced per raw material expended). This means that economically speaking, the trade-off is between time requirement and equipment size on one hand, and product loss on the other hand.

Each process was optimized with respect to yield and productivity, while main-

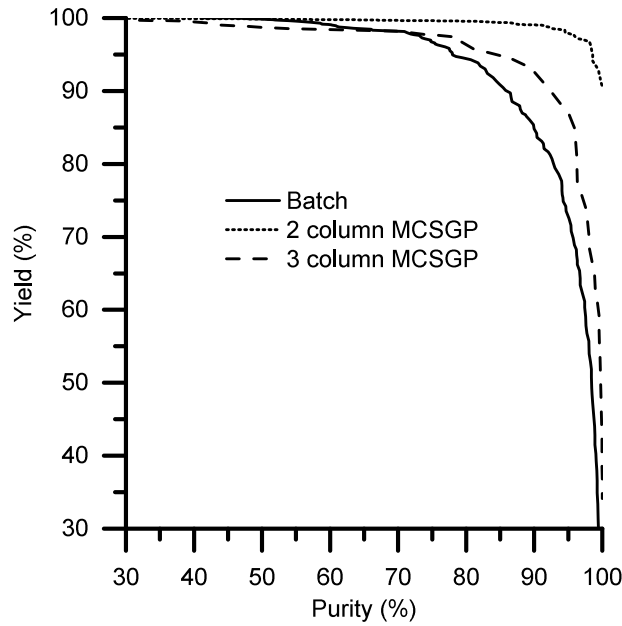


Figure 5.5: Purity-yield pareto fronts for the batch and MCSGP processes.

taining a certain purity value, in each case either 80%, 90% or 95%. Figure 5.6 shows the resulting pareto-curves for each process. In all three processes, the trade-off between productivity and yield got worse as the purity constraint became more strict, which was quite expected. Clearly, in the batch and 3-column processes, the maximum achievable yield strongly depended on the desired purity, which reflects the results from the purity-yield optimization in figure 5.5 above. This effect was much less pronounced in the 2-column process. For all three processes, the maximum achievable productivity decreased with increasing purity requirements, indicating that longer process times and/or smaller loading volumes were needed to fulfill the harder purity constraints.

Comparing the different processes at fixed purity levels (see figure 5.7, some interesting effects were observed: At the lower purity requirements, the batch process could achieve the highest productivity value out of the three processes, albeit not

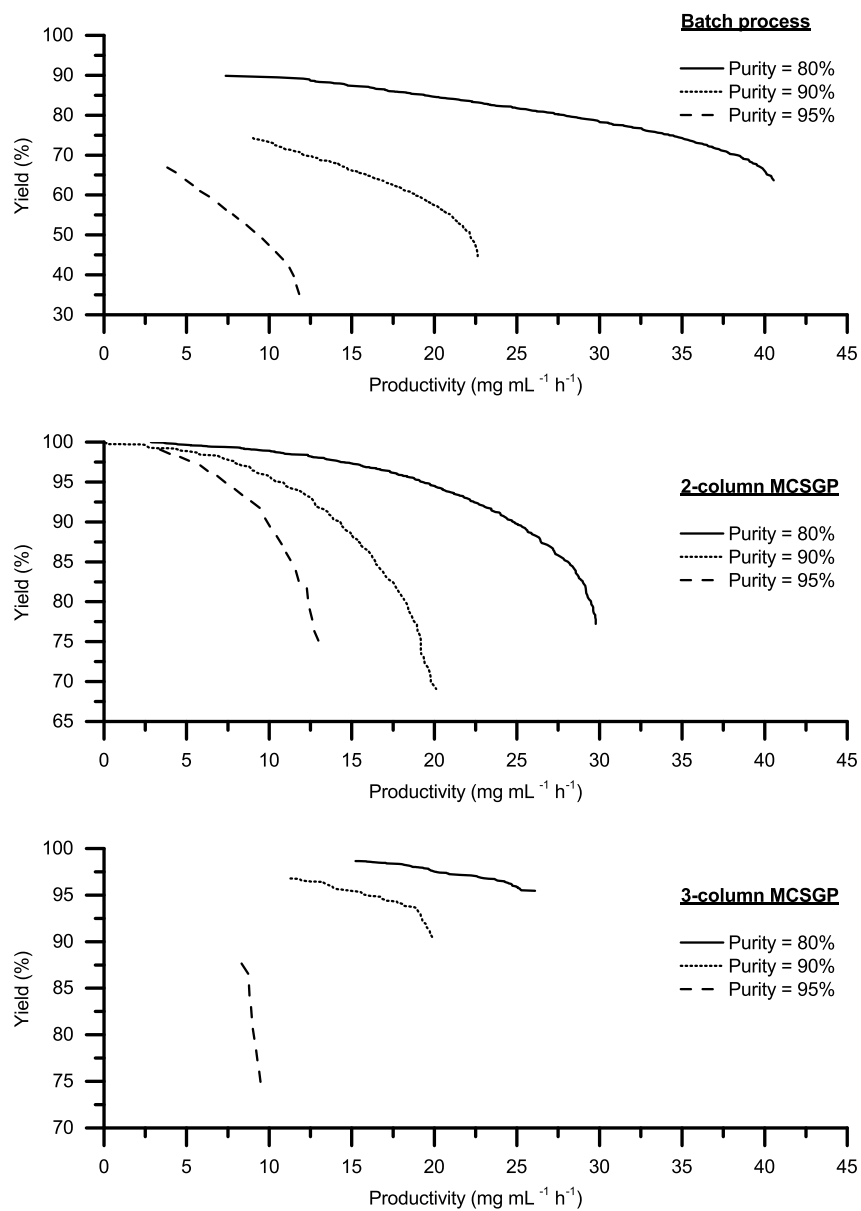


Figure 5.6: Productivity-yield pareto fronts for the batch and MCSGP processes, grouped by process.

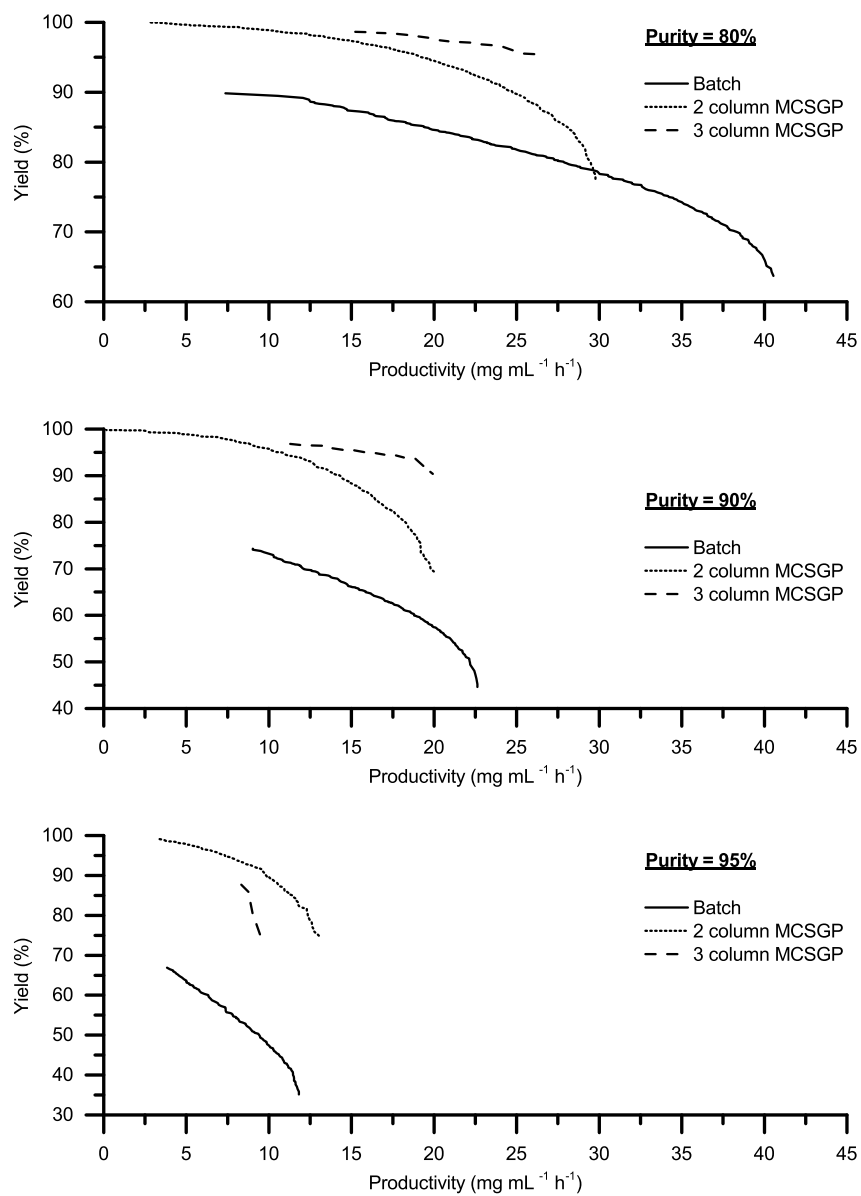


Figure 5.7: Productivity-yield pareto fronts for the batch and MCSGP processes, grouped by purity level.

without severely compromising the yield. This effect was similar to what has been observed for capture processes in the previous chapter (see 4.4, page 73): if the constraints originating from the separation problem are not limiting (the separation task is easy enough so that maximum flow rates and short gradients can be used), using multiple columns can actually be detrimental to productivity, because the loading and elution steps are not independent. This poses an additional constraint which the batch process does not have. In the 95% purity case however, the batch process fell short of the 2-column process in both objectives, because the yield was compromised so badly that the productivity suffered as well. In all cases, the multi-column processes had better yield and a better trade-off than the batch process. Among the multi-column processes, a similar inversion happened: At the lower purities (80% and 90%), the 3-column process showed a better trade-off than the 2-column process, while the 2-column process reached a higher maximum productivity. In the highest purity case again, the worse purity-yield trade-off of the 3-column process came into play, compromising yield enough to give the 2-column process a clear edge.

5.5.4 Influence of operating parameters

In order to visualize the impact of the different operating parameters on the purity and yield values, principle component analysis (PCA) was performed. Projecting the operating space on to the first two principle components, a 2-D representation of the influence of the operating parameters along the pareto fronts was obtained. Together with partial least squares regression (PLS), which provides a measure for the variable importance in projection (VIP) on the relevant sub-space and normalized regression coefficients for each variable, the most important variables were identified.

Batch polishing

Panel A in Figure 5.8 shows the scores and loadings for the first two principle components resulting from the PCA analysis for the batch process. The color indicates productivity, and since this is a visualization of a pareto-front, increasing productivity also indicates decreasing yield and vice versa. The different symbols represent the optimization runs at different purities (80%, 90% and 95%). On the axis, the percentage of variance that is explained by each principle component is noted as σ values, so 93.2% of the variability in the data set can be explained using only two linear combinations of the operating parameters, productivity and purity. The loadings for each variable, which are represented by the black lines, provide information about the correlation between the variables, where parallel lines indicate a strong correlation, and perpendicularity indicates no correlation. Several variables appeared to be correlated: Productivity was correlated with the gradient length, the modifier concentration at the end of the gradient, and the elution window; purity was correlated with the start point of the gradient; and the loading flow rate and volume were correlated. Note that in this analysis the flow rate during the gradient Q_{Grad} is missing, because every solution found by the optimizer had the same, that is maximal, gradient flow rate. This variable thus seemed to have no influence on the productivity-yield trade-off, or on the purity. Three clusters could be clearly identified in the data, which corresponded to the different purity levels. The clusters each appeared have a main direction that is more or less parallel to the other clusters, indicating that the variables changed in a similar fashion inside each cluster (moving along the productivity/yield pareto-front at a fixed purity), but that there were differences between the clusters. Using the correlations and the relative positioning of the clusters, it became clear that the main operating parameters influencing the purity were likely the gradient start and end point, as well as the start point of the product elution window. Indeed,

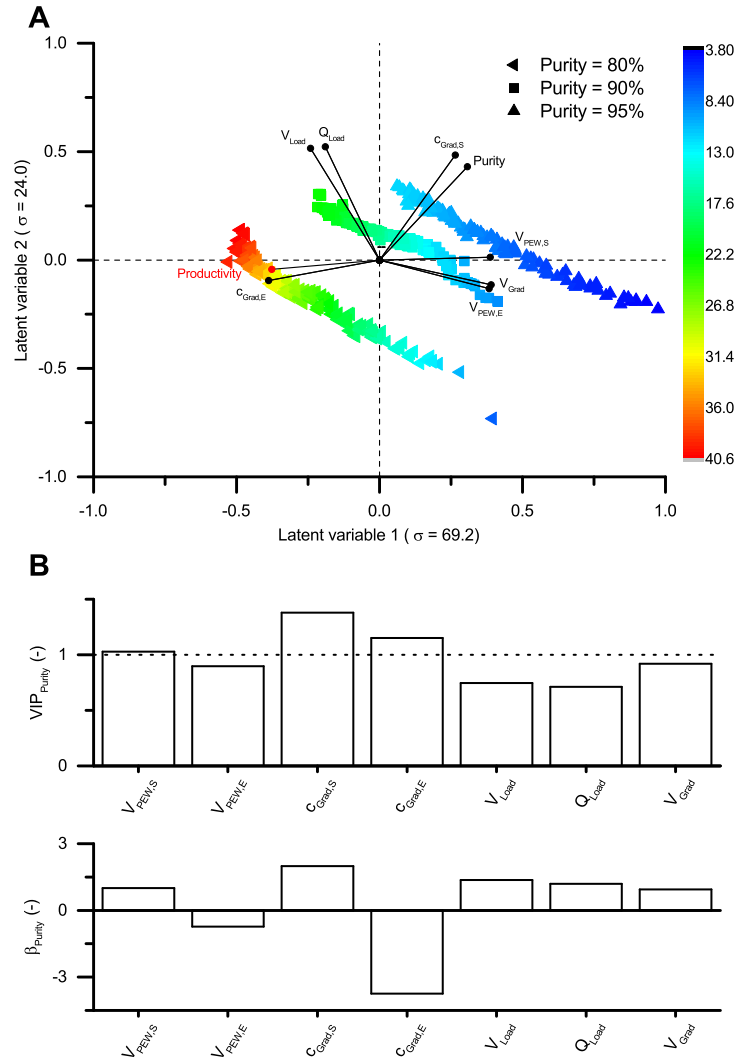


Figure 5.8: Panel A: PCA analysis of the productivity-yield pareto front for the batch process. Points indicate scores (projection of data points onto the new plane), with different symbols denoting different purity levels, lines indicate loadings (projection of operating parameters onto the new plane). Colors indicate productivity values, with red denoting high productivity and low yield, and blue the inverse case. The σ -values given in the axis labels indicate the percentage of variance in the data set explained by the latent variables. Panel B: Results of the PLS analysis for the purity. For each variable, the variable importance in projection is shown in the top axis and the normalized regression coefficient β is shown in the bottom axis.

the results of the PLS regression (panel B) suggested the same. A value for the variable importance in projection (VIP) larger than unity together with a large regression coefficient β suggests that a variable has a large influence on the purity. In this case, to influence the purity while keeping the productivity and yield pareto optimal, the most important variables were the gradient (both start and end points, as well as the duration) and to some degree the position of the product elution window. From the sign of the regression coefficients it followed that a higher purity could be achieved by increasing the start point of the gradient, decreasing the end point of the gradient and increasing its length, which corresponds to a shallower gradient. This behavior was of course very much expected. As for the product elution window, starting the collection later and finishing earlier increased purity, which was again no surprise because this corresponds to a narrower cut in the chromatogram.

Figure 5.9 shows the results of a PLS regression of productivity on each purity level, again with the variable importance in projection (VIP) in the top axis and the normalized regression coefficients β in the bottom axis. The level of the columns and the error bars correspond to the values calculated at the three different purity levels, where the column shows the middle value calculated in the regressions, and the error bars represent the high and low values. At all three purity levels, all variables except the start point of the gradient and the loading flow rate appeared to be important for changing productivity and yield in a pareto-optimal fashion. An increase in productivity (and corresponding decrease in yield) was observed when increasing the end point of the gradient and the load volume, or when decreasing the gradient duration. Since productivity is defined as amount produced per unit time and unit resin volume, it was very much expected that it increases when more product is loaded, or when the product is eluted earlier by having a steeper gradient. On the other hand, lower loading and a shallower gradient made the

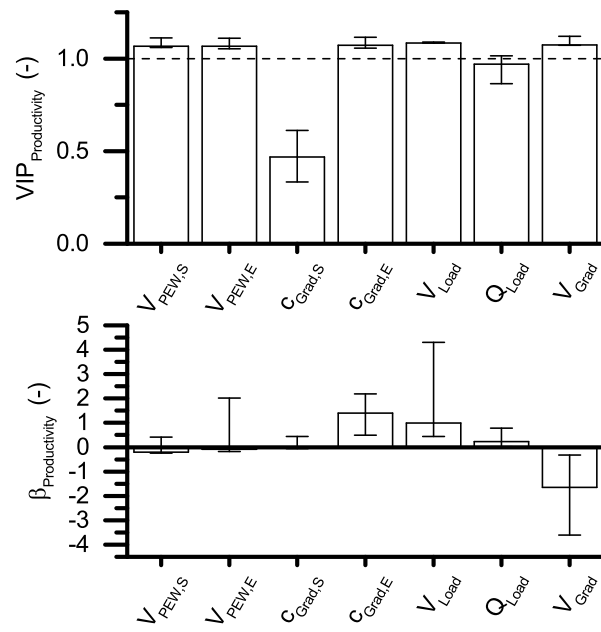


Figure 5.9: PLS regression results for productivity for the batch process. For each variable, the variable importance in projection is shown in the top axis and the normalized regression coefficient β is shown in the bottom axis.

separation easier, resulting in better yield. The one case where the position of the product elution window had a larger influence than in the others is at 80% purity. This effect could be observed because the purity requirement is not very strict, and the product elution window could be moved to a later position in the gradient, leading to contamination with strong impurity, but increasing the productivity through better recovery.

2-column MCSGP

Figure 5.10 shows the score/loading plot from the PCA analysis (panel A, top) and the PLS analysis with respect to purity (panel B) for the 2-column MCSGP process. Again, three clusters of data could be easily distinguished in the score/loading plot, corresponding to the three different purity levels. The clusters did not feature as clear a principle direction of change as in the batch case, nor were these directions parallel, indicating that there were differences in how to move along the productivity/yield pareto-front at each purity level. Not as much of the variance was explained as in the batch process, only 80% in these first two principle components. At least two clusters of correlated variables were clearly visible, in the bottom-left to top-right direction (V_W , DR_2 , V_{PEW} , Q_{Feed} , $c_{Grad,S/E}$ and Q_{PS}), and in the left to right direction (DR_1 , Purity, V_{WP} and Q_{PEW}). Combined with the variable importance in projection and the magnitude of the regression coefficients, some insight was gained about which variables seem to be important to reach a purity requirement in an optimal way. The important variables appeared to be: the width of the recycling windows (V_{WP} and V_{PS}), the flow rate in the product elution window Q_{PEW} , the gradient, and the dilution of the first recycling stream DR_1 . Regarding the recycling streams, it is important to realize that the end of the first recycling stream V_{WP} indicates the beginning of the product elution window. Therefore, as in the batch process, a later product collection resulted in

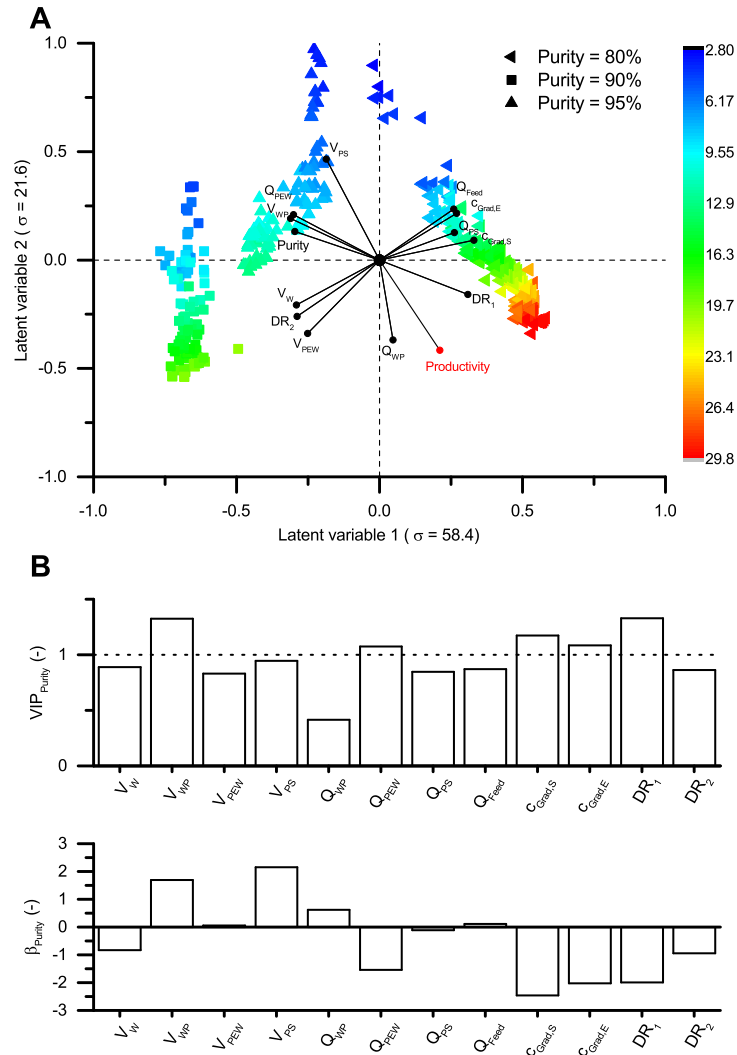


Figure 5.10: Panel A: PCA analysis of the productivity-yield pareto front for the 2-column process. Points indicate scores (projection of data points onto the new plane), with different symbols denoting different purity levels, lines indicate loadings (projection of operating parameters onto the new plane). Colors indicate productivity values, with red denoting high productivity and low yield, and blue the inverse case. The σ -values given in the axis labels indicate the percentage of variance in the data set explained by the latent variables. Panel B: Results of the PLS analysis for the purity. For each variable, the variable importance in projection is shown in the top axis and the normalized regression coefficient β is shown in the bottom axis.

better purity. Surprisingly, the width of the second window, during which product contaminated with strong impurity is recycled and which takes place after the product elution, seemed to also have a relatively large influence on the purity, judging from the normalized regression coefficients. This effect was most likely related to the gradient; a shallower gradient affords an easier separation, and a longer recycling window provides a shallower gradient. This same effect could be observed for changes in the gradient start and end points.

In terms of increasing the productivity in a pareto-optimal fashion with constrained purity, the picture was a bit less clear than in the batch process, but some main effects could still be identified (see Figure 5.11). At all three purity levels, increasing the width of the P/S recycling window and increasing the end point of the gradient resulted in better yield, but lower productivity. While it was clear that more recycling would result in better recovery, but a longer process and therefore lower productivity, it was not immediately obvious how a higher gradient end point will result in lower productivity but better yield. The increase in yield could be explained by the fact that with a steeper gradient, more product was pushed from the strong outlet, where most of the product losses occurred in this separation problem, towards the product elution window. However, since accumulation of strong impurity must be avoided, it was now necessary to have better separation between product and strong impurity, which could be achieved by a longer gradient or lower loading, both of which resulted in decreased productivity. The volume of eluted during the product elution window V_{PEW} and the flow rate during the product elution window Q_{PEW} showed interesting behavior, because they did not seem to have the same influence at different purity levels. Namely, at the 80% level, increasing the width of the product elution window resulted in a decrease in productivity, while at the other two levels, a wider window resulted in increased productivity. In the the latter case, the width of the product elution window

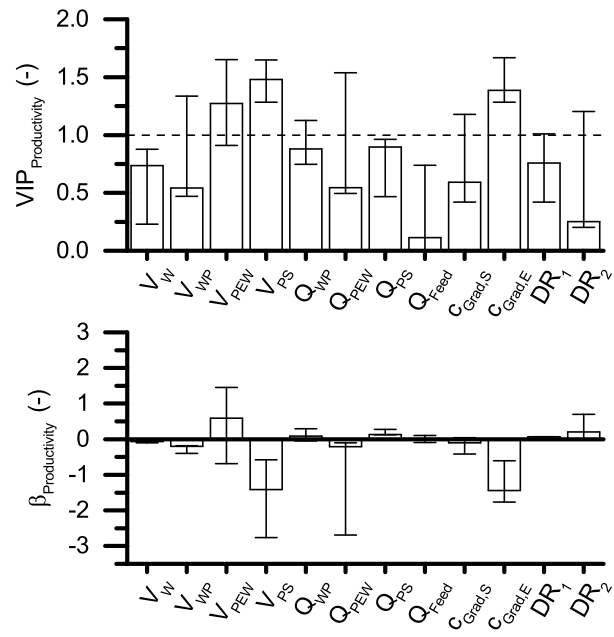


Figure 5.11: PLS regression results for productivity for the batch process. For each variable, the variable importance in projection is shown in the top axis and the normalized regression coefficient β is shown in the bottom axis.

dictated the loading amount, because the feed flow rate and the flow rate during the product elution window were more or less constant in all cases, therefore an increase in V_{PEW} would result in higher loading and therefore higher productivity. At the 80% purity level however, the width of the product elution window and the flow rate during the window were highly correlated, with the flow rate decreasing more than the volume, which lead to the interesting behavior that a narrower product elution window allowed more product to be loaded, and therefore higher productivity.

3-column MCSGP

Proceeding with the analysis for the 3-column process, again the three clusters of different purity are clearly visible in the projection on to first two principle components (91.4 % variance explained), shown in Figure 5.12 in the top panel A. The clearest correlations were found between purity, gradient end point and Q_1 , and between the gradient start point and Q_{Feed} . Note that two of the degrees of freedom are missing, namely the flow rate of the third pump during the interconnected phase Q_3 , which was equal to 0 in all optimal points found, and the flow rate of the product elution window Q_{PEW} , which was maximal in all points found. The variables t_{IC} and $c_{\text{Grad,E}}$ had the largest influence on purity, which was expected, because as in the batch process, a shallower gradient (longer gradient duration and lower end point) facilitates the separation. The flow rate of the first pump during the interconnected phase, Q_1 had a high importance in the projection found for the PLS regression with respect to purity, but a relatively small normalized regression coefficient, therefore it could be considered less important than the gradient and the duration of the interconnected time. Figure 5.13 shows the variable importance in projection and regression coefficients of the PLS regression with respect to productivity. Clearly, the variables determining the productivity (and,

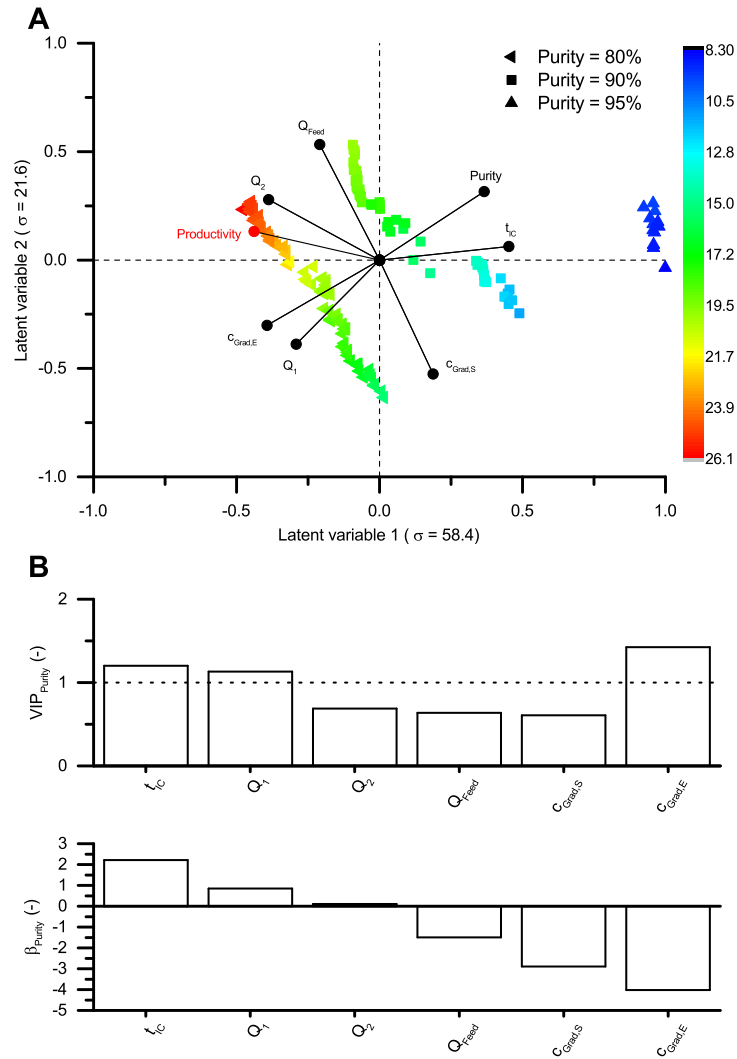


Figure 5.12: *Panel A: PCA analysis of the productivity-yield pareto front for the 2-column process. Points indicate scores (projection of data points onto the new plane), with different symbols denoting different purity levels, lines indicate loadings (projection of operating parameters onto the new plane). Colors indicate productivity values, with red denoting high productivity and low yield, and blue the inverse case. The σ -values given in the axis labels indicate the percentage of variance in the data set explained by the latent variables. Panel B: Results of the PLS analysis for the purity. For each variable, the variable importance in projection is shown in the top axis and the normalized regression coefficient β is shown in the bottom axis.*

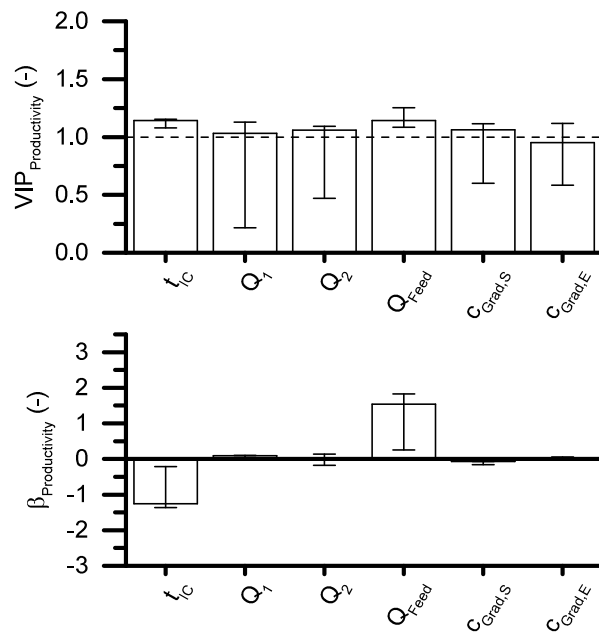


Figure 5.13: PLS regression results for productivity for the batch process. For each variable, the variable importance in projection is shown in the top axis and the normalized regression coefficient β is shown in the bottom axis.

in pareto-optimal fashion, the yield) were the interconnected time t_{IC} and the feed flow rate Q_{Feed} . During the interconnected time, the recycling takes place, it was therefore quite expected that an increase in interconnected time would increase the yield, but decrease productivity, due to the longer process duration. As in the batch process, a higher loading flow rate increases the load and therefore lead to increased productivity, but loading more makes the separation more difficult, resulting in lower yield. This was true at all three purity levels. Note that at the 80% purity level, a variable importance in projection larger than unity was calculated for all variables, indicating that they were important, but all variables except t_{IC} and Q_{Feed} had a small absolute value of β . This indicates that the process was more flexible at the lower purity level, but there were still only two main variables dictating the trade-off between productivity and yield.

5.5.5 Buffer consumption

In all processes, the buffer consumption increased with decreasing productivity (and increasing yield). Therefore, there was a trade-off between buffer consumption and yield. Figure 5.14 shows the buffer consumption as a function of yield for the pareto-optimal points found above. For each process, the buffer consumption increased with increasing yield and increasing purity constraint. The main determining factor for the buffer consumption was the gradient length in all processes at all purity levels. As shown above, a longer gradient lead to better separation and therefore higher yield and better maximal purity, but a longer process and therefore lower productivity. In terms of absolute values, the multi-column processes were comparable to each other, but clearly better than the batch process, especially at higher purities.

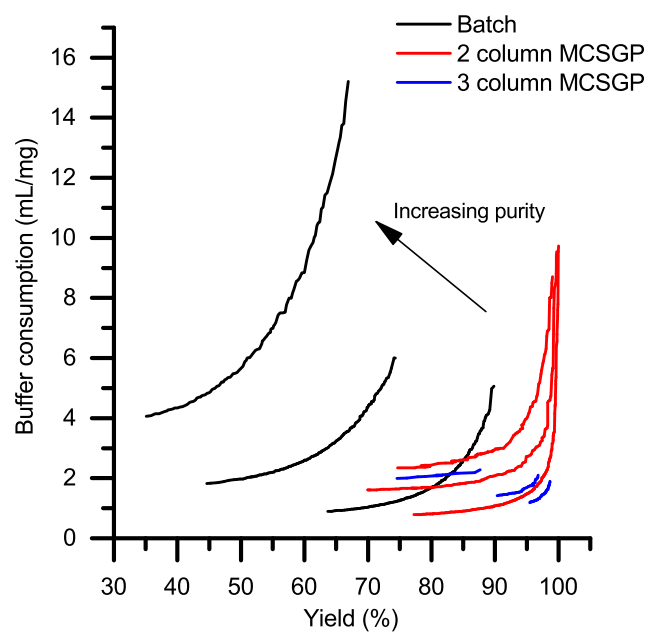


Figure 5.14: Buffer consumption as a function of yield for all processes and all three purity levels. The points correspond to the pareto-optimal productivity/yield points found above. For each process, the lowest line corresponds to 80% purity, the middle line to 90%, and the top line to 95% purity.

5.5.6 Stability analysis

The stability analysis was used to determine three factors for each process: what fraction of the runs fail at each purity; which variables are more prone to producing failures (if any); and what purity margin is needed to avoid failures across the pareto-front. Table 5.3 summarizes these values for the three processes. The multi-

Table 5.3: Stability analysis of the batch, 2- and 3-column MCSGP processes.

Process	Purity	Average failure rate	Purity margin	Sensitive variables
Batch	80%	32.3%	0.39%	Q_{Feed}
	90%	30.4%	0.17%	
	95%	23.0%	0.12%	
2-column MCSGP	80%	49.7%	2.47%	$Q_{\text{Feed}}, c_{\text{Grad}}$
	90%	13.1%	0.32%	
	95%	18.5%	0.37%	
3-column MCSGP	80%	5.32%	0.30%	$Q_{\text{Feed}}, c_{\text{Grad}}$
	90%	18.9%	0.20%	
	95%	15.6%	0.16%	

column processes appeared to be influenced less by the disturbances in general, which was most likely a consequence of their superior separation performance. The 2-column process appeared to be exceptionally unstable at 80% purity, where the productivity and therefore the loading was highest, which made the separation more difficult. For all processes however, only a very low purity margin (which is the maximum purity deficit among all the disturbed points) in the range of a few percentage points was needed to completely avoid any failed runs with the disturbances modeled. A large enough disturbance in any of the variables could cause the process to fail, but across all processes, the loading flow rate Q_{Feed} was particularly sensitive, which means disturbing it caused more failures compared to the other variables. In particular an increased value in Q_{Feed} was detrimental.

In addition, the gradient values were more decisive in the multi-column processes. This behavior was consistent with what was found in the PLS analysis of the optimization (see section 5.5.4, page 116), confirming that in order to reach higher purity, the load must be lowered and the gradient must be adjusted.

5.6 Concluding remarks

A charge variant separation of a monoclonal antibody of IgG₁-type on a DEAE-S ion exchange column, using a salt gradient, was modeled using a lumped kinetic model with Langmuir isotherms for each variant. The separation task proved to be very difficult, resulting in the well known purity/yield trade-off present in batch chromatography. Considering the high value of the products involved, this behavior warrants the use of multi-column processes which can strongly alleviate this trade-off. The model was therefore used to simulate and subsequently optimize batch separation and two different MCSGP processes, with two and three columns. During optimization, as many degrees of freedom were left available as possible, that is 8 for the batch and 3-column processes, and 12 for the 2-column process. Each process was first optimized with respect to purity and yield, which, as expected, resulted in pareto-optimal operating points. While the usage of multi-column processes could alleviate the trade-off, it could not be completely bypassed and was present in all three processes. However, the trade-off was much less pronounced in the multi-column processes. The 2-column MCSGP process showed the best trade-off, reaching 97.6% yield at 95% purity and 98.6% purity at 95% yield, thus almost completely breaking the trade-off situation. The 3-column process performed worse than the 2-column process, but still better than the batch process, reaching 87.5% yield at 95% purity and 84.3% purity at 95% yield. In the batch process, the trade-off was rather significant, resulting in just 73.9% yield at

95% purity and only 78.0% purity at 95% yield.

The second trade-off situation that was of interest in this difficult separation was the productivity/yield trade-off. At the lower two of the three different purity levels investigated (80%, 90% and 95%), fewer columns resulted in higher maximum productivity, i.e. the batch process could achieve higher productivity values than the 2-column process, which could achieve higher productivity values than the 3-column process. However, in the batch case, the trade-off had a large impact, resulting in very low yield values at high productivity. At the lower two purity values, the 2-column process exhibited a slightly worse trade-off than the 3-column process, meaning the 2-column process lost yield faster when increasing productivity. At the highest purity level, 95%, however, there was an inversion: Due to the worse purity/yield trade-off found in the 3-column process, at this level of purity the 2-column process dominated the other two processes completely.

Principle component analysis and partial least squares regression were used to determine the important variables in each process that determined purity and, with constrained purity, allowed to move along pareto-front on the yield/productivity plane. In all processes, the purity was mainly determined by the gradient, and therefore by the variables that influenced the gradient slope and duration. In terms of productivity and yield, the duration of the a process cycle and the load amount had a large impact. Longer cycles resulted in more time for the separation and recycling (in case of the multi-column processes), which increased yield, but made the processes less productive. Larger load amounts on the other hand made the separation more difficult, resulting in lower yield, but higher productivity. It is worth noting that all these relations are well known for batch processes, but appear to also apply to the 2- and 3-column MCSGP processes.

The buffer consumption was found to be related to productivity: Higher productivity resulted in lower buffer consumption for each process, while higher purity

requirement resulted in higher buffer consumption. The main parameter influencing the buffer consumption was the gradient length, with a longer gradient resulting in more buffer requirement, and, as noted above, the gradient length was also one of the main determining factors for the productivity/yield trade-off.

Process stability was investigated at different points along the productivity/yield pareto-curves for each process at each purity by introducing random disturbances in all input variables. If the purity requirement could not be met, a run was deemed a failure. All three processes showed significant failure rates even for small variations, with an average of 28.6%, 27.1%, and 12.2% of runs failing for the batch, 2- and 3-column processes respectively. However, only very small margins in purity would be needed to completely prevent any failures (0.40%, 2.5% and 0.30% for the batch, 2- and 3-column processes, respectively), owed to the fact that the pareto-optimal operating points are all right on the boundary of feasibility. The main variables responsible for failures were the gradients and the feed flow rates. Overall, it became clear that there is a step change in performance when going from single column batch chromatography to 2-column MCSGP, and only a marginal improvement at lower purities when going from 2-column MCSGP to 3-column MCSGP. Due to the linear increase of equipment cost with number of columns, the 2-column MCSGP process appears to be optimal for very difficult separation of high value products with strict product quality requirements.

Chapter 6

Conclusions and outlook

Chromatography has long been one of the most widely used separation techniques for difficult mixtures, both for analytical as well as for preparative purposes. With the advent of the simulated moving bed (SMB) process and later the multi-column counter-current solvent gradient purification (MCSGP) process, multi-column applications have become possible and ever more frequently applied. Due to the cyclic steady state that these multi-column processes reach, it is not immediately obvious how to optimally design such a process, owing to the internal recycling streams and long transients.

Empirical MCSGP design

In chapter 2, the application of MCSGP to the isolation and purification of human blood plasma proteins was examined. The first and simplest approach to designing a multi-column chromatographic process was highlighted here, which is an empirical design from a batch experiment. As an example target protein, α_1 -antitrypsin (AAT) was isolated from single donor, cryopoor, delipidated human blood plasma. The historic Cohn process for albumin production, where increasing amounts of

ethanol are added to cold plasma in order to precipitate different fractions of proteins, is still the backbone of industrial plasma fractionation processes. In these industrial applications, AAT is usually isolated from the Cohn fraction IV precipitate, where many impurities have already been removed. The approach presented in this work was therefore a much more difficult separation and could easily be applied in an industrial setting.

In the batch process, which was run as gradient ion-exchange chromatography on a fractogel EMD DEAE (M) resin, the well known trade-off situation between purity and yield could be observed: either a narrow, pure product fraction can be collected, which leads to the loss of all product eluting before and after the product elution window, or a wide product fraction is pooled, which leads to compromised purity due to the fact that impurities co-elute with the product. To alleviate this, the batch chromatogram was used to design an MCSGP process using empirical design rules. This MCSGP process managed to break the trade-off, reaching high purity and high yield simultaneously. Further product analysis by LC/MS/MS and size exclusion chromatography revealed the presence of several additional impurities compared to an industrial standard, but these are commonly removed by an orthogonal chromatography step.

Optimal CaptureSMB design

The CaptureSMB process was recently developed to increase resin capacity utilization and productivity in protein A capture steps. As with the MCSGP process, empirical design rules have been developed to set up a multi-column process from a batch experiment. Because design rules like these are expected to yield suboptimal process parameters, in chapter 3 a different approach was followed: Batch capture and the CaptureSMB process were modeled and optimized *in silico*. In a first step, batch breakthrough curves of a monoclonal antibody (mAb) on a protein

A column were fitted using a lumped kinetic model with an empirical correlation describing the decrease of mass transfer with increasing saturation of the resin. The resulting model was used to simulate the CaptureSMB process at different operating points, and comparison to experimental data showed that such a model can adequately predict CaptureSMB performance using just batch breakthrough curves. The model also allowed to look inside the columns by examining the internal concentration profiles calculated, and it was shown that the first column can be fully loaded while the all product is contained in only the two columns, therefore making a third column in the load train generally redundant.

In a second step, the batch and CaptureSMB models were used to optimize the two processes, using a genetic algorithm. Two optimization objectives were targeted: Resin capacity utilization, which determines how much product can be processed per resin volume and per cycle, and productivity, which determines how much product can be processed per resin volume and per time. The main cause of resin deterioration is the cleaning-in-place (CIP) step, which occurs once per cycle per column. Therefore, if the resin capacity utilization is higher, more mAb can be processed before the resin must be replaced, which, due to the high cost of protein A resin, can lead to major cost reductions. Productivity on the other hand is important simply because it allows faster processing of a given amount of product, which amounts to time savings and related cost savings. Rigorous optimization of both processes, with flow rate constraints and with the constraint that the breakthrough value at the end of the batch phase in CaptureSMB and at the end of the loading phase in the batch process cannot exceed 1%, showed that a trade-off between the two objectives is present in both processes. The CaptureSMB process however can reach a higher maximum capacity utilization and a higher productivity overall, and has a better trade-off, meaning that with increasing productivity the capacity utilization decreases more slowly than in the batch case.

Comparison of different multi-column capture processes

The CaptureSMB process was certainly not the first multi-column capture process to be developed, but arguably one of the least complex, owing to the fact that it only employs two columns, compared to several well known processes with 3, 4 or even more columns. In chapter 4, the 3- and 4-column periodic counter current chromatography (PCC) processes, which are closely related to the CaptureSMB process, were modeled and optimized along with batch capture and CaptureSMB itself, using the same tools as in chapter 3, but with a more advanced adsorption model. The new model replicated the behavior of the protein on the particle level in more detail, employing a shrinking core model to describe the adsorption of the mAb in the resin particles. As with the empirical mass transfer model, this was used to take the decrease in mass transfer into account, that occurs when the pores in the particle get filled with adsorbed protein, but with a more rigorous mechanistic approach. This led to a more accurate representation of the breakthrough curves, and therefore better model predictions.

As above, the model was then used to simulate and optimize the four different capture processes, using as a constraint that a column with no other column connected downstream may not exceed a breakthrough value of 1%. In addition, the flow rate was constrained by the pressure drop, and the interconnected time in the PCC processes was constrained by the fact that during this phase, one or two columns undergo recovery and regeneration, which must be finished before switching occurs. Optimizing again resin capacity utilization and productivity, pareto-optimal operating points were found for all 4 processes. Additionally, the influence of the CIP time, the feed concentration, the duration of the interconnected washing procedures and the length of a single column was examined. The final comparison showed that, depending on the objective and the feed concentration, different

processes are optimal. At low titers and medium titers, the CaptureSMB process proved optimal for maximizing productivity, but surprisingly, at high titers, the batch process exhibited the highest maximum productivity value among all the processes, albeit at a considerable reduction in capacity utilization. This was due to the fact that in the batch process, the loading and elution are completely decoupled, which means that very quick, fast loading can be used to maximize the productivity, while in the multi-column processes, the switching time is constrained by the recovery and regeneration phase, which happens simultaneously. In terms of maximizing the capacity utilization, all three multi-column processes proved equally optimal, reaching close to 100% capacity utilization in all cases. The trade-off situation, i.e. how much capacity utilization is lost when increasing productivity, was best in the CaptureSMB process at low and high titers, but at medium titers, the 3-column PCC process proved slightly more optimal in this regard. In summary, it was shown that there is a step change in performance between single column and multi-column chromatography, but there is no guaranteed increase in performance when using more than two columns.

Comparison of different multi-column polishing processes

In the last chapter, chapter 5, the focus was again on the polishing part of the downstream processing. Similarly to the many different multi-column capture processes available, the MCSGP process has been shown to operate in many different configurations, using 2, 3, 4, 5, 6 or even 8 columns. In order to assess the performance of the different processes, the two most representative ones, the 2- and 3-column MCSGP processes, along with batch polishing, were compared. Since so far, only empirical design rules exist to set up the MCSGP processes, it was unclear how to run the processes optimally. Given the large numbers of degrees of freedom in each of the processes, model-based optimization was the best way to

ensure that a comparison could be made at optimal operating points for each of the processes.

Using as an example problem the separation of charge variants of a mAb, a model was developed that could replicate the elution behavior of these charge variants under gradient conditions on an ion-exchange column. In a batch separation process, when there is overlap between the desired product and the impurities, a trade-off situation occurs: either a narrow, high-purity product fraction can be collected, resulting in yield losses, or a broad, but impure fraction can be pooled, which improves the yield but compromises purity. The MCSGP process was initially developed with the goal of breaking this trade-off. The first optimization task considered was therefore to optimize purity and yield. As expected, the batch process exhibited a significant trade-off, requiring to sacrifice a large part of the yield to achieve acceptable purity levels. For the MCSGP processes however, it was found that they too exhibited a trade-off between purity and yield, but at a much higher level, meaning that much less yield was lost when increasing the purity levels. Among the two MCSGP processes, the two-column process exhibited a better trade-off still than the 3-column process. The next interesting trade-off situation occurs when a working separation, that achieves the desired purity goal, has been established, but the loading and therefore the productivity should be increased. Optimizing for productivity and yield, while keeping the purity above a certain target value, showed that all three processes exhibit a trade-off between these two performance variables. The two-column process again showed the best performance overall, except at low purity requirements, where it could not reach the same maximum productivity values as the other two processes, but still showed the best yield. Again, there was a step change in performance from batch to two columns, but negligible improvements from two to three column. Surprisingly, when the purity constraint was rather low, the batch process showed the highest

maximum productivity by far, reiterating one of the findings of the previous chapter, that a single column, which completely decouples loading from the elution, can be the optimum configuration for maximum productivity, if the main factor determining productivity is the process time.

Each of the resulting pareto curves in the yield/productivity plane was analyzed using multivariate regression techniques, namely principle component analysis (PCA) and partial least squares regression (PLS), in order to identify the most important operating parameters in each of the processes. In general terms, it was shown that the same basic principles as in the batch process could be applied to the MCSGP processes, namely that the gradient is most important to achieve proper separation, that higher loading increases the productivity but makes the separation more challenging, and that faster process times make the separation faster, but more difficult.

The process understanding that arose from the rigorous modeling and optimization of these complex processes offers a opportunity to improve performance. The proof of the mere existence of trade-off situations in multi-column processes has already reshaped our understanding of what an optimal process might look like; in cases where there is a pareto-front, optimality is a very different concept from just finding one single optimal operating point. The identification of key process variables and how to reach and move along a pareto-curve greatly simplifies the research into better empirical design rules. In the case of CaptureSMB the increased process understanding has in practice already led to the development of a completely model-free, online optimizing control concept, that automatically finds pareto-optimal operating points and can move along pareto-curves. Developing such concepts for the much more complex MCSGP process is a more difficult matter, but the analysis provided here should act as a stepping stone in this direction.

Bibliography

- [1] J. Drews, Drug discovery: a historical perspective. *Science* 2000, 287 (5460), 1960–1964.
- [2] G. Walsh, Biopharmaceutical benchmarks 2014. *Nat Biotech* 2014, 32 (10), 992–1000.
- [3] H. Daniell, S. J. Streatfield, K. Wycoff, Medical molecular farming: production of antibodies, biopharmaceuticals and edible vaccines in plants. *Trends in Plant Science* 2001, 6 (5), 219 – 226.
- [4] S. Assady, G. Maor, M. Amit, J. Itskovitz-Eldor, K. L. Skorecki, M. Tzukerman, Insulin production by human embryonic stem cells. *Diabetes* 2001, 50 (8), 1691–1697.
- [5] E. B. Jensen, S. Carlsen, Production of recombinant human growth hormone in escherichia coli: Expression of different precursors and physiological effects of glucose, acetate, and salts. *Biotechnology and Bioengineering* 1990, 36 (1), 1–11.
- [6] A. Beck, T. Wurch, C. Bailly, N. Corvaia, Strategies and challenges for the next generation of therapeutic antibodies. *Nature reviews. Immunology* 2010, 10 (5), 345–352.
- [7] G. P. Cereghino, J. L. Cereghino, C. Ilgen, J. M. Cregg, Production of recombinant proteins in fermenter cultures of the yeast pichia pastoris. *Current Opinion in Biotechnology* 2002, 13 (4), 329 – 332.
- [8] A. A. Shukla, J. Thömmes, Recent advances in large-scale production of monoclonal antibodies and related proteins. *Trends in Biotechnology* 2010, 28 (5), 253 – 261.
- [9] E. J. Cohn, L. E. Strong, W. L. Hughes, D. J. Mulford, J. N. Ashworth, M. Melin, H. L. Taylor, Preparation and properties of serum and plasma proteins. iv. a system for the separation into fractions of the protein and lipoprotein components of biological tissues and fluids1a,b,c,d. *Journal of the American Chemical Society* 1946, 68 (3), 459–475.
- [10] P. Kistler, H. Nitschmann, Large scale production of human plasma fractions. *Vox Sanguinis* 1962, 7 (4), 414–424.

- [11] T. Burnouf, Modern plasma fractionation. *Transfusion Medicine Reviews* 2007, 21 (2), 101 – 117.
- [12] T. Burnouf, Recombinant plasma proteins. *Vox Sanguinis* 2011, 100 (1), 68–83.
- [13] S. Moore, D. S. Pepper, J. D. Cash, Platelet antiheparin activity. *Biochimica et Biophysica Acta (BBA) - Protein Structure* 1975, 379 (2), 370 – 384.
- [14] W. R. Church, R. L. Jernigan, J. Toole, R. M. Hewick, J. Knopf, G. J. Knutson, M. E. Nesheim, K. G. Mann, D. N. Fass, Coagulation factors v and viii and ceruloplasmin constitute a family of structurally related proteins. *Proceedings of the National Academy of Sciences* 1984, 81 (22), 6934–6937.
- [15] S. P. Bajaj, S. I. Rapaport, S. F. Brown, Isolation and characterization of human factor VII. activation of factor VII by factorXa. *Journal of Biological Chemistry* 1981, 256 (1), 253–259.
- [16] L. O. Andersson, N. Forsman, K. Huang, K. Larsen, A. Lundin, B. Pavlu, H. Sandberg, K. Sewerin, J. Smart, Isolation and characterization of human factor VIII: molecular forms in commercial factor VIII concentrate, cryoprecipitate, and plasma. *Proceedings of the National Academy of Sciences* 1986, 83 (9), 2979–2983.
- [17] R. G. D. Scipio, M. A. Hermodson, S. G. Yates, E. W. Davie, A comparison of human prothrombin, factor IX (christmas factor), factor X (stuart factor), and protein S. *Biochemistry* 1977, 16 (4), 698–706.
- [18] K. Kurachi, G. Schmer, M. A. Hermodson, D. C. Teller, E. W. Davie, Characterization of human, bovine, and horse antithrombin III. *Biochemistry* 1976, 15 (2), 368–373.
- [19] R. Pannell, D. Johnson, J. Travis, Isolation and properties of human plasma α -1-proteinase inhibitor. *Biochemistry* 1974, 13 (26), 5439–5445.
- [20] M. Steinbuch, R. Audran, The isolation of igg from mammalian sera with the aid of caprylic acid. *Archives of Biochemistry and Biophysics* 1969, 134 (2), 279 – 284.
- [21] H. Chaplin, S. Cohen, E. Press, Preparation and properties of the peptide chains of normal human 19s γ -globulin (IgM). *Biochemical Journal* 1965, 95 (1), 256.
- [22] J. Viikari, Precipitation of plasma lipoproteins by PEG-6000 and its evaluation with electrophoresis and ultracentrifugation. *Scandinavian Journal of Clinical and Laboratory Investigation* 1976, 36 (3), 265–268.
- [23] T. Burnouf, Chromatography in plasma fractionation: benefits and future trends. *Journal of Chromatography B: Biomedical Sciences and Applications* 1995, 664 (1), 3 – 15.

- [24] H. E. Conrad, *Heparin-binding proteins*. Academic Press, 1997.
- [25] T. Yatohgo, M. Izumi, H. Kashiwagi, M. Hayashi, Novel purification of vitronectin from human plasma by heparin affinity chromatography. *Cell Structure and Function* 1988, 13 (4), 281–292.
- [26] T. Burnouf, M. Radosevich, Affinity chromatography in the industrial purification of plasma proteins for therapeutic use. *Journal of Biochemical and Biophysical Methods* 2001, 49 (1–3), 575 – 586.
- [27] G. Guiochon, A. Felinger, D. G. Shirazi, *Fundamentals of preparative and nonlinear chromatography*. Academic Press, 2006.
- [28] M. Mazzotti, G. Storti, M. Morbidelli, Optimal operation of simulated moving bed units for nonlinear chromatographic separations. *Journal of Chromatography A* 1997, 769 (1), 3 – 24.
- [29] E. R. Francotte, P. Richert, Applications of simulated moving-bed chromatography to the separation of the enantiomers of chiral drugs. *Journal of Chromatography A* 1997, 769 (1), 101 – 107.
- [30] C. M. Grill, L. Miller, T. Q. Yan, Resolution of a racemic pharmaceutical intermediate: A comparison of preparative hplc, steady state recycling, and simulated moving bed. *Journal of Chromatography A* 2004, 1026 (1–2), 101 – 108.
- [31] P. C. Wankat, Simulated moving bed cascades for ternary separations. *Industrial & Engineering Chemistry Research* 2001, 40 (26), 6185–6193.
- [32] G. Paredes, S. Abel, M. Mazzotti, M. Morbidelli, J. Stadler, Analysis of a simulated moving bed operation for three-fraction separations (3F-SMB). *Industrial & Engineering Chemistry Research* 2004, 43 (19), 6157–6167.
- [33] G. Ströhlein, L. Aumann, M. Mazzotti, M. Morbidelli, A continuous, counter-current multi-column chromatographic process incorporating modifier gradients for ternary separations. *Journal of Chromatography A* 2006, 1126 (1–2), 338 – 346.
- [34] G. Köhler, C. Milstein, Continuous cultures of fused cells secreting antibody of predefined specificity. *nat* 1975, 256, 495–497.
- [35] A. L. Nelson, E. Dhimolea, J. M. Reichert, Development trends for human monoclonal antibody therapeutics. *Nature reviews Drug discovery* 2010, 9 (10), 767–774.
- [36] J. G. Elvin, R. G. Couston, C. F. van der Walle, Therapeutic antibodies: Market considerations, disease targets and bioprocessing. *International journal of pharmaceuticals* 2013, 440 (1), 83–98.

- [37] B. Kelley, Industrialization of mab production technology: The bioprocessing industry at a crossroads. *mAbs* 2009, 1 (5), 443–452.
- [38] S. Hober, K. Nord, M. Linhult, Protein a chromatography for antibody purification. *Journal of Chromatography B* 2007, 848 (1), 40 – 47.
- [39] H. Hjelm, K. Hjelm, J. Sjöquist, Protein a from staphylococcus aureus. its isolation by affinity chromatography and its use as an immunosorbent for isolation of immunoglobulins. *FEBS Letters* 1972, 28 (1), 73–76.
- [40] A. A. Shukla, P. Hinckley, Host cell protein clearance during protein a chromatography: Development of an improved column wash step. *Biotechnology Progress* 2008, 24 (5), 1115–1121.
- [41] C. Jiang, J. Liu, M. Rubacha, A. A. Shukla, A mechanistic study of protein a chromatography resin lifetime. *Journal of Chromatography A* 2009, 1216 (31), 5849 – 5855.
- [42] R. Godawat, K. Brower, S. Jain, K. Konstantinov, F. Riske, V. Warikoo, Periodic counter-current chromatography – design and operational considerations for integrated and continuous purification of proteins. *Biotechnology Journal* 2012, 7 (12), 1496–1508.
- [43] M. Angarita, T. Müller-Späth, D. Baur, R. Lievrouw, G. Lissens, M. Morbidelli, Twin-column CaptureSMB: A novel cyclic process for protein a affinity chromatography. *Journal of Chromatography A* 2015, 1389, 85 – 95.
- [44] F. Steinebach, M. Angarita, D. J. Karst, T. Müller-Späth, M. Morbidelli, Model based adaptive control of a continuous capture process for monoclonal antibodies production. *Journal of Chromatography A* 2016, 1444, 50 – 56.
- [45] S. Kukkonen, J. Lampinen, GDE3: the third evolution step of generalized differential evolution. in *Evolutionary Computation, 2005. The 2005 IEEE Congress on*, volume 1, 443–450 Vol.1.
- [46] E. Mahajan, A. George, B. Wolk, Improving affinity chromatography resin efficiency using semi-continuous chromatography. *Journal of Chromatography A* 2012, 1227, 154 – 162.
- [47] J. Pollock, G. Bolton, J. Coffman, S. V. Ho, D. G. Bracewell, S. S. Farid, Optimising the design and operation of semi-continuous affinity chromatography for clinical and commercial manufacture. *Journal of Chromatography A* 2013, 1284, 17–27.
- [48] M. Holzer, H. Osuna-Sanchez, L. David, Multicolumn chromatography. *Bio-Process Intl* 2008, 6, 74–82.
- [49] C. K. Ng, F. Rousset, E. Valery, D. G. Bracewell, E. Sorensen, Design of high productivity sequential multi-column chromatography for antibody capture. *Food and Bioproducts Processing* 2014, 92 (2), 233 – 241.

- [50] M. Bisschops, L. Frick, S. Fulton, T. Ransohoff, Single-use, continuous-countercurrent, multicolumn chromatography. *BioProcess Int* 2009, 7 (6), S18–S23.
- [51] M. Krättli, F. Steinebach, M. Morbidelli, Online control of the twin-column countercurrent solvent gradient process for biochromatography. *Journal of Chromatography A* 2013, 1293, 51 – 59.
- [52] L. Aumann, M. Morbidelli, A semicontinuous 3-column countercurrent solvent gradient purification (MCSGP) process. *Biotechnology and bioengineering* 2008, 99 (3), 728–733.
- [53] J. Travis, J. Bowen, D. Tewksbury, D. Johnson, R. Pannell, Isolation of albumin from whole human plasma and fractionation of albumin-depleted plasma. *Biochemical Journal* 1976, 157 (2), 301–306.
- [54] L.-O. Andersson, T. Barrowcliffe, E. Holmer, E. Johnson, G. Sims, Anti-coagulant properties of heparin fractionated by affinity chromatography on matrix-bound antithrombin III and by gel filtration. *Thrombosis Research* 1976, 9 (6), 575 – 583.
- [55] H. A. Sober, F. J. Gutter, M. M. Wyckoff, E. A. Peterson, Chromatography of proteins. II. fractionation of serum protein on anion-exchange cellulose. *Journal of the American Chemical Society* 1956, 78 (4), 756–763.
- [56] A. Dromard, M. Exertier, C. Rollin, J. Tayot, M. Tardy, Fractionation/purification of plasma by ion exchange chromatography. 1987, US Patent 4,675,384.
- [57] N. L. Anderson, N. G. Anderson, The human plasma proteome history, character, and diagnostic prospects. *Molecular & cellular proteomics* 2002, 1 (11), 845–867.
- [58] S. Gallant, S. Vunnum, S. Cramer, Optimization of preparative ion-exchange chromatography of proteins: linear gradient separations. *Journal of Chromatography A* 1996, 725 (2), 295 – 314.
- [59] L. Aumann, M. Morbidelli, A continuous multicolumn countercurrent solvent gradient purification (MCSGP) process. *Biotechnology and Bioengineering* 2007, 98 (5), 1043–1055.
- [60] T. Müller-Späth, M. Krättli, L. Aumann, G. Ströhlein, M. Morbidelli, Increasing the activity of monoclonal antibody therapeutics by continuous chromatography (MCSGP). *Biotechnology and bioengineering* 2010, 107 (4), 652–662.
- [61] F. Steinebach, T. Müller-Späth, M. Morbidelli, Continuous counter-current chromatography for capture and polishing steps in biopharmaceutical production. *Biotechnology Journal* 2016, 11 (9), 1126–1141.

- [62] T. Mueller-Spaeth, G. Stroehlein, O. Lyngberg, D. Maclean, Enabling high purities and yields in therapeutic peptide purification using multicolumn countercurrent solvent gradient purification. *Chimica Oggi–Chemistry Today* 2013, 31 (5), 56–60.
- [63] A. Jungbauer, Continuous downstream processing of biopharmaceuticals. *Trends in Biotechnology* 2013, 31 (8), 479 – 492.
- [64] M. Krättli, T. Müller-Späth, M. Morbidelli, Multifraction separation in countercurrent chromatography (MCSGP). *Biotechnology and Bioengineering* 2013, 110 (9), 2436–2444.
- [65] T. Müller-Späth, L. Aumann, L. Melter, G. Ströhlein, M. Morbidelli, Chromatographic separation of three monoclonal antibody variants using multicolumn countercurrent solvent gradient purification (MCSGP). *Biotechnology and Bioengineering* 2008, 100 (6), 1166–1177.
- [66] O. Ludemann-Hombourger, R. M. Nicoud, M. Bailly, The “VARICOL” process: A new multicolumn continuous chromatographic process. *Separation Science and Technology* 2000, 35 (12), 1829–1862.
- [67] S. Abel, M. U. Bäbler, C. Arpagaus, M. Mazzotti, J. Stadler, Two-fraction and three-fraction continuous simulated moving bed separation of nucleosides. *Journal of Chromatography A* 2004, 1043 (2), 201 – 210.
- [68] S. Ghose, D. Nagrath, B. Hubbard, C. Brooks, S. M. Cramer, Use and optimization of a dual-flowrate loading strategy to maximize throughput in protein-a affinity chromatography. *Biotechnology Progress* 2004, 20 (3), 830–840.
- [69] R. Hahn, P. Bauerhansl, K. Shimahara, C. Wizniewski, A. Tscheliessnig, A. Jungbauer, Comparison of protein a affinity sorbents: II. mass transfer properties. *Journal of Chromatography A* 2005, 1093 (1–2), 98 – 110.
- [70] R. L. Fahrner, D. H. Whitney, M. Vanderlaan, G. S. Blank, Performance comparison of protein a affinity-chromatography sorbents for purifying recombinant monoclonal antibodies. *Biotechnology and Applied Biochemistry* 1999, 30 (2), 121–128.
- [71] V. Warikoo, R. Godawat, K. Brower, S. Jain, D. Cummings, E. Simons, T. Johnson, J. Walther, M. Yu, B. Wright, J. McLarty, K. P. Karey, C. Hwang, W. Zhou, F. Riske, K. Konstantinov, Integrated continuous production of recombinant therapeutic proteins. *Biotechnology and Bioengineering* 2012, 109 (12), 3018–3029.
- [72] G. Guiochon, Preparative liquid chromatography. *Journal of Chromatography A* 2002, 965 (1–2), 129 – 161.

- [73] K.-U. Klatt, F. Hanisch, G. Dünnebier, S. Engell, Model-based optimization and control of chromatographic processes. *Computers & Chemical Engineering* 2000, 24 (2–7), 1119 – 1126.
- [74] K. Kaczmarski, M. Mazzotti, G. Storti, M. Morbidelli, Modeling fixed-bed adsorption columns through orthogonal collocations on moving finite elements. *Computers & Chemical Engineering* 1997, 21 (6), 641 – 660.
- [75] S. Golshan-Shirazi, G. Guiochon, Analytical solution for the ideal model of chromatography in the case of a langmuir isotherm. *Analytical Chemistry* 1988, 60 (21), 2364–2374.
- [76] N. Forrer, A. Butté, M. Morbidelli, Chromatographic behavior of a polyclonal antibody mixture on a strong cation exchanger column. part I: Adsorption characterization. *Journal of Chromatography A* 2008, 1214 (1–2), 59 – 70.
- [77] C. Orellana, C. Shene, J. Asenjo, Mathematical modeling of elution curves for a protein mixture in ion exchange chromatography applied to high protein concentration. *Biotechnology and Bioengineering* 2009, 104 (3), 572–581.
- [78] C. A. Brooks, S. M. Cramer, Steric mass-action ion exchange: Displacement profiles and induced salt gradients. *AIChE Journal* 1992, 38 (12), 1969–1978.
- [79] W.-D. Chen, X.-Y. Dong, Y. Sun, Analysis of diffusion models for protein adsorption to porous anion-exchange adsorbent. *Journal of Chromatography A* 2002, 962 (1–2), 29 – 40.
- [80] H. Thomas, B. C. de Neuville, G. Storti, M. Morbidelli, M. Joehnck, M. Schulte, Role of tentacles and protein loading on pore accessibility and mass transfer in cation exchange materials for proteins. *Journal of Chromatography A* 2013, 1285, 48 – 56.
- [81] B. C. de Neuville, H. Thomas, M. Morbidelli, Simulation of porosity decrease with protein adsorption using the distributed pore model. *Journal of Chromatography A* 2013, 1314, 77 – 85.
- [82] T. Müller-Späth, G. Ströhlein, L. Aumann, H. Kornmann, P. Valax, L. Delegrange, E. Charbaut, G. Baer, A. Lamproye, M. Jöhnck, M. Schulte, M. Morbidelli, Model simulation and experimental verification of a cation-exchange igg capture step in batch and continuous chromatography. *Journal of Chromatography A* 2011, 1218 (31), 5195 – 5204.
- [83] C. K. Ng, H. Osuna-Sanchez, E. Valéry, E. Sørensen, D. G. Bracewell, Design of high productivity antibody capture by protein a chromatography using an integrated experimental and modeling approach. *Journal of Chromatography B* 2012, 899, 116 – 126.
- [84] A. C. Hindmarsh, ODEPACK, a systematized collection of ODE solvers. *IMACS transactions on scientific computation* 1983, 1, 55–64.

- [85] A. C. Hindmarsh, NetLib ODEPACK. <http://www.netlib.org/odepack/>, 2001, [Online; accessed 06/2013].
- [86] G. Carta, A. Jungbauer, *Protein chromatography: process development and scale-up*. John Wiley & Sons, 2010.
- [87] D. L. Hacker, M. De Jesus, F. M. Wurm, 25 years of recombinant proteins from reactor-grown cells — where do we go from here? *Biotechnology Advances* 2009, 27 (6), 1023–1027.
- [88] D. Low, R. O’Leary, N. S. Pujar, Future of antibody purification. *Journal of Chromatography B* 2007, 848 (1), 48–63.
- [89] J. Andersson, B. Mattiasson, Simulated moving bed technology with a simplified approach for protein purification: Separation of lactoperoxidase and lactoferrin from whey protein concentrate. *Journal of Chromatography A* 2006, 1107 (1–2), 88–95.
- [90] N. Gottschlich, V. Kasche, Purification of monoclonal antibodies by simulated moving-bed chromatography. *Journal of Chromatography A* 1997, 765 (2), 201–206.
- [91] M. Schulte, J. Strube, Preparative enantioseparation by simulated moving bed chromatography. *Journal of Chromatography A* 2001, 906 (1–2), 399–416.
- [92] A. Ljunglöf, R. Hjorth, Confocal microscopy as a tool for studying protein adsorption to chromatographic matrices. *Journal of Chromatography A* 1996, 743 (1), 75–83.
- [93] J. Hubbuch, T. Linden, E. Knieps, A. Ljunglöf, J. Thömmes, M.-R. Kula, Mechanism and kinetics of protein transport in chromatographic media studied by confocal laser scanning microscopy: Part I. the interplay of sorbent structure and fluid phase conditions. *Journal of Chromatography A* 2003, 1021 (1–2), 93–104.
- [94] T. Linden, A. Ljunglöf, L. Hagel, M.-R. Kula, J. Thömmes, Visualizing patterns of protein uptake to porous media using confocal scanning laser microscopy. *Separation science and technology* 2002, 37 (1), 1–32.
- [95] S. R. Dziennik, E. B. Belcher, G. A. Barker, A. M. Lenhoff, Effects of ionic strength on lysozyme uptake rates in cation exchangers. I: Uptake in SP sepharose FF. *Biotechnology and bioengineering* 2005, 91 (2), 139–153.
- [96] L. E. Weaver, G. Carta, Protein adsorption on cation exchangers: Comparison of macroporous and gel-composite media. *Biotechnology progress* 1996, 12 (3), 342–355.
- [97] M. Nativ, S. Goldstein, G. Schmuckler, Kinetics of ion-exchange processes accompanied by chemical reactions. *Journal of Inorganic and Nuclear Chemistry* 1975, 37 (9), 1951–1956.

- [98] P. A. Marichal-Gallardo, M. M. Álvarez, State-of-the-art in downstream processing of monoclonal antibodies: Process trends in design and validation. *Biotechnology Progress* 2012, 28 (4), 899–916.
- [99] T. Müller-Späth, L. Aumann, G. Ströhlein, H. Kornmann, P. Valax, L. Delegrange, E. Charbaut, G. Baer, A. Lamproye, M. Jöhnck, M. Schulte, M. Morbidelli, Two step capture and purification of IgG2 using multicolumn countercurrent solvent gradient purification (MCSGP). *Biotechnology and Bioengineering* 2010, 107 (6), 974–984.
- [100] A. A. Shukla, B. Hubbard, T. Tressel, S. Guhan, D. Low, Downstream processing of monoclonal antibodies—application of platform approaches. *Journal of Chromatography B* 2007, 848 (1), 28 – 39.
- [101] D. M. Ruthven, C. Ching, Counter-current and simulated counter-current adsorption separation processes. *Chemical Engineering Science* 1989, 44 (5), 1011 – 1038.
- [102] F. Charton, R.-M. Nicoud, Complete design of a simulated moving bed. *Journal of Chromatography A* 1995, 702 (1), 97 – 112.
- [103] M. Juza, M. Mazzotti, M. Morbidelli, Simulated moving-bed chromatography and its application to chirotechnology. *Trends in Biotechnology* 2000, 18 (3), 108 – 118.
- [104] R. Wooley, Z. Ma, N.-H. L. Wang, A nine-zone simulating moving bed for the recovery of glucose and xylose from biomass hydrolyzate. *Industrial & Engineering Chemistry Research* 1998, 37 (9), 3699–3709.
- [105] Y. Xie, C. Y. Chin, D. S. C. Phelps, C.-H. Lee, K. B. Lee, S. Mun, N.-H. L. Wang, A five-zone simulated moving bed for the isolation of six sugars from biomass hydrolyzate. *Industrial & Engineering Chemistry Research* 2005, 44 (26), 9904–9920.
- [106] K. Hashimoto, S. Adachi, H. Noujima, H. Maruyama, Models for the separation of glucose/fructose mixture using a simulated moving-bed adsorber. *Journal of Chemical Engineering of Japan* 1983, 16 (5), 400–406.
- [107] V. G. Mata, A. E. Rodrigues, Separation of ternary mixtures by pseudo-simulated moving bed chromatography. *Journal of Chromatography A* 2001, 939 (1–2), 23 – 40.
- [108] J. S. Hur, P. C. Wankat, New design of simulated moving bed (SMB) for ternary separations. *Industrial & engineering chemistry research* 2005, 44 (6), 1906–1913.
- [109] T. Müller-Späth, L. Aumann, M. Morbidelli, Role of cleaning-in-place in the purification of mab supernatants using continuous cation exchange chromatography. *Separation Science and Technology* 2009, 44 (1), 1–26.

- [110] S. S. Farid, Process economics of industrial monoclonal antibody manufacture. *Journal of Chromatography B* 2007, 848 (1), 8 – 18.
- [111] I. Jolliffe, *Principal component analysis*. Wiley Online Library, 2002.
- [112] H. Wold, Partial least squares. *Encyclopedia of statistical sciences* 1985.

Curriculum Vitae

Personal information

Name: Daniel Baur
Date and place of birth: April 4th, 1988 (Zurich, Switzerland)
Nationality: Switzerland

Education

2012 – 2017 PhD studies in the group of Prof. Dr. Massimo Morbidelli at the Institute for Chemical- and Bioengineering, Department of Chemistry and Applied Biosciences, ETH Zurich, Switzerland (Design, modeling and optimization of multi-column chromatographic processes)
2010 – 2011 MSc in Chemical- and Bioengineering, ETH Zurich
2007 – 2010 BSc in Chemical Engineering, ETH Zurich
2000 – 2006 University entrance diploma with ancient Greek major (formerly type A), Kantonsschule Oerlikon, Zurich
1994 – 2000 Elementary school Huerstholz, Zurich

Research and teaching

2015, 2016 Co-organizer and lecturer in “Short Course on Continuous Chromatography”, ETH Zurich
2012 – 2014 Lecturer “Statistical and Numerical Methods for Chemical Engineers”, Department of Mathematics, ETH Zurich
2011 Master thesis in the group of Prof. Dr. Massimo Morbidelli (Model predictive control of the multicolumn countercurrent solvent gradient purification (MCSGP) process with limited feedback)

List of publications

- **D. Baur**, M. Angarita, T. Müller-Späth, M. Morbidelli, Twin-column affinity capture: current developments in continuous protein A affinity chromatography. *Chimica Oggi-Chemistry Today* 2017, 35, 8 – 10.
- **D. Baur**, M. Angarita, T. Müller-Späth, M. Morbidelli, Optimal model-based design of the twin-column CaptureSMB process improves capacity utilization and productivity in protein A affinity capture. *Biotechnology Journal* 2016, 11, 135 – 145.
- **D. Baur**, M. Angarita, T. Müller-Späth, F. Steinebach, M. Morbidelli, Comparison of batch and continuous multi-column protein A capture processes by optimal design. *Biotechnology Journal* 2016, 11, 920 – 931.
- R. Khalaf, **D. Baur**, D. Pfister, Optimization of reversed-phase chromatography methods for peptide analytics. *Journal of Chromatography A* 2015, 1425, 198 – 203.
- M. Angarita, T. Müller-Späth, **D. Baur**, R. Lievrouw, G. Lissens, M. Morbidelli, Twin-column CaptureSMB: A novel cyclic process for protein A affinity chromatography. *Journal of Chromatography A* 2015, 1389, 85 – 95.
- M. Angarita, P. Arosio, T. Müller-Späth, **D. Baur**, R. Falkenstein, W. Kuhne, M. Morbidelli, Role of urea on recombinant Apo A-I stability and its utilization in anion exchange chromatography. *Journal of Chromatography A* 2014, 1354, 18 – 25.
- M. Bavand, **D. Baur**, M. Angarita, R. Lievrouw, G. Lissens, G. Ströhlein, T. Müller-Späth, M. Morbidelli, Increasing Capacity Utilization in Protein A Chromatography. *Biopharm International* 2013, 26.

Conference proceedings

- **D. Baur**, M. Angarita, F. Steinebach, T. Müller-Späth, M. Morbidelli, Modeling and Optimization of the Twin Column CaptureSMB Process. SPICA 2014, Basel, Switzerland.
- **D. Baur**, T. Müller-Späth, M. Morbidelli, Purification of Proteins from Human Blood Plasma by MCSGP. SPICA 2012, Brussels, Belgium.

Poster proceedings

- **D. Baur**, M. Angarita, T. Müller-Späth, F. Steinebach, M. Morbidelli, Comparison of Multi-Column Continuous Protein A Capture Processes. PREP 2015, Philadelphia, PA.
- **D. Baur**, T. Müller-Späth, M. Morbidelli, Purification of proteins from human blood plasma by multicolumn countercurrent solvent gradient purification. PREP 2013, Boston, MA.